THE IN VITRO METABOLISM OF THREE ANTICANCER DRUGS

by

Yun Fan

B.S., West China University of Medical Sciences, 1996

M.S., West China University of Medical Sciences, 2001

Submitted to the Graduate Faculty of

School of Pharmacy in partial fulfillment

of the requirements for the degree of

Doctor of Philosophy

University of Pittsburgh

2007

UNIVERSITY OF PITTSBURGH

SCHOOL OF PHARMACY

This dissertation was presented

by

Yun Fan

It was defended on

March 23, 2007

and approved by

Samuel M. Poloyac, Assistant Professor, Pharmaceutical Sciences

RamanVenkataramanan, Professor, Pharmaceutical Sciences

Jack C. Yalowich, Associate Professor, Pharmacology

Michael A. Zemaitis, Professor, Pharmaceutical Sciences

Billy W. Day, Professor, Pharmaceutical Sciences

THE IN VITRO METABOLISM OF THREE ANTICANCER DRUGS

Yun Fan, Ph.D.

University of Pittsburgh, 2007

Etoposide is a widely used topoisomerase II inhibitor particularly useful in the clinic for treatment of disseminated tumors, including childhood leukemia. However, its use is associated with the increased risk of development of secondary acute myelogenous leukemias. The mechanism behind this is still unclear. It was hypothesized that etoposide *ortho*-quinone, a reactive metabolite previously shown to be generated *in vitro* by myeloperoxidase, the major oxidative enzyme in the bone marrow cells from which the secondary leukemias arise, might be a contributor to the development of treatment-related secondary leukemias. Experiments showed that the glutathione adduct of etoposide *ortho*-quinone was formed in myeloperoxidase-expressing human myeloid leukemia HL60 cells treated with etoposide, that its formation was enhanced by addition of the myeloperoxidase substrate hydrogen peroxide, and that the glutathione adduct level was dependent on myeloperoxidase. Both the normoisotopic and a stable isotope-labeled version of the glutathione adduct were synthesized. The latter was used for liquid chromatography-mass spectrometry-based quantitative analyses of the adduct formed by the cells.

Discodermolide and dictyostatin are two strucuturally related natural products that possess potent microtubule stabilizing activity. Discodermolide advanced to Phase II clinical trials, but the trials were halted for unannounced reasons. Here, both agents were found to be extensively metabolized by human liver microsomes *in vitro*. In order to determine the metabolic

soft spots in the molecules, the chemical structures of the metabolites of discodermolide and dictyostatin were elucidated by liquid chromatography-mass spectrometry. At least eight metabolites of discodermolide and six metabolites of dictyostatin were formed in human liver microsomes *in vitro*. The terminal diene groups on discodermolide and dictyostatin were found to be the metabolic soft spots. Results from these studies can be used in future medicinal chemistry design and synthesis work to decrease metabolic rate and improve drug metabolism and pharmacokinetic properties, therefore decreasing the doses needed and perhaps even the toxicity.

TABLE OF CONTENTS

LIST OF TABLES

LIST OF FIGURES

PREFACE

Although this dissertation reports work that I did, it is truly the product of a group effort of the many people who gave me sound advice and constructive criticism. All of this helped me to shape this dissertation into its final form. I would like to express my sincere thanks to my advisor, Prof. Billy W. Day, for his guidance of this project, his total support of the dissertation work, and his encouragement of my entering into the mixture of chemistry, toxicology and drug metabolism reported here. He was an excellent mentor during my Ph.D. program.

In addition, I am extremely grateful to my committee members, Professors Samuel M. Poloyac, Raman Venkataramanan, Jack C. Yalowich and Michael A. Zemaitis. Their guidance, advice and comments were valuable to me. I wish to acknowledge Dr. Emanuel M. Schreiber and Ms. Angela Giorgianni, who helped me on the etoposide work. I want to thank Prof. Wen Xie, my rotation advisor, who helped me understand regulatory mechanisms of drug metabolism. In particular, I thank Dean Patricia Kroboth from the bottom of my heart for her support.

I am also deeply indebted to my family, who have always trusted and supported me. They provide the source of my motivation to do everything.

Finally, I would like to thank all the faculty, staff and graduate students in the Day lab and in the School of Pharmacy for their support, and the TATRC/DoD (USAMRAA Prime Award W81XWH-05-2-0066) and the NIH (R01 CA090787 and P01 CA078039) for financial support during these studies.

1.0 INTRODUCTION

1.1 OVERVIEW

An understanding of the metabolism of chemicals is important in the drug discovery and development processes. Most compounds that have failed in development or after being approved have done so because of undesirable side effects or toxicities (so-called adverse drug reactions). These toxicities may be observed in a short period of time after administration, or sometimes they are only detected after long term use. In most cases, biotransformation of parent compounds often contributes to idiosyncratic adverse drug reactions. Toxicities induced by biotransformation can be caused by metabolites themselves, or by reactive metabolites formed. The biotransformation leading to reactive metabolites is known as "bioactivation". There are several mechanisms of bioactivation-induced adverse drug reactions, and some functional groups are particularly susceptible to bioactivation. Another reason that a compound fails in clinical trials is poor pharmacokinetic properties. Recently, a trend in the drug discovery process is to elucidate the chemical structures of metabolites of the parent compound in an early stage so as to determine the metabolic "soft spots" (the sites on the chemical structure which can be attacked by metabolic enzymes) in the compound. Characterization of metabolites formed *in vitro* or *in vivo* has therefore become more and more crucial in the drug development stage and even in the early drug discovery stage. There are several approaches for metabolite structure elucidation,

including liquid chromatogram-masspectrometry (LC-MS/MS) and liquid chromatogram-nulcear magnetic resonance(LC-NMR). LC-MS/MS is the most common technique applied in metabolite identification.

Etoposide is an approved anticancer drug, discodermolide is an investigational new anticancer drug that progressed to Phase II trials, and dictyostatin is a lead agent that could perhaps displace/replace discodermolide. Etoposide is a topoisomerase II inhibitor that has been widely used for decades. However, the use of etoposide, often in children with cancer, is associated with an increased risk of the development of secondary leukemias. The mechanism behind this adverse drug reaction is still unknown, but it is suspected to include local metabolism by cells that give rise to the secondary leukemias. Discodermolide and dictyostatin are two microtubule stabilizing agents derived from different marine sponges. Their metabolism has not been studied. It is important to find out the metabolic soft spots of discodermolide and dictyostatin to perhaps provide means for improving their pharmacokinetic and toxicological properties. The metabolism of these three agents is the subject of this dissertation.

1.2 BIOACTIVATION AND ADVERSE DRUG REACTIONS

Adverse drug reactions are a major problem in drug development and a common cause of drug recalls and labeling changes. Over 10% of the drugs approved by FDA from 1975 to 2000 had to be withdrawn from the US market or be fitted with new warning(s) in their labels (Lasser KE, *et al.*, 2002). One of the reasons that certain adverse drug reactions are not recognized before drug approval is the small numbers of patients enrolled in clinical trials that is not sufficient to reveal these negative effects (Uetrecht JP, 2000). The other reason might be the

variability among patients in gender, genetic background, underlying disease, and co-administrated drugs (Kaplowitz N, 2004). Adverse drug reactions are categorized into several types. The most common type of adverse drug reactions are predictable reactions, sometimes referred to as type A reactions, and most adverse drugs reactions (76-95%) belong to this category (Davies DM, 1985). These adverse drug reactions are usually identified based on the pharmacology of the drug in preclinical toxicological evaluations. If toxicity is observed in animals at the concentration with anticipated clinical efficacy, the further development of the drugs will be stopped. However, some adverse drug reactions do not involve the known pharmacological properties of drugs and the dose-response relationship is not well defined. These adverse drug reactions are termed idiosyncratic adverse drug reactions. The prediction of idiosyncratic adverse drug reactions is impossible at present not only because the incidence rate is extremely low, but also because such events typically emerge only after weeks or months of therapy; sometimes they are observed only several years after therapy (Uetrecht JP, 2000). Based on the reasons above, idiosyncratic adverse drug reactions are usually observed only after the drugs are approved and widely used. Idiosyncratic adverse drug reactions are a major reason for drug withdrawal in drug development and after the launch into the market. Some drugs induce idiosyncratic adverse drug reactions prior to metabolism, but most of them are caused by reactive metabolites (Uetrecht JP, 2000). A lot of evidence has been accumulated to show that inadequate detoxification of reactive metabolites is the major cause of tissue necrosis, carcinogenicity and immune toxicity. In order to decrease idiosyncratic adverse drug reactions, it is imperative that the fundamental mechanisms behind these reactions with reactive metabolites are well understood.

1.2.1 The mechanism of bioactivation-induced adverse drug reactions

Clinical and experimental evidence shows that idiosyncratic adverse drug reactions are mediated by immunological responses, in some cases, or are at least recognized by the immune system. For example, idiosyncratic liver injury caused by drugs are often accompanied by some clinical symptoms of immune response (Banks et al., 1995); Antibodies against reactive metabolite-modified proteins have been found in serum, and the presence of antibodies is associated with liver injury (Bougie et al., 1997). Dramatic responses to such agents have been reported (Greaves et al., 2001). It is well known that low molecular weight compounds can not trigger the immune response unless they covalently bind to or chemically alter proteins or other biomacromolecules. Most idiosyncratic adverse drug reactions are caused by reactive metabolites of drugs rather than by the drugs themselves. However, the presence of circulating antibodies alone is merely a marker for the immune response. In fact, experimental data suggests that the liver injury seen in these cases is actually caused by cytotoxic T cells. Most drugs that cause idiosyncratic adverse drug effects can be converted to reactive metabolites. On the other hand, it is not true that drugs that are converted to reactive metabolites to some degree are always associated with an unacceptable risk of idiosyncratic adverse drug reactions. The risk of idiosyncratic adverse drug reactions is also influenced by two other factors: one is the amount of reactive metabolite(s) that actually binds to macromolecules; the other is the specificity of macromolecules bound by reactive metabolites. Meanwhile, the dose of the drug administered can also influence the observation of idiosyncratic adverse reactions. If the dose used is low enough, the probability that it will cause adverse reactions is also low, even though the drug can be efficiently converted to reactive metabolite(s).

There may be other risk factors, in addition to covalent binding, that induce adverse reactions. This is because the normal reaction to the foreign proteins, the category in which covalently modified proteins should be placed, is tolerance. The modified protein alone is generally not sufficient to cause idiosyncratic adverse drug reactions (Bonierbale E et al., 1999). Meanwhile, if the covalent binding were the only cause of idiosyncratic adverse drug reactions, it appears that the binding of reactive metabolites only to the enzyme that formed them is unlikely to be associated with adverse reactions. One good example is tienilic acid. Tienilic acid can cause idiosyncratic liver toxicity, however it is known to only bind to CYP450 (Bonierbale E et al., 1999). These observations imply that other factors might contribute to idiosyncratic adverse drug reactions. More recent concepts have invoked the necessity of a "danger signal". There might be some factors that act as danger signals, including cellular stress, cell damage, etc. For example, a reactive metabolite can cause upregulation of costimulatory signals on T cells (Uetrecht JP, 1999; Pirmohamed et al., 2002).

Understanding the mechanisms underlying idiosyncratic adverse drug reactions is important. Such an understanding can provide a basis to identify susceptible populations, identify biomarkers associated with increased risk and assist in lead selection. Although in the past several decades, major progress has been made in understanding of idiosyncratic adverse drug reactions at the molecular level, the underlying mechanisms are still not clear. There are several possible reasons why the mechanisms are still unclear, including the difference between human and experimental animal immune systems in many aspects, the availability of animal disease models for studying immune response, and the general artificial state of experimental systems used in drug studies.

1.2.2 Bioactivation pathways of organic functional groups

Macromolecules, including proteins and DNA, in living tissues are essential components for life-sustaining process. In order to maintain the functions of proteins and DNA, their structure and sequence should remain intact. If these two fundamental elements of biochemical process are disrupted, for example by irreversible covalent binding of reactive metabolites, can manifest into cellular damage in some cases, or trigger an immune response. In attempts to identify potential idiosyncratic adverse drug reactions, promising drug candidates are generally evaluated for toxicity in animal models prior to administration to humans. However, not all toxicity caused by reactive metabolites can be identified in preclinical studies due to the limited numbers of animal disease models as well as the metabolic differences between animals and humans. Furthermore, the number of animals used in preclinical studies is far too low to reveal the typical incidence frequency of idiosyncratic adverse drug reactions seen in humans. In order to minimize reactive metabolite-mediated safety issues, the formation of reactive metabolites should be reduced. Several common functional groups that have the potential to form reactive metabolites are described below.

Aromatic Amines. The bioactivation of aromatic amines is initiated by the formation of the *N*-hydroxylamine intermediate as shown in Figure 1.1. The reactive *N*-hydroxylamine metabolites can undergo conjugation to generate *N*-*O*-acetyl conjugates, thereby forming an excellent leaving group (acetate). Under the right conditions, this can lead to a highly reactive nitrenium ion, which may be the ultimate reactive intermediate involved in DNA adduct and covalent protein binding. The reactive *N*-hydroxylamine can also undergo two-electron oxidation to generate the more reactive nitroso intermediate resulting in DNA and protein binding. A noteworthy example is procainamide, an aromatic amine. The utility of procainamide has been

hampered by its adverse drug reactions. *N*-Hydroxyprocainamide and nitrosoprocainamide have been observed to result from incubation with mouse liver microsomes *in vitro*, as well as *in vivo* (Freeman RW, et al., 1981). The covalent binding of reactive metabolites of procainamide can be prevented by the addition of reducing agents to reduce them to aromatic amines.

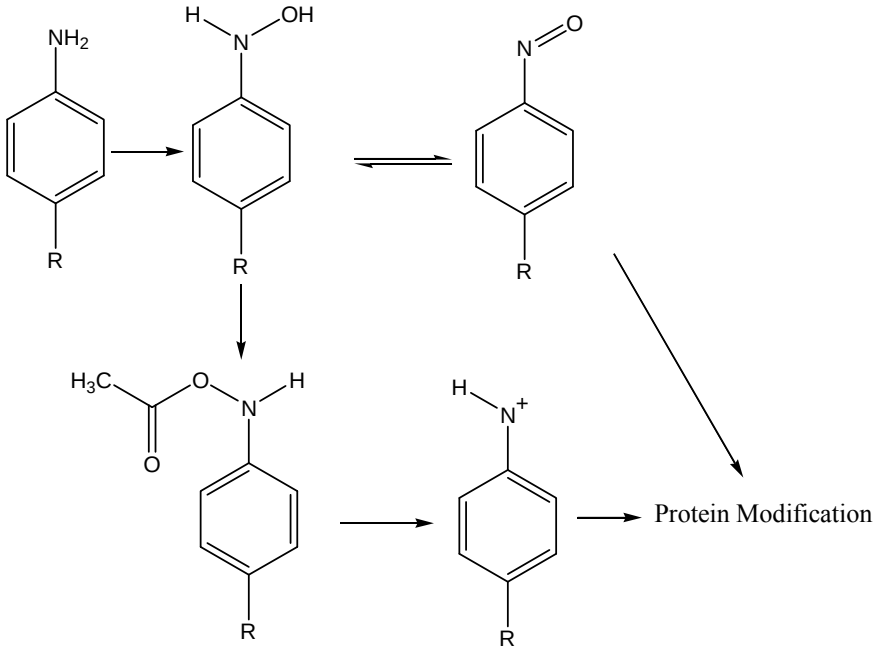

Figure 1.1 Bioactivation of aromatic amine.

Aromatic nitro compounds. Aromatic nitro drugs are similar to aromatic amines in that they can also be converted to hydroxylamine and nitroso intermediate metabolites. The formation of nitroso intermediate metabolite is initiated by the reduction of the nitro group (Figure 1.2), often by nitroreductases in gut bacteria. A well-known example of a drug that causes idiosyncratic adverse drug reactions is talcapone. Talcapone is a drug that was approved for the treatment of Parkinson's disease. It was withdrawn from the market because of a high incidence of liver toxicity (Watkins P, 2000). The nitro group in talcapone was shown to in fact

be reduced to the nitroso and hydroxylamine intermediates, reactive metabolites that are presumed to be responsible for the idiosyncratic adverse drug reactions (Jorga K, et al., 1999).

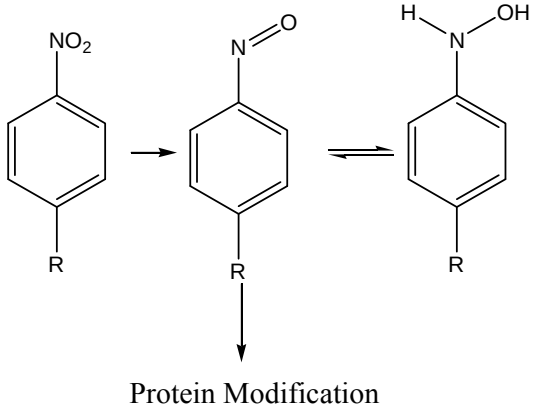

Figure 1.2 Bioactivation of aromatic nitro compounds.

Hydrazine containing drugs. Hydrazine-based drugs have the potential to cause idiosyncratic adverse drug reactions. For instance, isoniazid is associated with a relatively high incidence of severe hepatotoxicity and this is well stated on its warning label. The mechanism of hydrazine drug-induced idiosyncratic adverse drug reactions is thought to be related to the bioactivation of hydrazines. Hydrazines appear to be oxidized by peroxidases to diazines and diazonium ions, two reactive intermediates. Diazonium ions can further lose nitrogen to form very reactive radicals or carbocations. These very reactive species can then covalently modify macromolecules.

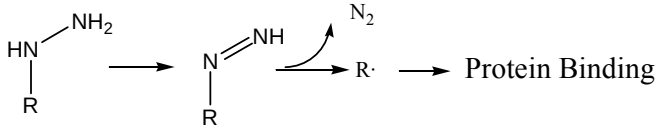

Figure 1.3 Bioactivation of hydrazine.

Quinone-imine reactive metabolites. Quinone-imines are reactive electrophiles that readily form conjugates with proteins and endogenous glutathione (GSH) through Michael reactions. Such a metabolite is likely responsible for the idiosyncratic adverse drug reactions

associated with some drugs (Clarke JB, et al., 1991), particularly the liver toxicity caused by high doses of acetaminophen. Quinone-imine formation occurs during normal biological oxidation of parent compounds.

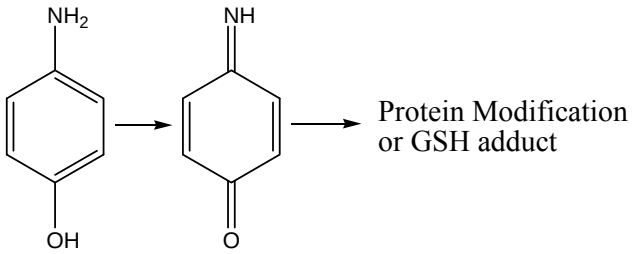

Figure 1.4 Bioactivation of 1,4-aminophenol.

Quinones. Quinones are Michael acceptors and can covalently react with cellular electrophiles such as proteins and DNA, resulting in cell damage and an immune response. They can not only cause macromolecule modification by direct reaction, but also initiate redox cycles through their hydroquinone and semiquinone forms, finally leading to the formation of reactive oxygen species. Quinones are typically generated from aromatic compounds through oxidation.

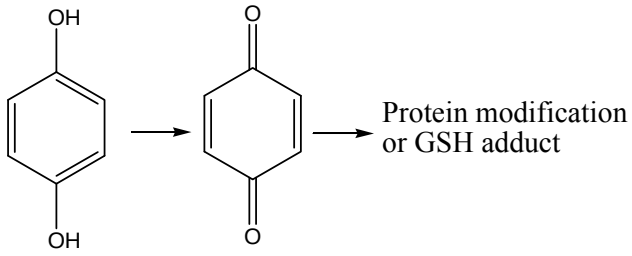

Figure 1.5 Bioactivation of 1,4-hydroquinone.

Furans. Furan is an environmental contaminant in smog, tobacco smoke and canned foods. Furan is a known hepatic and renal toxicant. It is also a potential human carcinogen (Sirica AE, 1996). Bioactivation of furan moiety is believed to be a major cause of idiosyncratic adverse drug reactions in molecules that contain them. Furan is first converted to an epoxide, which can be converted to toxic butene-1,4-dial (Chen LJ, et al., 2006). The hepatocarcinogen

aflatoxin B1 is activated to its ultimate carcinogenic form by this mechanism (Guengerich FP, et al., 1998).

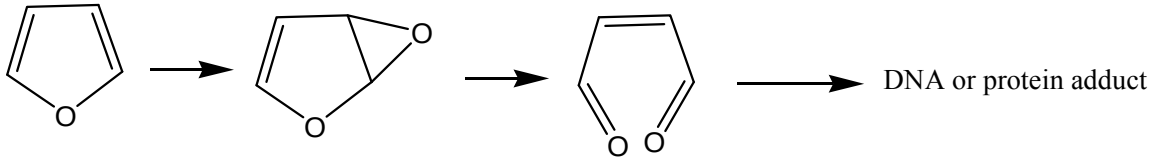

Figure 1.6 Bioactivation of furan.

1.2.3 Enzymes responsible for the formation of reactive metabolites

The cytochrome P450 system is the essential group of enzymes associated with reactive metabolite formation. It is also the dominant system of enzymes in the liver, which is the major organ of drug bioactivation (Rooney PH, et al., 2004). Cytochromes P450 are responsible for the oxidation of a wide range of drug substrates, and comprise the major route of what is termed Phase I metabolism. Phase I metabolism is conversion of endo- and xenobiotics to more polar compounds through an oxidation that generally leads to addition of an oxygen atom to the xenobiotic. However, the liver is not the only target organ in which idiosyncratic adverse drug reactions take place; other organs and tissues, such as intestine, kidney, skin, lung, etc., contain different cytochrome P450 subfamily (Rooney PH, et al., 2004). These organs and tissues contribute to idiosyncratic adverse drug reactions to some degree. Bioactivation reactions can also be attributed to the action of flavin-containing monoxygenase (FMO), but the functional groups affected by these enzymes are limited to certain nitrogen- and sulfur-containing groups on drug substrates (Cashman JR, 2000). In addition, monoamine oxidases (MAOs) (Gong B, et al., 2006) and heme-containing peroxidases (O'Brien PJ, 2000) can contribute to the

bioactivation of drugs. One target tissue for idiosyncratic adverse drug reactions, the bone marrow, is likely associated with peroxidase-catalyzed metabolic bioactivation (Ju C, et al., 1998).

Peroxidases play an important role in drug metabolism and can lead to the formation of reactive metabolites. Such reactive metabolites might give rise to cellular oxidative stress and protein binding to specific enzymes, and finally cause idiosyncratic adverse drug reactions and even cancer. The native peroxidases are heme-containing enzymes that catalyze the oxidation of a variety of xenobiotics using hydrogen peroxide (H_2O_2). Myeloperoxidase (MPO) is one of the members of the peroxidase family. MPO contributes 2-5% dry weight of the human neutrophil. In addition to neutrophils, MPO is also present in monocytes, tissue macrophages, Kupffer cells and bone marrow CD34+ myeloid progenitor cells (Brown KE, et al., 2001; Schattenberg DG, et al., 1994). MPO is a unique enzyme among all peroxidases and is most commonly associated with its catalysis of chloride oxidation to produce hypochlorous acid (HOCl). The high peroxidase activity in neutrophils has been attributed to MPO, which provides an antibacterial system in human body. It has been reported that secondary leukemias induced by chronic exposure to etoposide might be associated with MPO-catalyzed oxidation. It has been hypothesized that MPO-catalyzed etoposide oxidation causes radical production and reactive metabolite formation, further increasing cellular oxidative stress and the inactivation of etoposide's molecular target, topoisomerase II. This combination of events may finally lead to secondary leukemias (Kagan VE, et al., 1999; Fan Y, et al., 2006). Studies, including one reported in this dissertation, have shown that incubation of HL60 cells, a myeloid leukemia cell line that contains MPO, with etoposide and hydrogen peroxide leads to the formation of GSH thiyl radicals and the etoposide *ortho*-quinone GSH adduct.

The Phase II enzymes are usually considered as pure detoxification pathways. These enzymes catalyze conjugation of xenobiotics (including drugs) and their more polar Phase I metabolites to hydrophilic functional groups, such as glucuronic acid, GSH and sulfate. The result is a dramatic decrease in the lipophilicity of drugs and an increase in their elimination. However, this is not always true. Conjugation pathways can result in the formation of electrophilic reactive metabolites (Banoglu E, 2000; Glatt H, 2000; Ritter JK, 2000). Glucuronidation of certain carboxylic acids results in the formation of electrophilic acyl glucuronides, some of which have been noted to covalently modify macromolecules. This covalent binding has the potential to inactive metabolic enzymes and lead to the loss of cell membrane integrity. The sulfation and acetylation of -OH groups on drugs can provide a good leaving group and therefore facilitate the formation of electrophilic reactive metabolites. Aromatic amine metabolites are an excellent example. Although it is less common to some extent, the conjugation with GSH can sometimes generate reactive metabolites (Monks TJ, et al., 1990).

1.3 METABOLITE IDENTIFICATION APPROACHES

Identification of the metabolites generated by biotransformation processes is a crucial task in various stages of drug discovery and development. In the early drug discovery stage, it is necessary to identify the metabolic soft spots of compounds that show low metabolic stability. The result can provide information for further structure modifications of lead compounds and improvement of the metabolic and pharmacokinetic properties. The purpose of metabolite identification at this stage is to: 1) lower intrinsic clearance in order to increase systemic

exposure to the drug; and 2) decrease the potential for the formation of reactive metabolites generated by bioactivation in a particular structure/backbone/scaffold series. Identification of unknown metabolites in biological matrices is a difficult task due to the complexity of the matrices, varying in chemical structures and in concentration. Because of its superb speed, selectivity, and sensitivity, liquid chromatography-tandem mass spectrometry (LC-MS/MS) is without question the best technique for identification of unknown metabolites among a wide array of analytical techniques and methods (Kostiainen R, et al., 2003; Clarke NJ, et al., 2001; Tozuka Z, et al., 2003). The traditional metabolite identification procedure is as follows. Metabolites and the parent drug are separated by high performance liquid chromatography, then a full scan mass spectrum (MS) and a product ion (MS/MS) fragmentogram are generated by the mass spectrometric system. The molecular weight and chemical structure of metabolites can be elucidated based on such data; the latter particularly through the product ion spectra of metabolites. MS/MS data often can provide sufficient structure information for metabolite identification of candidate drugs. Multiple stage MS experiments (MS^n) are also widely used to generate complementary structure information (Tomer KB, 2001). In many situations, other parallel techniques, such as precursor ion scans, neutral loss ion scans, an accurate mass measurement on an instrument capable of high resolution mass spectrometry, and data-dependent scans can also facilitate the structure elucidation of metabolites present in a complex biological matrix. Furthermore, some chemical related techniques, including hydrogen/deuterium (H/D) exchange and chemical derivatives, can give more useful information about the chemical structures of metabolites. However, LC-MS cannot always determine the geometry and can only very rarely determine the stereochemistry of substituents within the eluting metabolites (Lindon JC, et al., 1997). Furthermore, it is difficult to obtain MS data for compounds that are thermally

labile or that are difficult to ionize in modern MS ionization sources (Dachtler M, et al., 2001). Therefore, nuclear magnetic resonance (NMR) is often a necessary method to be used to generate more detailed information, especially in regard to stereochemistry. Nowadays, modern two-dimensional, high field NMR can be performed in some cases on the small amounts of metabolites isolated from biological systems.

In MS, the product ion scan mode is the most common scan technique used for metabolite identification. This scan function is available on most types of mass analyzers, such as triple quadrupole, 3D and linear ion trap, and ion cyclotron resonance Fourier transform (FT) MS systems. It also can be performed on some hybrid mass spectrometers, including quadrupole-linear ion trap (Q-Trap) and quadrupole-time of flight (Q-TOF) MS systems. A typical product ion scan experiment includes three steps (Figure 1.7). The first step is the selection of the parent (precursor) ion of interest to be fragmented. The second step is the fragmentation of the parent ion by various energetic techniques, e.g., collision-induced dissociation. The third step is obtainment of the full scan of the product (a.k.a. daughter) ions obtained by fragmentation in the second step. The interpretation of the product ion spectra (MS/MS data) usually provides enough data to intelligently propose chemical structures of metabolites generated by biotransformation.

In addition to the product scan mode, there are other scan techniques that can be performed, but only on some types of instruments. Precursor ion scan mode and neutral loss ion scan mode are two of the relatively commonly used scan techniques. Usually, these two ion scan modes can be performed on a triple quadrupole mass spectrometer. They are powerful tools for detecting metabolites in complex biological matrix. If a drug can produce a characteristic neutral product ion that corresponds to a specific structural feature after fragmentation, that specific neutral loss can be used for detecting metabolites related to the

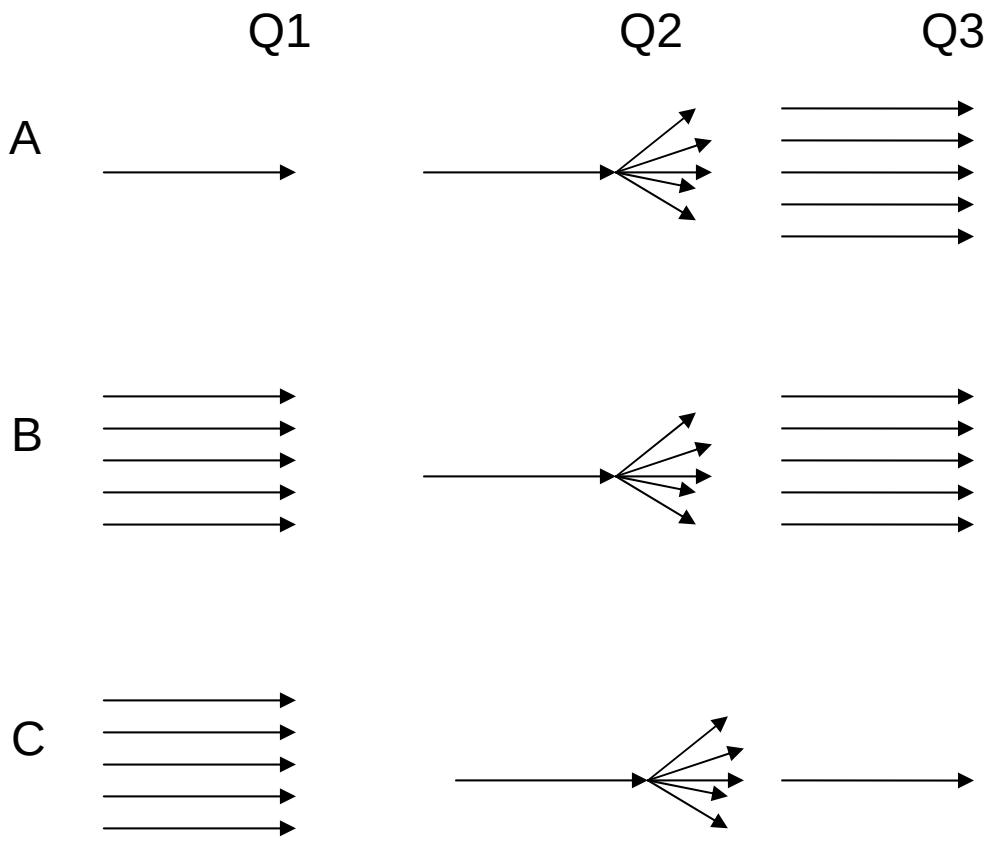

Figure 1.7 Different ion scan modes in triple quadrupole mass analyzer: A. product ion scan; B. neutral loss ion scan; C. precursor ion scan. (multiple arrows: full scan mode; single arrow: selective ion mode, arrows in Q2: collision induced dissociation.)

parent drug. A typical neutral loss ion scan experiment (Figure 1.7) performed on a triple quadrupole mass spectrometer is set to full scan both in Q1 and Q3, but the mass difference of Q1 and Q3 full scan is fixed. This difference corresponds to the neutral loss of the molecular ion during collision-induced dissociation. Therefore, only those molecular ions that give rise to this common neutral loss are recorded in the final mass spectral data file. The neutral loss scan mode is widely used in the detection of Phase II metabolites, which usually generate neutral fragments during fragmentation. For example, GSH conjugates and adducts show a neutral loss of 129, glucuronide conjugates give a neutral loss of 176, and sulfate conjugates show a neutral loss of 80 (Prakash C, et al., 1997; Davoine C, et al., 2005). The precursor ion scan mode can also be

used as a powerful tool for detecting target metabolites if the drug produces a characteristic fragment ion corresponding to a specific chemical structure feature after collision-induced dissociation. In a precursor scan experiment (Figure 1.7), Q1 is set to full scan mode and Q3 is set to select the product ion scan in which only a characteristic fragment ion can be detected. Thus, precursor ions generating this common fragment ion can be recorded in the MS/MS analytical data file. Precursor ion scanning is very useful in discovery stages where radiolabeled compounds are not available. Neutral loss ion scan and precursor ion scan can dramatically reduce the consumption of samples and increase analytical efficiency.

MS/MS scanning (MS^2) is usually referred to as the first stage product ion scan. Further fragmentation of select product ions produced by MS^2 is called MS^3. Continuous fragmentation of product ions from the previous stage leads to what are known as MS^n experiment and the resulting multiple stage mass spectra. A scheme of multiple stage ion scanning performed in an ion trap mass analyzer is illustrated in Figure 1.8. The MS^n results are a very useful means for structure elucidation of unknown metabolites because such results can not only provide a convenient way for fragment assignment, but also give rise to a wealth of information about chemical structures of metabolites in a single analysis. This type of scan is not available to all kinds of mass analyzers. Only those instruments that trap ions, such as 3D and linear ion traps (including the hybrid quadrupole-ion trap (Q-TRAP)), and FT-ion cyclotron resonance (FT-ICR) systems, can perform these multiple stage ion scans. This method is very useful to determine the sites of biotransformation. In some cases, it can also differentiate the chemical structures of the fragment ions that own the same mass charge ratio. Thus, it is very helpful to run multiple stage ion scan experiment when an MS/MS scan can not give rise to enough information for structure elucidation.

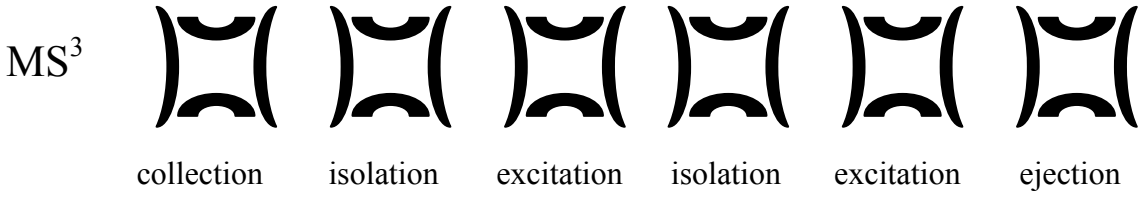

Figure 1.8 The scheme of a MS^3 experiment in ion trap. The experiment is initiated by the collection of the ion currant, followed by the isolation of the parent ion, excitation of the parent ion, isolation of the fragment ion, excitation of the fragment ion and the ejection of the secondary fragment ions generated by the secondary excitation.

Accurate mass measurement can be crucial in distinguishing essentially isobaric molecular ions and in assigning fragment ions for elucidation of fragmentation mechanisms (Ma S, et al., 2006). Accurate mass measurement can help confirm the molecular formula of both parent ions and fragment ions under investigation. Accurate mass measurement is usually performed with several types of mass analyzers owning higher mass accuracy, e.g., those containing TOF and FT-ICR analyzers. This experiment can also performed with hybrid mass analyzers, like linear ion trap-FT-ICR or QqTOF systems (Sanders M, et al., 2006).

Hydrogen/deuterium exchange experiments are a strategy widely used for elucidation of mass spectral fragmentation mechanisms (Ma S, et al., 2006). The biotransformation of drugs usually introduces polar functional group such, as hydroxyls, or alters some functional groups, such as amines. The biotransformation will lead to a number of exchangeable hydrogen atoms, which can be exchanged with deuterium. H/D exchange experiments can in fact be performed on-line when the water in the reversed phase HPLC mobile phase is replaced by heavy, deuterium-containing water (^2H_2O, a.k.a. D_2O). Hydroxylation of the parent drug introduces an additional exchangeable hydrogen atom, which can be detected by H/D exchange experiments on-line. The more the hydroxyl groups in chemical structures of metabolites, the higher purity of D_2O required.

1.4 METABOLIC STABILITY

Drug development is a time-consuming process. The average development time of a new drug is around twelve years, and the cost in 2004 was approximately $900 million (Kola I, et al., 2004). The major reason for the failures in drug development is poor metabolic and pharmacokinetic properties (Kola I, et al., 2004). Previously, drug metabolism studies were performed at a late stage of drug development, such as in clinical studies. Nowadays, pharmaceutical companies have introduced many new methods to improve the metabolic and pharmacokinetic properties at an earlier stage in drug development process, and even at drug discovery phase. The study of *in vitro* metabolic stability is one of them (Plant N, 2004).

In vitro models to study drug metabolic stability include incubations of lead agents with liver microsomes and/or hepatocytes. Liver microsomes are the most common tool used to study metabolic stability. Compared with hepatocytes, microsomes are very stable during prolonged storage and more convenient to use. Usually, pooled liver microsomes from different donors are used in order to minimize the difference of enzyme activity from each donor. In addition to CYP enzymes, there are other enzymes present in microsomes, such as flavin-containing monoxygenase (FMO) and UDP-glucuronosyltransferase (UGT). Microsomal systems have several advantages, such as easy use and preparation, a maintenance-free nature, high enzyme concentrations, and high stability. Hepatocytes are also valuable for metabolic stability studies. This model includes all Phase I and Phase II enzymes in liver, as well as the co-factors for enzyme activities. However, the availability of fresh hepatocytes and the short lifetimes of the cells hamper the widespread deployment of this model. Although *in vitro* models can minimize the inter-species difference in drug metabolism enzymes, it is important to keep in mind that they represent a simplistic view of the *in vivo* systems in which drug biotransformation takes place.

Therefore, researchers must pay attention to this point when predictions of drug metabolism *in vivo* are made with data collected from *in vitro* systems.

Metabolic stability studies using liver microsomes as the model are performed based on the following assumptions: 1) *in vitro* metabolism represents the metabolism *in vivo*; 2) the liver is the major organ for drug metabolism; and 3) the major elimination pathway of oxidative metabolism is mediated in the first step by CYP enzymes. In the present studies, the *in vitro* half-life approach utilizing liver microsomes was used to evaluate the metabolic stability of compounds. This approach, reported in Chapter 5, is the most widely used model for *in vitro* metabolism because of its simplicity. In this method, the natural log scale of the percentage of parent compound remaining versus time is plotted. The percentage of parent compound remaining is calculated by comparing the amount of compound remaining at different times to the amount of compound present at 0 min (t = 0). The slope of the line resulting from regression analysis is –k, and the half life ($t_{1/2}$) is calculated using the formula

$$t_{1/2} = 0.693/k$$

1.5 ETOPOSIDE, DISCODERMOLIDE, AND DICTYOSTATIN

Etoposide. Etoposide (a.k.a. VP-16) is one of the most widely used anticancer agents. It is a semi-synthetic derivative of a natural product from *Podophyllum peltatum* (Pommier Y, et al., 1985).

The anticancer mechanism of etoposide is based on its inhibitory effects on the DNA rejoining catalyzed by the ATP-utilizing enzyme topoisomerase IIα (Topo II) (Pommier Y, et al., 1985). Topo II is an essential DNA binding protein responsible for double strand cleavage of DNA. It allows the passage of one DNA strand across another to relieve torsional stress during replication and transcription, and allows for separation of daughter DNA strands during mitosis. Topo II is a target for a number of clinically effective anticancer agents. These drugs interfere with topo II's activity by stabilizing topo II/DNA binding in a covalent cleavable complex, which prevents subsequent reannealing activity and leads to sustained DNA strand breaks.

Numerous groups have reported in the past ten years that the same treatment schedules associated with the impressive clinical efficacy of VP-16 are also associated with an increased risk of secondary treatment-related acute myeloid leukemia (t-AML) (Pui CH, et al., 2000; Winick NJ, et al., 1993). t-AML is characterized by distinct translocations involving the chromosome 11q23 region. An 8.3-kb breakpoint cluster region of the MLL gene that encompasses exons 5 through 11 has been found to be associated with myeloid leukemia arising subsequent to treatment with topo II inhibitors such as VP-16 (Pui CH, et al., 1989; Pedersen-Bjergaard J, et al., 1994). The MLL gene encodes a 3969 amino acid protein whose function likely regulates transcription of genes important in hematopoietic differentiation. In t-AML, the MLL gene is recombined with a variety of chromosomal partners. *MLL* partners with over 40 different genes to create leukemogenic gene fusions. (Eguchi M, et al, 2005). Each translocation

yields in-frame fusions in the derivative chromosome 11, likely resulting in functional chimeric proteins. Hence, 11q23 translocations of MLL are considered to be likely causative for t-AML (Popovic R, et al., 2005).

Chromosome band 11q23 translocation breakpoints within the centromeric portion of the MLL breakpoint cluster region have been identified to be in close proximity to etoposide-induced Topo II cleavage sites (Aplan PD, et al., 1996). A double strand DNA cleavage site has been identified within the telomeric portion of the MLL breakpoint cluster region in malignant cell lines and in normal peripheral blood lymphocytes treated with etoposide (Nasr F, et al., 1997). These drug-induced DNA cleavage sites map to the same region as a consensus Topo II cleavage site within the MLL breakpoint cluster region. These investigations suggest that site-specific cleavage within the MLL breakpoint cluster region induced by Topo II inhibitors may be an early marker of apoptosis, or may lead to translocations and secondary leukemias (Ng A, et al., 2000). These results imply that myeloid progenitor cells may be unusually susceptible targets for the leukemogenic effects of etoposide.

In summary, etoposide is converted to several metabolites, such as the hydroxyl acid, the *cis*-lactone, the E-ring catechol, and a glucuronide (Relling MV, et al., 1994; Watanabe Y, et al., 2003). Some oxidative enzymes, e.g., peroxidases, tyrosinase and cytochrome P450 isozymes, can also generate intermediate phenoxyl radical species leading to the catechol, the *ortho*-quinone and semiquinone metabolites of etoposide. Covalent reaction of etoposide *ortho*-quinone with DNA and protein has been reported in isolated microsomal or DNA preparations (Haim N, et al., 1987). In addition, *ortho*-quinone-mediated inactivation of single and double stranded DNA has been associated with direct adduct formation, and has been demonstrated to induce Topo II-mediated DNA cleavage (van Maanen JM, et al., 1985). Therefore, etoposide

ortho-quinone may play an important role in etoposide's action, as well as toxicities. Its overproduction in MPO+ cells may make this stem cell population particularly susceptible to the recombinogenic events related to MLL translocations.

Previous studies show that there is a correlation between adduct formation, Topo II inhibition and cytotoxicity for the *ortho*-quinone, and the results suggest that Topo II poisoning by the *ortho*-quinone is due to chemical modification of Topo II (Gantchev TG, et al., 1998). In the present studies, direct chemical adduction between etoposide *ortho*-quinone and cysteine sulfhydryls was assessed, as was the formation of the metabolite and adducts in human cells containing MPO. The results provided detailed information about the production of this metabolite in hematopoietic cells, and perhaps a better understanding of the mechanism by which etoposide therapy leads to the formation of secondary leukemias.

Discodermolide. Microtubules are an important target for cancer therapy, e.g., a microtubule stabilizer, paclitaxel, has been used successfully in the treatment of different type of cancers, particularly solid tumors (Flechon A, et al. 2006). Microtubules are one of the principal components of the cytoskeleton, and the dynamic structure of microtubules, provides a somewhat cancer -selective means of treatment by agents that alter microtubule dynamics. Microtubules are composed of monomers containing a heterodimeric protein, tubulin, which includes the subunits α-tubulin and β-tubulin. Microtubules are polar structures with two distinct ends: a fast-growing plus end and a slow-growing minus end. This polarity is an important consideration in determining the direction of movement of motor proteins along microtubules (Rungger-Brandle E, et al., 1983). The assembly and disassembly of microtubules is a dynamic progress. During or shortly after polymerization, the GTP bound to β-tubulin is hydrolyzed to

GDP and this GTP hydrolysis weakens the binding affinity of tubulin for adjacent molecules, thereby favoring depolymerization and resulting in the dynamic behavior of microtubules (Mareel MM, et al., 1985). Microtubules are particularly critical for mitosis, so drugs that affect microtubule assembly are powerful weapons in the treatment of cancer.

Paclitaxel was the first microtubule stabilizing agent on the market. It has been used for over a decade. It is isolated from the extracts of the bark of the pacific yew, *Taxus brevifolia*, and was initially identified as a cytotoxic agent (Wani MC, et al., 1971). Although paclitaxel is one of the most effective chemotherapeutic drugs, it has several limitations: 1) it is susceptible to several forms of mechanism-based drug resistance, such as the efflux pump P-glycoprotein (Pgp; a.k.a. ABCB1)-mediated drug resistance and selection of mutant or overexpression of unaffected β-tubulin (Iwahana M, et al., 1998; Fukushima M, et al., 2000); 2) the aqueous solubility of paclitaxel is poor, ca. 7 μM (Rowinsky EK, 1997); and 3) its structural complexity makes it difficult to synthesize from readily available and inexpensive raw materials.

To overcome these drawbacks, new generation microtubule stabilizing agents with increased efficacy and/or better synthetic accessibility have been sought. One of the most interesting drugs in this regard is discodermolide. (+)-Discodermolide was initially isolated from a marine sponge, *Discodermia dissoluta*, and was incorrectly identified as an immunosuppressive agent (Gunasekera SP, et al., 1990). Later, it was demonstrated that this compound could cause cell cycle arrest at mitosis in a variety of cell lines at low concentrations, ranging from 3 to 80 nM, and treated cells that survived (i.e., did not apoptose) eventually exited mitosis with micronuclei (Hung DT, et al., 1996). Isolated tubulin treated with discodermolide forms abnormal microtubules, and these microtubules show increased stability against cold-induced depolymerization (ter Haar E, et al., 1996). Discodermolide has been found to bind

either to the same site on microtubules as paclitaxel or to an overlapping site, and discodermolide's affinity for the same site as paclitaxel is higher (Kowalski, RJ, et al. 1997). It is believed that discodermolide can stabilize mitotic spindle microtubule dynamics and inhibit the rate and extent of shortening instead of changing the amount of polymerized tubulin (ter Haar E, et al., 1996). Compared with paclitaxel, discodermolide is substantially more potent in most cell lines tested (Mani S, et al., 2004). It is not a substrate of P-gp (Kowalski RJ, et al., 1997). It is also able to induce apoptosis in cell lines that are resistant to paclitaxel due to mutations in β-tubulin, while another type of new microtubule stabilizers, the epothilones, do not (Kowalski RJ, et al., 1997). Intriguingly, the combination of paclitaxel with discodermolide demonstrates synergistic effects in enhancement of cell death, suppression of microtubule dynamics and induction of mitotic arrest, and this synergic effect was not observed for combinations of paclitaxel with epothilones (Honore et al., 2004; Hamel E, et al., 2006). Discodermolide has a somewhat simpler chemical structure than does paclitaxel. Total syntheses of discodermolide has been reported by several groups (e.g., Paterson I I, et al., 2000; Smith AB, et al., 2005; Harried SS, et al., 2003) and it has been produced by full synthesis at large scale (Francavilla C, et al., 2003). The aqueous solubility of discodermolide is also much higher than that of paclitaxel (Kowalski RJ, et al., 1997).

However, discodermolide has some features that impact its clinical development. Its maximum tolerated dose in rats is only ca. 1.0 mg/kg (Mita C, et al., 2003). Preclinical ADME studies show that discodermolide is rapidly cleared from plasma (Mita C, et al., 2003). In order to increase metabolic stability mediated by CYP enzymes, decrease the dose of administered, and therefore decrease the toxicity of discodermolide, its metabolism by pooled human liver

microsomes was examined here. Several metabolites were detected *in vitro*, and a soft spot for biotransformation was identified.

Dictyostatin. Marine organisms are proving to be a rich source of bioactive secondary metabolites with potential anticancer properties (Gunasekera SP, et al., 1990). In fact, many microtubule stabilizing agents, such as discodermolide, eleutherobin and laulimalide, come from extracts of marine organisms. Although their chemical structures share little similarities, all of them have a very similar mechanism of action.

A novel 22-membered macrocyclic lactone, (–)-dictyostatin, was initially isolated from a Republic of Maldives marine sponge of *Spongia* species in 1994 and found to strongly inhibit the growth of murine P388 lymphocytic leukemia cells (Pettit GR, et al., 1994). Later, dictyostatin was found to arrest cells in the G2/M phase of the cell cycle and to induce the polymerization of tubulin *in vitro*. Like discodermolide, the microtubules induced by dictyostatin are resistant to cold temperatures (Isbrucker RA, et al., 2003). Dictyostatin and discodermolide share a high degree of homology in their chemical structures. Total synthesis of dictyostatin has recently been reported by several groups (Shin Y, et al., 2004; Paterson I, et al., 2004; O'Neil GW, et al., 2006; Ramachandran PV, et al., 2007). Similar to discodermolide, dictyostatin is also highly potent against paclitaxel-resistant human cancer cell lines overexpressing active P-glycoprotein (Isbrucker RA, et al., 2003). The studies described in this dissertation indicate that dictyostatin is metabolically unstable, albeit less so than discodermolide, and is extensively transformed by pooled human liver microsomes. It was no surprise that the same soft spot as found in discodermolide was found for biotransformation of dictyostatin. The data discovered in this work

may prove useful in designing analogues with improved metabolic and pharmacokinetic properties.

2.0 MYELOPEROXIDASE-CATALYZED METABOLISM OF ETOPOSIDE TO ITS QUINONE AND GLUTATHIONE ADDUCT FORMS IN HL60 CELLS

Yun Fan, Emanuel M. Schreiber, Angela Giorgianni, Jack C. Yalowich, and Billy W. Day

Department of Pharmaceutical Sciences, Proteomics Core Lab, Department of Pharmacology, and Department of Chemistry, University of Pittsburgh, Pittsburgh, Pennsylvania 15261

Reproduced with permission from [Yun Fan, Emanuel M. Schreiber, Angela Giorgianni, Jack C. Yalowich, and Billy W. Day. Myeloperoxidase-Catalyzed Metabolism of Etoposide to Its Quinone and Glutathione Adduct Forms in HL60 Cells. *Chem. Res. Toxicol.,* 19 (7), 937 -943, 2006]

2.1 ABSTRACT

Etoposide is a widely used antineoplastic agent that has provided great success in the treatment of childhood leukemias and other malignancies. Unfortunately, its use is associated with increased risk of development of secondary acute myelogenous leukemias involving translocations at the *MLL* gene in chromosome band 11q23. Previous studies showed that the phenoxyl radical of etoposide can be generated by myeloperoxidase (MPO), an enzyme prevalent in myeloid progenitor cells that can derive myelogenous leukemias. Disproportionation of this radical leads to formation of the redox active etoposide *ortho*-quinone metabolite. We hypothesized that etoposide *ortho*-quinone could be formed in myeloid progenitor cells and might contribute to the development of treatment-related secondary leukemias. Etoposide *ortho*-quinone is an inherently unstable compound and readily reacts with glutathione in aqueous media without any requirement for catalytic assistance from glutathione *S*-transferase. We looked for the presence of its glutathione adduct as an indicator of etoposide *ortho*-quinone in cells. MPO-expressing human myeloid leukemia HL60 cells were treated with etoposide for 0.5 h in the presence and absence of the cosubstrate of MPO, hydrogen peroxide. Cell lysates and medium were analyzed by LC-ESI-ion trap-MS and MS/MS, which yielded clear evidence of the intracellular formation of the etoposide *ortho*-quinone-glutathione adduct. A stable isotope-labeled form of the GSH adduct was synthesized and employed as an isotope dilution internal

standard in LC-ESI-quadrupole-MS analyses. The glutathione adduct level was dependent on the concentration of etoposide added to the cells. More importantly, the formation of the glutathione adduct was significantly suppressed by the pretreatment of HL60 cells with the heme synthesis inhibitor succinylacetone ($p < 0.001$), which resulted in a decreased level and activity of MPO. These results are consistent with the idea that MPO is responsible for the conversion of etoposide to its *ortho*-quinone in these cells.

2.2 INTRODUCTION

Etoposide is one of the several widely used cancer chemotherapeutic DNA topoisomerase II (Topo II) inhibitors. It is a semisynthetic derivative of the natural product podophyllotoxin, which is one compound present in an extract from the plants *Podophyllum peltatum and Podophyllum emodi*. Etoposide inhibits Topo II-catalyzed DNA rejoining and stabilizes the enzyme-DNA cleavage complex (Pommier Y, et al., 1985). Several metabolites of etoposide have been identified in humans, such as its hydroxyl acid, *cis*-(picro)lactone, catechol, and glucuronide (Stewart CF, 1994). It has been reported that etoposide catechol formation is catalyzed by CYP3A4 and CYP3A5 (Relling MV, et al., 1994; Zhuo X, et al., 2004; Zheng N, et al., 2004) and that of the glucuronide by UGT1A1 (Watanabe Y, et al., 2003). Etoposide and its catechol also can be converted by one-electron (1-e^-) oxidation to their respective phenoxyl radicals (i.e., the semiquinone from the catechol) by peroxidases and prostaglandin synthetase (Haim N, et al., 1986; Haim N, et al., 1987; Van Maanen JM, et al. 1988; Kagan VE, et al., 2001). An additional 1-e^- oxidation or disproportionation of these phenoxyl radical species can convert them to the etoposide *ortho*-quinone metabolite. Formation of this etoposide metabolite

has recently been demonstrated in humans (Zhuo X, et al., 2004; Zheng N, et al., 2004). Use of etoposide in the clinic is accompanied by an increased risk of development of secondary leukemias specifically treatment-related acute myeloid leukemia (t-AML) characterized by translocations of the *MLL* gene involving the chromosome 11q23 region (Felix CA, 1998; Felix CA, 2001; Shearer P, et al., 2001; Wierecky J, et al., 2005; Josting A, et al., 2003). Despite this recognized epidemiological link, the mechanism(s) behind the high susceptibility of myeloid progenitors, such as CD34+ cells, to the leukemogenic effects of etoposide remains unclear (Libura J, et al., 2005). It is not known why etoposide preferentially causes myeloid leukemias but not other types of leukemias.

Because CD34+ myeloid precursor cells in early stages of maturation contain relatively high levels of the 1-e^- oxidizing enzyme myeloperoxidase (MPO) (Strobl H, et al., 1993), we previously hypothesized that oxidative activation of the phenolic moiety of etoposide by MPO may be responsible for converting this drug to a more genotoxic and carcinogenic species (Kagan VE, et al., 2001). In support of this hypothesis, we used both purified MPO and MPO-rich HL60 myeloid leukemia cells as surrogates for CD34+ cells to directly demonstrate (i) 1-e^- metabolic oxidation of etoposide to its phenoxyl radical (etoposide-$O^{\bullet}$) accompanied by generation of thiyl radicals and oxidation of protein sulfhydryl groups and (ii) MPO-dependent enhancement of etoposide-induced Topo II-DNA complex formation (Kagan VE, et al., 2001). Both the formation of etoposide-$O^{\bullet}$ and the increase in etoposide activity were prevented by use of MPO inhibitors and nutritional antioxidants, such as the free radical scavenger vitamin C and analogues of vitamin E (Kagan VE, et al., 2001; Kagan VE, et al., 1998). In addition, inhibition of MPO activity in HL60 cells was associated with decreased etoposide-induced DNA strand breakage, diminished oxidative DNA damage, and reduced cleavage of the *MLL* gene known to

be associated with t-AML (Yalowich JC, et al., 2004). These results led to the idea that nutritional strategies can be utilized to minimize etoposide conversion to etoposide-O$^{\bullet}$ and to possibly prevent t-AML (Kagan VE, et al., 1999; Maellaro E, et al., 1996; Kagan VE, et al., 1994; Kagan VE, et al., 1998; Tyurina YY, et al., 1995). Because MPO may also catalyze the formation of a 2-e^- oxidation product of etoposide, the chemically reactive metabolite etoposide *ortho*-quinone (Maanen JMS, et al., 1988), we now further posit that this metabolite of etoposide may contribute to the genotoxic and leukemogenic action of etoposide. It is known that oxidative formation of 8-hydroxy-2'-deoxyguanine and endonuclease generation of apurinic sites on DNA (Chung MH, et al., 1991; Demple B, et al., 1994) can result in poisoning of Topo II and activation of DNA double strand cleavage (Kingma PS, et al., 1997; Sabourin M, et al., 2000). Hence, MPO-catalyzed oxidation of etoposide to its *ortho*-quinone may potentiate Topo II-mediated recombination events through redox-cycling mechanisms.

To test this hypothesis, it is first necessary to determine if the etoposide *ortho*-quinone is formed in myeloid lineage cells. In the present work, we demonstrate that etoposide *ortho*-quinone is produced in myeloid HL60 cells and readily forms conjugates with GSH and that these conjugates are detectable and quantifiable. Furthermore, we show that the formation of the GSH adduct depends on the MPO activity in the cells.

To further understand the mechanism of reaction with GSH in vivo, we required authentic reference metabolites, as well as an analytical method to quantify these compounds. We report the synthesis and characterization of these compounds, as well as the measurement of their metabolically generated forms in HL60 cells exposed to etoposide. The data obtained should facilitate future studies of therapy-related secondary leukemias and the assessment of the importance of MPO-catalyzed oxidative activation of etoposide in this process.

2.3 MATERIALS AND METHODS

Instruments. ^{1}H and ^{13}C NMR spectra were obtained on a Varian Mercury 400 spectrometer operating at 400 or 100 MHz using the residual proton (2.54 or 7.26 ppm) or ^{13}C (44.5 or 77.4 ppm) signals from the deuterated solvent, d_6-DMSO or $CDCl_3$, as the internal reference. Infrared spectra were recorded on a Nicolet Avatar 360 FT-IR spectrophotometer. MALDI-TOF and MALDI-TOF/TOF mass spectra were obtained using α-cyano-4-hydroxycinnamic acid as the matrix on an Applied Biosystems 4700 instrument. Synthesized compounds were purified over C_{18} columns on a Dionex Summit HPLC. LC-MS/MS analyses were performed on a ThermoFinnigan Deca XP Plus ion trap system equipped with a ThermoFinnigan Surveyor HPLC. Stable isotope dilution quantitative studies were performed by LC-MS on a ThermoFinnigan MSQ single quadrupole system. UV spectra were obtained on a Shimadzu UV160U spectrophotometer.

Chemicals. Etoposide was obtained from Polymed Therapeutics Inc. (Houston, TX). [$^{13}C_2{}^{15}N$-Gly]Glutathione was purchased from Toronto Research Chemicals, Inc. (North York, ON, Canada). Triton X-100 (*t*-octylphenoxypolyethoxyethanol) was from Bio-Rad Laboratories (Richmond, CA). Acetonitrile (HPLC grade) and sodium periodate were from Fisher Scientific. Water was deionized and distilled from $KMnO_4$. Stock solutions were stored at –20 °C. Other reagents were from Sigma Chemical Co. (St. Louis, MO) and were of the highest available quality.

Synthesis of Etoposide *ortho*-Quinone and Catechol. The target compounds were prepared by a previously reported method (Pang S, et al., 2001) with minor modifications. Etoposide (390 mg, 663 μmol) was dissolved in dioxane (7.2 mL) and H_2O (14.1 mL). $NaIO_4$ (4.2 mL of a 0.5 M aqueous solution) was added with stirring. The reaction mixture stirred in the

dark at 10 ± 4 °C for 4 h and then treated to saturation with solid $(NH_4)_2SO_4$. The resulting solution was extracted with CH_2Cl_2 (1 × 10 mL and then 5 × 5 mL). The organic phases were combined, washed with H_2O (5 × 5 mL), dried with $MgSO_4$, and filtered. After evaporation, the residue was recrystallized from CH_2Cl_2/diethyl ether. The solid was filtered, washed with diethyl ether three times, and taken to complete dryness under vacuum to give 304 mg (80%) of the product as a purple powder, which was stored protected from light; mp 200-210 °C. ^{1}H NMR ($CDCl_3$): δ4.15 (2H, m), 4.60 (1H, d, *J* = 7.7 Hz), 4.70 (1H, q, *J* = 5.0 Hz), 4.90 (1H, d, *J* = 3.4 Hz), 5.98 (2H, d, *J* = 1.0 Hz). MS (ESI) *m*/*z* calculated for $[M+H]^+$ $C_{29}H_{29}O_{13}$ (centroid), 573.5; found, 573.5.

The catechol was prepared as follows. Etoposide *ortho*-quinone (148 mg, 253 μmol) was dissolved in dioxane (2.5 mL) and H_2O (5 mL) under nitrogen and cooled to 0 °C. $NaBH_4$ (1 M in THF, 1.4 mL) was added dropwise with stirring. After 10 min, 0.6 mL of 1 M HCl was added to quench the reaction. The catechol was extracted with CH_2Cl_2 (5 × 5 mL), the combined organic extracts were washed with H_2O, dried with Mg_2SO_4, and filtered, and the solvent was evaporated. The resulting residue was crystallized with CH_2Cl_2/diethyl ether to give a white powder in 60% yield; mp 230-231 °C. ^{1}H NMR ($CDCl_3$): δ4.15 (2H, m), 4.60 (1H, d, *J* = 7.7 Hz), 4.70 (1H, q, *J* = 5.0 Hz), 5.98 (2H, d, *J* = 1.0 Hz). MS (ESI) *m*/*z* calculated for $[M + H]^+$ $C_{29}H_{31}O_{13}$ (centroid), 575.5; found, 575.5.

Synthesis of Etoposide *ortho*-Quinone-Glutathione Adduct. Etoposide *ortho*-quinone (114.5 mg, 200 μmol) was dissolved in dioxane (2.5 mL) and mixed with GSH (61.5 mg, 200 μmol) dissolved in 5 mL of H_2O. The mixture was stirred in the dark at room temperature for 4 h. The resulting solution was lyophilized to give a pale yellow powder (170 mg, 96% crude yield). Purification was conducted by HPLC over a Vydac C4 column (250 mm × 10 mm, 300 Å

pore size, 5 μm particle size) using 254 nm as the primary monitoring wavelength (4:1 H_2O/CH_3CN, flow rate of 1.5 mL/min). The HPLC analysis showed the crude product to be of 90% purity. The fractions containing the desired product were combined and lyophilized to give a white solid; mp 185-190 °C. ^{1}H NMR (d_6-DMSO): δ1.39 (3H, d, J = 5.0 Hz), 2.05 (2H, m), 2.90 (2H, m), 3.42 (1H, t, J = 7.6 Hz), 3.68 (3H, m), 3.75 (3H, s), 4.15 (2H, m), 4.30 (1H, m), 4.68 (1H, d, J = 7.6 Hz), 4.76 (1H, q, J = 5.0 Hz), 4.95 (1H, d, J = 3.4 Hz), 6.06 (2H, d, J = 1.0 Hz), 6.35 (1H, s), 6.55 (1H, s), 6.95 (1H, s), 7.03 (1H, s). ^{13}C NMR (d_6-DMSO): δ21.3, 27.7, 32.5, 42.2, 53.1, 53.9, 61.1, 63.7, 63.8, 66.1, 66.7, 67.3, 70.9, 73.4, 91.7, 99.6, 169.0, 171.4, 172.0, 172.9. IR cm^{-1} (KBr): 3293 (H-bond OH), 3056, 2925, 1725 (C=O), 1650 (C=C), 1534 (C=C). HRMS (MALDI) m/z calculated for $[M + H]^+$ $C_{38}H_{46}N_3O_{19}S$, 880.2446; found, 880.2373. MALDI-TOF-TOF-MS of the quasimolecular ion (m/z 880.3 ± 30 ppm) yielded fragment ions of m/z 805.2 $[M+H–Gly]^+$, m/z 751.2 $[M+H–Glu]^+$, m/z 674.1 $[M+H–206]^+$, and m/z 545.1 $[M+H–Glu–206]^+$.

A similar procedure was used at the 3 μmol scale for the preparation of the stable isotope-labeled [$^{13}C_2$,^{15}N-Gly]glutathione adduct of etoposide *ortho*-quinone. HRMS (positive ion MALDI) m/z calculated for $[M+H]^+$ $^{12}C_{33}{}^{13}C_2H_{46}{}^{14}N_2{}^{15}NO_{19}S$, 883.2484; found, 883.2383. MALDI-TOF/TOF-MS/MS analysis of the quasimolecular ion (m/z 883.3 ± 30 ppm) yielded fragment ions of m/z 754.2 $[M+H–Glu]^+$, m/z 677.1 $[M+H–206]^+$ and m/z 548.1 $[M+H–Glu–206]^+$.

Cell Culture. HL60 cells were cultured in phenol red-containing RPMI 1640 medium with 15% fetal bovine serum at 37 °C under a 5% CO_2, humidified atmosphere. The density of cells (in log-phase growth) at the time of experimentation was 5×10^5 cells/mL.

MPO Activity of HL60 Cells. The MPO activity of HL60 cells was determined using the guaiacol oxidation assay (Pinnix IB, et al., 1994). Cells were pelleted by centrifugation and then suspended in L1210 buffer (25 mM HEPES and 5 mM NaH_2PO_4, pH 7.4, containing 10 mM glucose, 115 mM NaCl, 5 mM KCl, and 1 mM $MgCl_2$) to a concentration of 1×10^7 cells/mL. The cell suspension was frozen at –20 °C and subsequently thawed. The lysate from 5×10^6 cells was added to a reaction mixture containing 3.75 mM 3-amino-1,2,4-triazole, 0.02% (v/v) cetyltrimethylammonium bromide, 100 μM PMSF, 0.1% (v/v) Triton X-100, 13 mM guaiacol, and 670 μM H_2O_2. The activity was monitored by changes in absorption at 470 nm (ε_{470} = 26.6 $mM^{-1}cm^{-1}$). On average, the MPO activity of cell homogenates was about 40 nmol of guaiacol oxidized /min/1×10^6 cells at 25 °C.

For suppression of MPO activity, HL60 cells were incubated for 68 h with succinylacetone (200 μM) dissolved in RPMI 1640 medium. Cell viability was determined microscopically by Trypan blue dye exclusion to be 98%, and MPO activity was determined by UV spectrophotometry as outlined above.

Western Blotting for MPO. Whole cell lysates were prepared from pelleted HL60 cells (2×10^7) and K562 cells (5×10^6) by the addition of 2× SDS-polyacrylamide gel electrophoresis sample buffer [50 mM Tris-HCL, pH 6.8, 1% (w/v) SDS, 10% (v/v) glycerol, and 0.5% (v/v) 2-mercaptoethanol], followed by boiling for 5 min and brief sonication. Protein samples of HL60 (2 μg) and of K562 (40 μg) cell lysate were resolved using 10% (w/v) SDS-polyacrylamide gel electrophoresis and then transferred to nitrocellulose. Visual inspection of Ponceau S-stained nitrocellulose membranes was used to ensure equivalent loading/transfer of the lysates. Membranes were blocked with nonfat dry milk (3% w/v) in PBS containing 0.05% (w/v) Tween 20 and then incubated with 1:40000 dilutions of primary rabbit anti-MPO antibodies kindly

provided by Dr. William Nauseef, University of Iowa School of Medicine. The secondary donkey anti-rabbit antibody used at 1:20000 dilution was purchased from Jackson Immuno-Research Laboratories (Westgrove, PA). Bound secondary antibody was detected using enhanced chemiluminescence (NEN, Boston, MA).

Treatment of HL60 Cells with Etoposide and H_2O_2. HL60 cells, with or without previous succinylacetone pretreatment, at a density of 1×10^6 cells/mL in L1210 buffer were incubated in the presence or absence of the given concentrations of etoposide (predissolved in DMSO, the final concentration of which was 0.1%) and H_2O_2 for 30 min at 37 °C in aerobic conditions in the dark. Cells were then harvested by centrifugation at 3000 rpm for 4 min, and the pellet was frozen at -80 °C. After thawing, etoposide and its derivatives were extracted with 100 μL of cold MeOH.

Determination of Glutathione Adduct in HL60 Cells Using LC-MS/MS. The extract was injected into a ThermoFinnigan Surveyor HPLC equipped with a prepacked Pico Frit C18 column (7.5 μm × 10 cm, New Objectives, Inc.) and segregated at a flow rate of 160 nL/min beginning with 19:1 H_2O-CH_3CN containing 0.1% (v/v) aqueous HCO_2H that was changed linearly over 25 min to 1:1 H_2O-CH_3CN containing 0.1% (v/v) aqueous HCO_2H. The effluent was monitored for positive ions in the *m*/*z* 400-1800 range with a ThermoFinnigan LCQ DECA XP Plus ion trap mass spectrometer fitted with a New Objectives nanoelectrospray ionization source. The spray voltage was 1.43 kV. The capillary temperature was 180 °C, and the capillary voltage was 3.3 V. Ion trap MS/MS analyses for the parent ion of the GSH adduct at *m*/*z* 880.0 were performed with 35% normalized collision energy. Data were processed with Xcalibur software.

Quantification of the Glutathione Adduct in HL60 Cells Using LC-MS. Cell extracts were treated with the synthetic etoposide *ortho*-quinone-[$^{13}C_2$,^{15}N-Gly]glutathione adduct and analyzed by LC-ESI-MS on a Thermo-Finnigan MSQ single quadrupole system. Analyses were performed in selected ion monitoring (SIM) mode with an ionization voltage of 3.2 kV and cone voltage of 60 V at a temperature of 300 K. Separation was performed using a Waters YMC ODSAQ column (2.0 mm × 150 mm) with a mobile phase of 4:1 H_2O-CH_3CN containing 0.1% (v/v) HCO_2H at a flow rate of 0.2 mL/min, giving a pressure of 2500 psi. The injection volume was 10 μL.

Statistical Analysis. The means of the GSH adduct formed between two groups (plus or minus succinylacetone treatment) were compared by Student's two-tailed *t*-test.

2.4 RESULTS

Synthesis of Metabolites. Etoposide was converted to its *ortho*-quinone and catechol in good yields (Figure 2.1) using the published methods of periodate oxidative demethylation and subsequent borohydride reduction (Pang S, et al., 2001). When the *ortho*-quinone was mixed with GSH in aqueous medium, the conjugate addition product (adduct) formed directly and in high yield without need for a transferase enzyme (Figure 2.1). These standard compounds were characterized spectroscopically, and their HPLC retention characteristics were examined. Analysis of the synthesized GSH adduct by MALDI-TOF-MS showed the *m*/*z* of the all-^{12}C form of the protonated GSH adduct $[M+H]^+$ to be 880.2373, 8 ppm from the calculated exact mass of the structure shown in Figure 2.1. The structure was further confirmed by using MALDI-TOF/TOF-MS/MS analysis (Figure 2.2). Structures of the fragment ions were reasonably

assigned. For example, the fragment ion at *m*/*z* 754.2 confirmed the presence of the glutamate moiety, and the fragment ion at *m*/*z* 677.1 confirmed the sugar moiety on the etoposide portion of the structure.

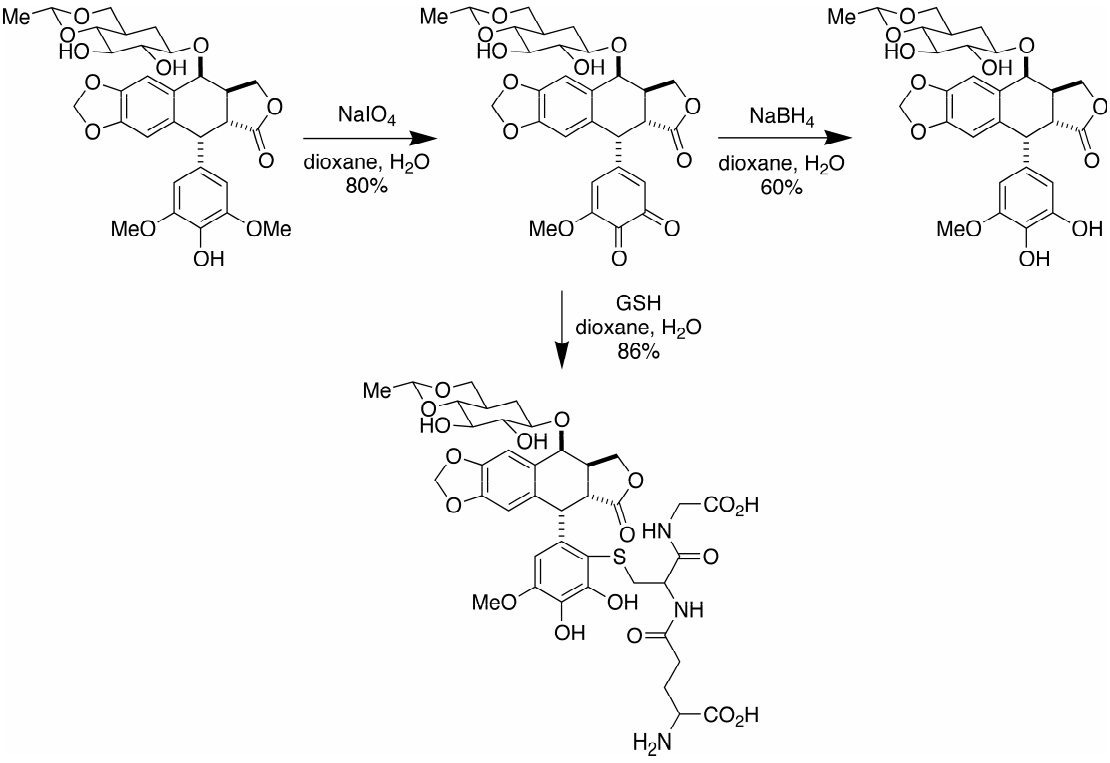

Figure 2.1 Synthesis of etoposide metabolites.

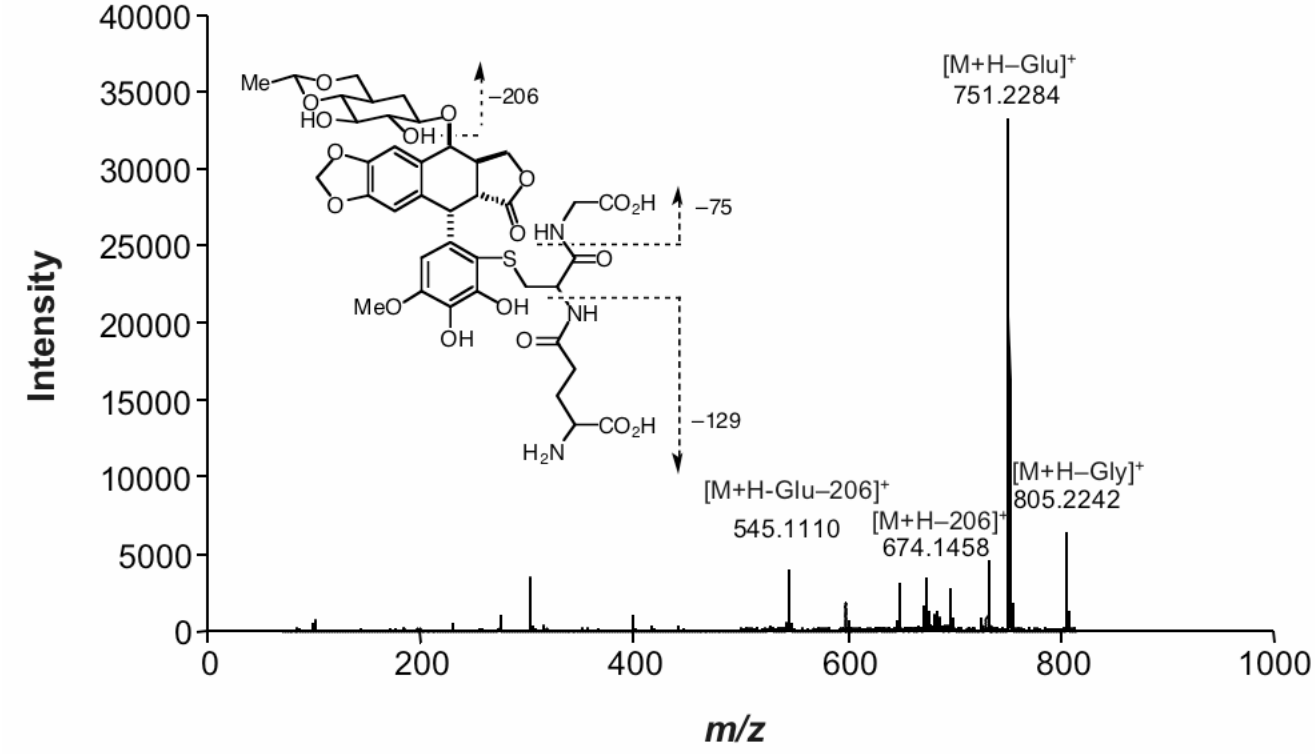

Figure 2.2 MALDI-TOF/TOF-MS/MS fragmentation spectrum of the $[M+H]^+$ ion (*m/z* 880) of synthetic etoposide *ortho*-quinone-glutathione adduct.

Determination of the Etoposide *ortho*-Quinone-GSH Adduct in HL60 Cells Using LC-MS/MS. HL60 cells were found to produce the GSH adduct of etoposide *ortho*-quinone. The adduct was detected by nanoelectrospray LC-ion trap-MS and -MS/MS. As shown in Figure 2.3, extracts of HL60 cells treated with 25 μM etoposide and 100 μM H_2O_2 showed a peak with a retention time of 16.4 min as detected at *m*/*z* 880.3, consistent with the $[M+H]^+$ ion of the etoposide *ortho*-quinone GSH adduct and with the synthetic material. At the same time, another known etoposide metabolite, its catechol, was also detected in these extracts of the HL60 cells at

a retention time of 17.7 min. The $[M+H]^+$ ion of the catechol was at *m*/*z* 575.2, which, along with the retention time, was consistent with the synthetic material. The structure of the GSH conjugate was confirmed by ion trap MS/MS by exciting the *m*/*z* 880.3 ion (Figure 2.4). The product ion spectrum showed production of diagnostic ions common to previously reported GSH adducts, including an abundant y2 ion at *m*/*z* 750.9 and a moderately abundant b2 ion at *m*/*z* 804.95 as expected for the structure depicted in Figure 2.4. Although the most abundant product ions were due to fragmentation within the GSH moiety, some product ions yielded information regarding the linkage between etoposide *ortho*-quinone and GSH. For example, the product ion at *m*/*z* 544.95 corresponds to $[M+H–Glu–206]^+$ and the fragment ion at *m*/*z* 674.0 corresponds to $[M+H–206]^+$. The results were similar to the product ions of the synthetic GSH adduct observed by using MALDI-TOF-TOF (Figure 2.2). The product ion of *m*/*z* 604.98 was derived from the cleavage of the thioether moiety. Loss of water produced the fragment ions of *m*/*z* 862.23 $[M+H–H_2O]^+$, *m*/*z* 733.87 $[M+H–Glu–H_2O]^+$, *m*/*z* 527.79 $[M+H–Glu–206–H_2O]^+$. The product ion of *m*/*z* 692.10 was the C2 ion derived from the product ion, which lost a glutamate moiety, and *m*/*z* 647.97 was the a2 ion derived from $[M+H–Glu]^+$.

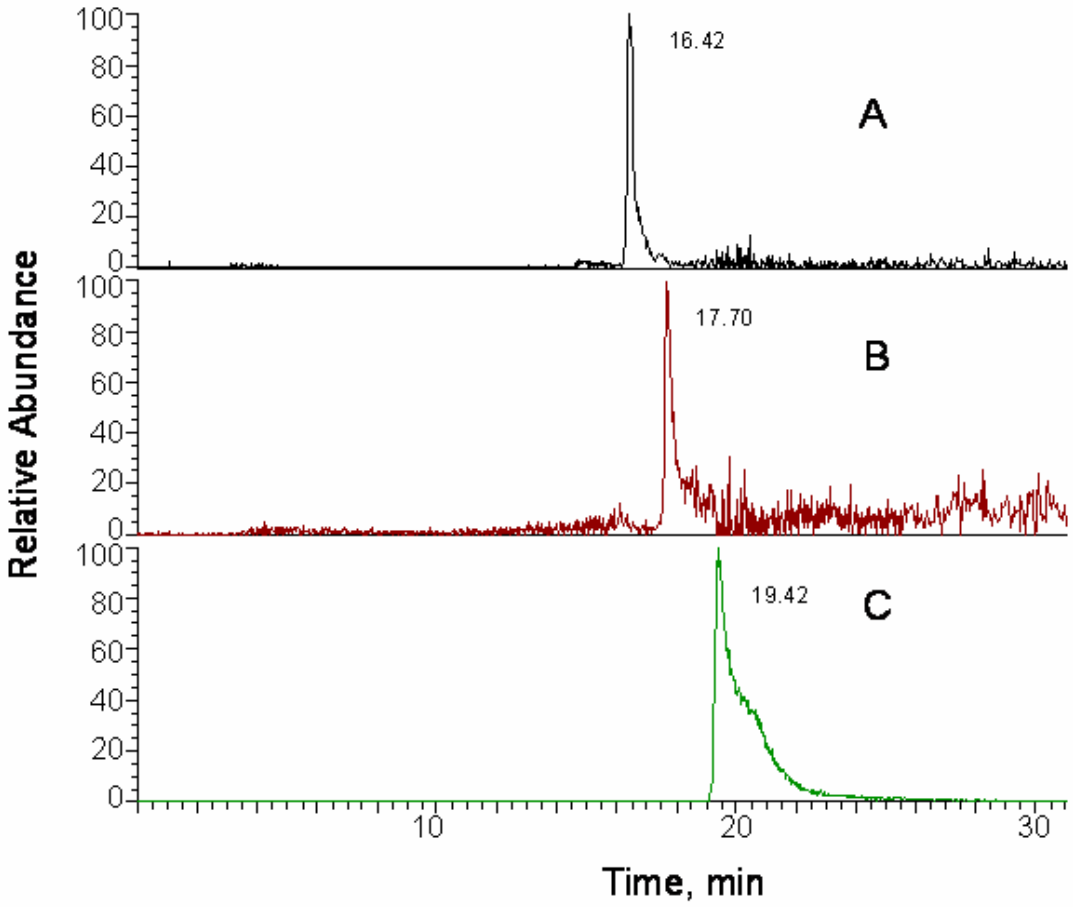

Figure 2.3 LC-ESI-ion trap MS analysis (positive ion, *m/z* 400-1800) of the etoposide *ortho*-quinone-GSH adduct formed in HL60 cells when treated with etoposide and H_2O_2 at 37ºC for 0.5h. (A) Extrated ion chromatogram showing the retention time of the adduct (*m/z* 880).(B) Extracted ion chromatogram showing the retention time of etoposide catechol (*m/z* 575). (c) Extracted ion chromatogram showing the retention time of etoposide (*m/z* 589).

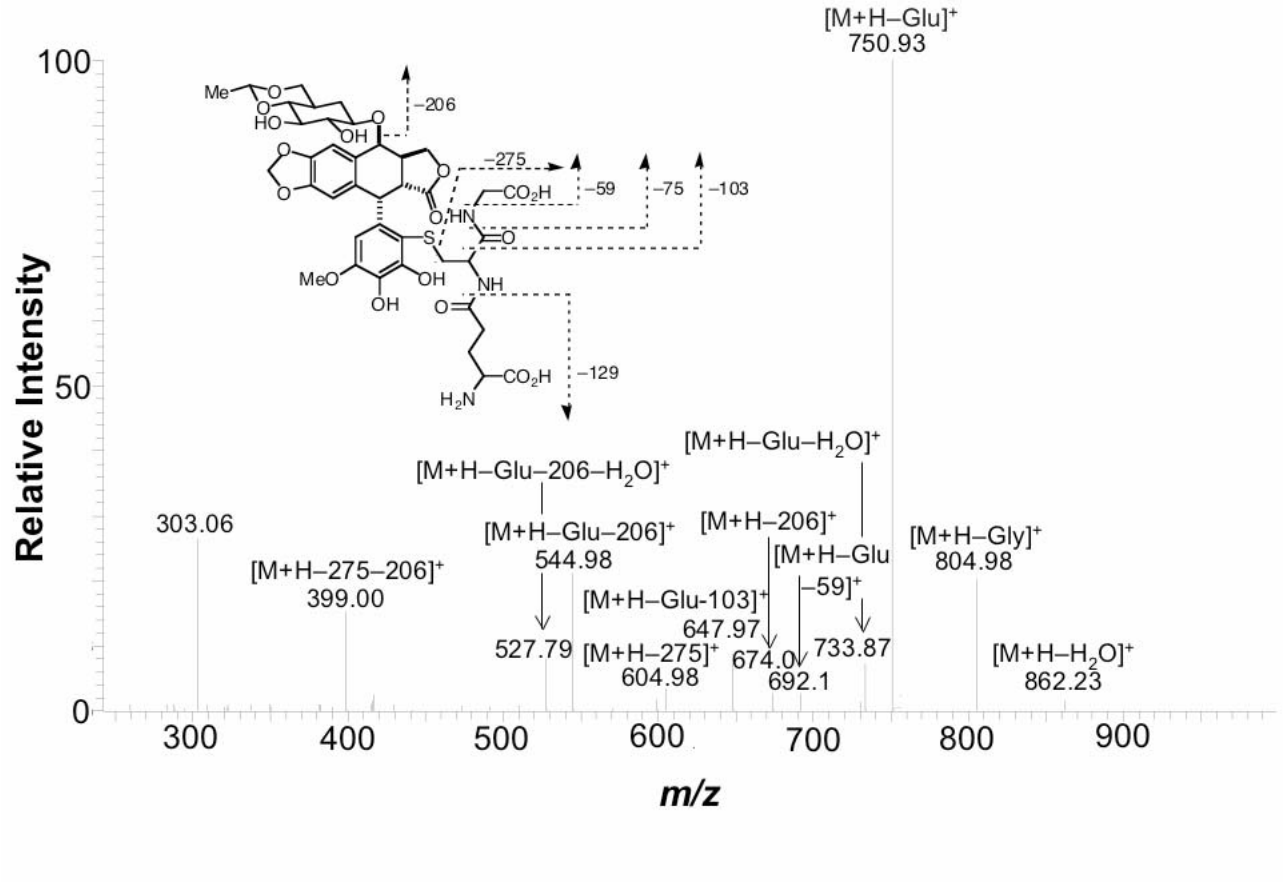

Figure 2.4 LC-ESI-ion trap MS/MS fragment ion spectrum of the $[M+H]^+$ precursor ion (*m/z* 880) of the etoposide *ortho*-*quinone*-GSH adduct formed in HL60 cells.

MPO Activity and Protein Levels. As shown in Figure 2.5, the activity of MPO significantly decreased when HL60 cells were pretreated for 68 h with the heme synthesis inhibitor succinylacetone (Nonaka T, et al., 1992). As expected, succinylacetone did not prevent production of the pre/pro forms of MPO in the HL60 cells but rather that of mature, heme-containing MPO protein (Figure 2.6). Human leukemia K562 cells, which do not produce mature MPO protein, were used as a comparative negative blotting control.

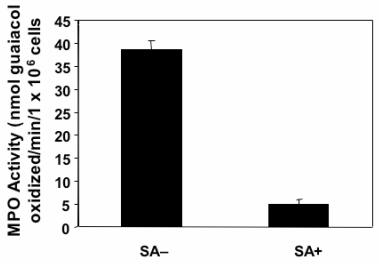

Figure 2.1 Significant difference in the myeloperoxidase (MPO) activity in HL60 cells without (SA–) or with (SA+) (P<0.05, N=7).

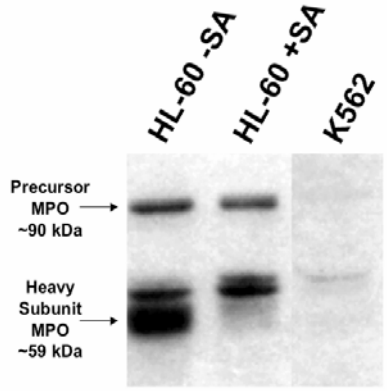

Figure 2.2 Western blot analysis of myeloperoxidase (MPO) protein levels in HL60 cells without (–SA) or with (+SA).

MPO and Etoposide Dependency in the Production of the GSH Conjugate. HL60 cells, with and without the 68 h pretreatment with succinylacetone to reduce the MPO level, were incubated with a range of etoposide concentrations. For quantification of the GSH adduct, we used a single quadrupole LC-MS system, the stable isotope-labeled form of the adduct as an internal standard, and selected ion monitoring. As can be seen in the chromatograms shown in Figure 2.7, no adduct formed in the absence of etoposide. When the HL60 cells were treated with 25 μM etoposide, a small peak appeared at 7.0 min. The *m*/*z* signal and retention time of this analyte correlated exactly with that of the synthetic GSH adduct of etoposide *ortho*-quinone. The synthetic, stable isotope-labeled [$^{13}C_2{}^{15}$N-Gly] form of the adduct (200 pmol/sample) was added after the cell lysis step as an internal standard for isotope dilution quantitative studies. The amount of etoposide *ortho*-quinone-GSH conjugate from cells treated with 25 μM etoposide was dramatically increased by adding 100 μM H_2O_2, an MPO cosubstrate. This increase indicated that the endogenous concentration of H_2O_2 in the cells was low (likely because of catalase) and it was necessary to add more H_2O_2 to increase the rate and extent of the reaction. As shown in Figure 2.8, the GSH adduct formed in HL60 cells with succinylacetone pretreatment (for 25 μM treatment, $n = 8$) was significantly decreased as compared with the group without succinylacetone pretreatment ($p < 0.001$). These results indicated that the generation of the etoposide *ortho*-quinone conjugate with GSH depended on the level of mature and catalytically active MPO in HL60 cells.

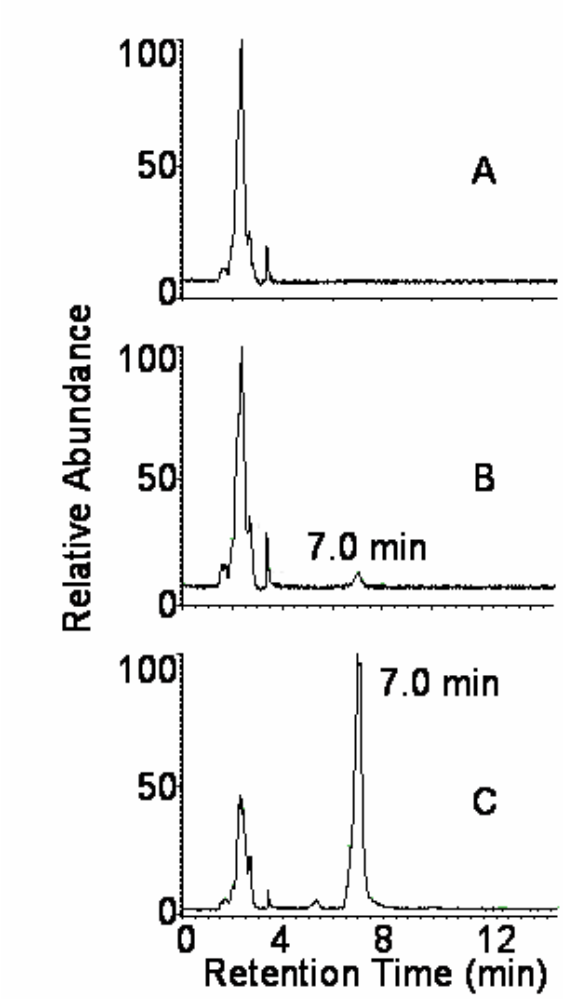

Figure 2.7 Total ion chromatograms from LC-ESI-quadrupole MS analyses of methanolic extracts of HL60 cells treated with etoposide and/or H_2O_2 at 37ºC for 0.5h. (A) Control HL60 cells (no etoposide, no H_2O_2). (B) HL60 cells treated with 25μM etoposide (no H_2O_2)-note the formation of the quinine-glutathione adduct at a retention time of 7min. (C) HL60 cells treated with 25μM etoposide and 100μM H_2O_2–note the markedly increased level of the adduct at 7 min.

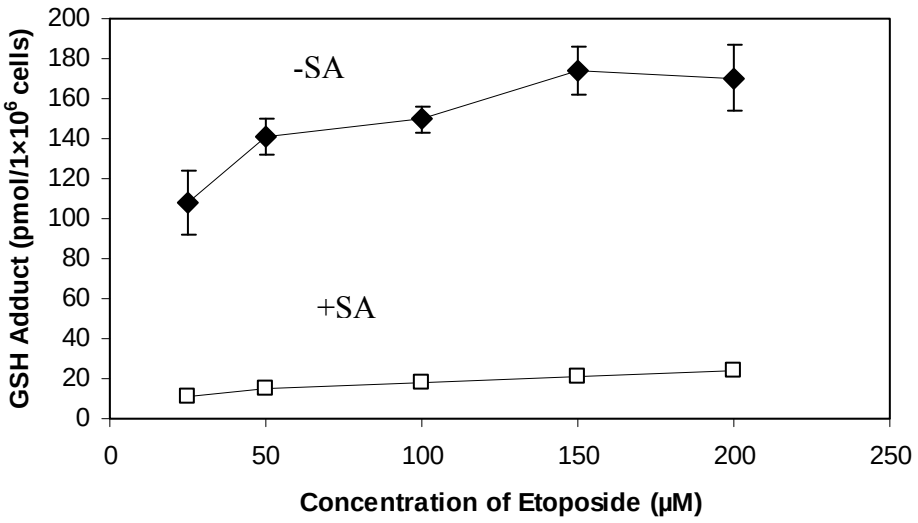

Figure 2.8 The formation of etoposide *ortho*-quinone-glutathione adduct in HL60 cells pretreated with (open squares) or without (closed diamonds) succinylacetone (SA) (P<0.001; for the 25μM treatment, N=8; for other concentration, N=3).

Also shown in Figure 2.8 are the concentration dependency profiles of the GSH adduct formation for the two groups (with and without succinylacetone pretreatment). Succinylacetone pretreatment blocked *ortho*-quinone formation at all concentrations of etoposide studied by 90% or more. This result confirmed the conclusion that the formation of the GSH adduct depends on the level of MPO in intact HL60 cells.

2.5 DISCUSSION

The results presented here demonstrate that etoposide undergoes MPO-catalyzed metabolic activation in HL60 cells to form etoposide *ortho*-quinone, which binds to GSH covalently. MPO-rich HL60 cells were utilized as a convenient cellular surrogate for the myeloid progenitor CD34+ cell population that expresses MPO (Strobl H ,*et al*., 1993) and is the likely

origin for the myeloid leukemias induced by etoposide (Libura J, *et al*., 2005). We hypothesize that the genotoxic and carcinogenic effects of etoposide occur in myeloid progenitor CD34+ cells due to MPO-catalyzed oxidation of etoposide to its *ortho*-quinone. Hence, etoposide may cause myeloid but not other leukemia types because its quinone, formed due to MPO, induces greater Topo II-mediated DNA cleavage and therefore recombination events than does unmetabolized etoposide (Felix CA, 1998; Felix CA, 2001; Gantchev TG, *et al*., 1998; Lovett BD, *et al*., 2001).

The etoposide *ortho*-quinone GSH adduct formed in HL60 cells was isolated, and its structure was verified by comparison of its mass spectral and chromatographic properties to those of synthetically prepared material. The level of the GSH adduct in HL60 cells, and by direct inference the MPO-mediated formation of the quinone, was substantially blocked by decreasing the levels of mature MPO after pretreatment with the heme synthesis inhibitor succinylacetone. MPO-catalyzed production of this etoposide metabolite was further established because addition of hydrogen peroxide, the necessary cosubstrate for MPO activity, bolstered production of the *ortho*-quinone. Finally, MPO appears to be the primary determinant of etoposide oxidative metabolism because the cytochromes P450 known to cause etoposide oxidations are not expressed appreciably in the undifferentiated HL60 cells used in this present work (Yu LJ, *et al*., 2001) nor in myeloid CD34+ precursors (Soucék P, *et al*., 2005). GSH, the most abundant intracellular nonprotein thiol, can react nonenzymatically and/or via catalytic assistance of gluthione *S*-transferase with electrophiles and free radicals. Etoposide *ortho*-quinone was found to react nonenzymatically with GSH in vitro to give the conjugate addition product. It is unknown at present if glutathione-*S*-transferase catalyzes this reaction in HL60 cells. Previous *in vitro* work (Gantchev TG, *et al*., 1998) demonstrates that GSH prevents

trapping of Topo II/DNA cleavable complexes by etoposide *ortho*-quinone, suggesting (to those authors) that the covalent adduct of etoposide *ortho*-quinone with GSH is inactive. It is not known, however, if the etoposide *ortho*-quinone-GSH adduct can act as a Topo II poison in a cellular context, which will be the subject of future studies.

Previous work has shown that etoposide undergoes 1-e^- oxidation to form its phenoxyl radical, which can be reduced by GSH (Kagan VE, et al., 1999). In the present study, we provide conclusive evidence that etoposide *ortho*-quinone, a 2-e^- oxidation product, is generated by MPO in intact, undifferentiated HL60 cells through detection of its conjugate with GSH. It is unclear at present if the quinone is formed by two MPO-mediated 1-e^- oxidation steps or by disproportionation of the 1-e^- oxidation product, etoposide-$O^{\bullet}$. Etoposide *ortho*-quinone has been suggested to be responsible in part for the cyto- and genotoxic effects of etoposide due to its ability to poison Topo II and stabilize Topo II/DNA covalent complexes *in vitro* (Gantchev TG, *et al*., 1998; Lovett BD, *et al*., 2001). As a quinone, it could conceivably also participate in redox cycling to generate reactive oxygen species, leading to an increase in oxidative DNA damage and an enhancement of recombination events linked to Topo II poisoning (Kingma PS, *et al*., 1997).

Results from the present work indicate that a concentration of etoposide as low as 25 μM is sufficient to trigger MPO-catalyzed oxidation to the *ortho*-quinone and yield detectable levels of its GSH adduct. This concentration of etoposide is well within the range attainable in plasma during commonly used regimens of chemotherapy and much below the plasma concentration of etoposide during a high-dose etoposide chemotherapy regimen (Nguyen L, *et al*., 1998; Rick O, *et al*., 1998).

Our results indicate that in the presence of exogenously added H_2O_2 the adduct concentrates in HL60 cells. Incubations with HL60 cells (1×10^6 cells/mL) were performed using etoposide (25-200 μM) in a final volume of 1 mL (25-200 nmol/1×10^6 cells). Under these conditions, conversion of 25 μM etoposide to the GSH adduct ranged from ~0.11-0.18 nmol/1×10^6 cells, a maximal conversion of 0.4%. Although this represents a small conversion of total drug, our results indicate that the etoposide *ortho*-quinone-GSH adduct concentrated within cells. For example, at 25 μM extracellular etoposide, the intracellular etoposide *ortho*-quinone-GSH adduct concentration was found to be 170 μM. At higher etoposide concentrations, there was an increase in GSH adduct formation that plateaued at a concentration of 275 μM, suggesting saturation of MPO-catalyzed oxidative activation of etoposide and subsequent steady state formation of the *ortho*-quinone metabolite.

Measurement of reduced GSH within HL60 cells using an established technique (Kagan VE, *et al*., 2001) yielded a level of 2.9 nmol/1×10^6 cells. Using the intracellular water content for HL60 cells of 0.6 μL/1×10^6 cells (Karasavvas N, *et al*., 2005), the GSH concentration was estimated to be 4.8 mM. Because the maximal consumption of GSH based on formation of the etoposide *ortho*-quinone-GSH adduct is ~275 μM, there is very little depletion of the overall intracellular antioxidant reserve within cells by GSH conjugation to etoposide metabolites. It is more likely that oxidative stress caused by MPO-catalyzed oxidative activation of etoposide (Kagan VE, *et al*, 2001) is related to redox cycling of etoposide-O$^{\bullet}$ and/or to cycling by etoposide *ortho*-quinone itself rather than by adduct-induced GSH depletion.

In conclusion, the data presented demonstrate that etoposide *ortho*-quinone generated by MPO-catalyzed oxidation of etoposide can be captured by GSH in intact HL60 cells to give a mass spectrometrically detectable and quantifiable adduct. The ability to detect, characterize, and

quantify the GSH adduct in intact HL60 cells is important for future investigations of the mechanism(s) of etoposide-associated secondary leukemias and for estimating the risk of treatment-related secondary leukemias. Using myeloid progenitor CD34+ cells, future studies will be directed toward a better understanding of the role of etoposide metabolites in the myeloid leukemogenic process frequently associated with the clinical use of this antineoplastic agent.

2.6 ACKNOWLEDGMENT

This research was supported by grants from the NIH (R01 CA090787) and the TATRC/DoD (USAMRAA Prime Award W81XWH-05-2-0066). We thank Prof. Ian Blair for several very useful communications, Prof. Samuel Poloyac for allowing use of his LC-MS instrument, and Prof. Valerian Kagan for his continued enthusiasm for this line of research.

3.0 METABOLISM OF (+)-DISCODERMOLIDE IN POOLED HUMAN LIVER MICROSOMES

3.1 INTRODUCTION

(+)-Discodermolide (Figure 3.1) is a natural product originally isolated from a marine sponge, *Discodermia dissoluta* (Gunaskekera *et al*., 1990).

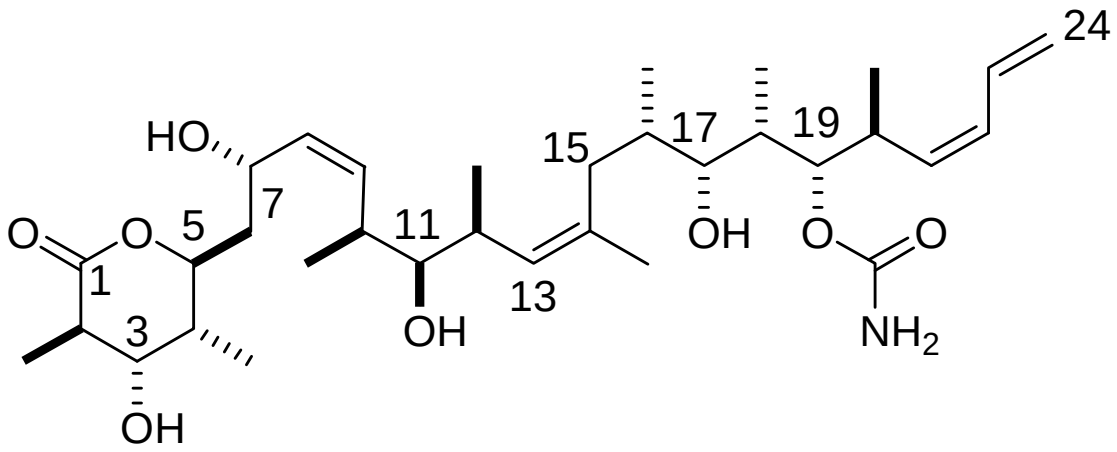

Figure 3.1 The chemical structure of (+)-discodermolide.

It was first introduced as an immunosuppressive agent (Longley *et al*., 1993), but then its mechanism of action was found to actually be potent microtubule stabilization (ter Haar *et al*.,

1996; Kowalski *et al*., 1997). Unlike paclitaxel, a microtubule-stabilizing anticancer drug on the market, discodermolide is not a substrate for the P-glycoprotein efflux pump (Kowalski et al., 1997). Discodermolide retains its antiproliferative potency againts β-tubulin mutant cells, unlike the epothilones (He et al., 2001). Although they compete for binding to microtubules, when discodermolide and paclitaxel are combined, there is a significant increase in antiproliferative activity against both cell lines and xenografts in mice (Huang et al., 2006). The potency and novel structure of (+)-discodermolide make it a promising candidate for clinical development as an anticancer drug.

Over the late 1990's and early 2000's, Novartis Corp. developed discodermolide to the stage of Phase II clinical trials in humans. Abruptly in late 2004, the company announced the withdrawal of the agent from development, without explanation (Novartis, 2004). It is suspected that undue toxicities were noted during dose escalation, but no official or scientific report has emerged to explain this action. Interestingly, only some scant pharmacokinetic data and no metabolic studies of discodermolide have been reported (Mani, et al., 2004). The numerous allylic positions, pendant methyl groups and double bonds in the molecule led to the hypothesis that the compound is extensively metabolized by cytochromes P450, The present studies were then undertaken to address this hypothesis, to provide information on the metabolic stability of discodermolide and to begin to determine structures of metabolites from human liver microsomes.

3.2 MATERIALS AND METHODS

Chemicals. Discodermolide was synthesized by Novartis Corp. and provided as a gift by Drs. Kenneth Bair and Fred Kinder. HPLC grade acetonitrile and water were purchased from Burdick & Jackson (Muskegon, MI). All other chemicals were purchased from Sigma-Aldrich (St.Louis, MO).

Human Liver Microsomes. Pooled human liver microsomes were purchased from BD Gentest (Woburn, MA). The cytochrome P450 content was 0.33 nmol/mg of protein.

Microsomal Incubations. A typical incubation mixture (0.5 mL) contained 0.1 mg/mL of microsomal protein, 10 μM discodermolide and 1 mM NADPH in 100 mM phosphate buffer, pH 7.4. The incubation was carried out for 15 min at 37 ºC and stopped by addition of 0.5 mL of cold acetonitrile to precipitate proteins. Samples were centrifuged and the supernatant was evaporated on a SpeedVac. Controls were the incubation without NADPH. (+)-Discodermolide was incubated at a concentration of 10 μM with pooled human liver microsomes for 0, 15, 30 and 60 min to determine the time period that gave rise to the maximum number of metabolites. Although some increase in metabolite concentrations was observed at the latter two time points, the 15 min incubation time gave rise to the same number of metabolites in the same relative abundances and was therefore chosen for detailed analyses.

LC-MS Analysis. Reverse phase HPLC separations were carried out using a prepacked Pico Frit C18 column. The mobile phase consisted of 0.1% formic acid in water (solvent A) and 0.1% formic acid in acetonitrile (solvent B). The elution program was as follows: isocratic at

23% B for 5 min, linear gradient from 23% to 70% B over 10 min, isocratic at 70% B for 10 min, linear gradient from 70% to 95% B over 1 min, isocratic at 95% B for 4 min. The flow rate was 160 nL/min. The column effluent was fed into a Thermo Finnigan LCQ Deca XP Plus mass spectrometer equipped with a nanoelectrospray source. Spray voltage was set at 1.43 kV, capillary temperature at 180 ºC and capillary voltage at 40 V. The normalized collision energy used was 35%. Accurate mass analyses were performed on an ABI QSTAR Elite Qq-TOF system equipped with a Nanospray II source. The ionspray voltage was 2.5 kV and the ion source temperature was 120 ºC. The Qq-TOF was tuned to 13,000 resolution at half maximum. Reserpine ($[M+H]^+$ at *m/z* 609.2812) was used as the autocalibration mass. The obtained mass accuracy of metabolites was $\pm$ 10 ppm.

3.3 RESULTS

Identification of Metabolites. At least eight metabolites of discodermolide were detected by LC-MS analysis after incubation of the compound with pooled human liver microsomes. The chromatogram of metabolites and discodermolide is shown in Figure 3.2A. The chromatogram of control sample is shown in Figure 3.2B.

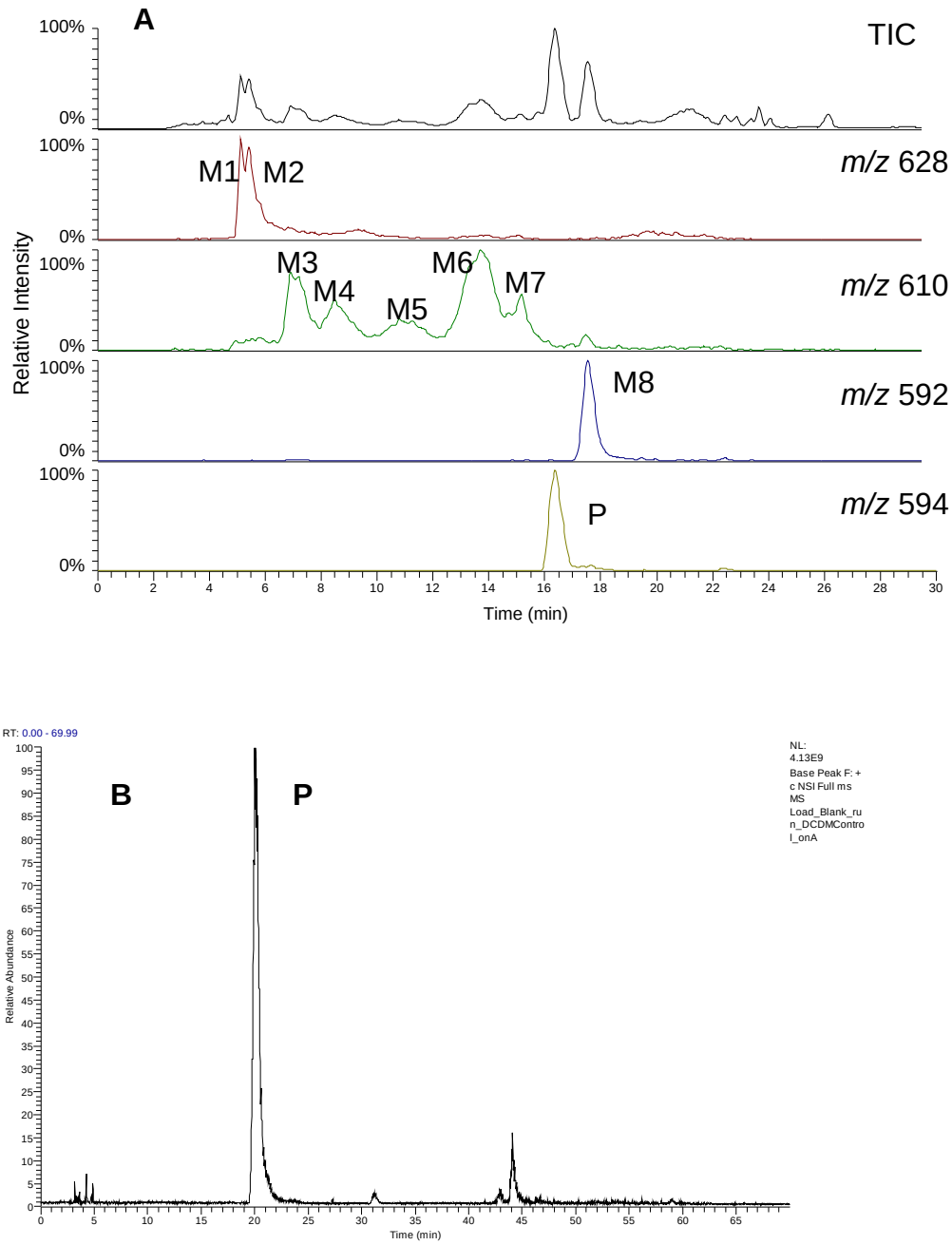

Figure 3.1 (A) Positive ion LC-MS/MS total ion chromatogram and extracted ion chromatograms of 10 μM (+)-discodermolide and its metabolites after incubation with pooled human liver microsomes for 15min with NADPH. (B) The total ion chromatogram of the control incubation (without NADPH).

The metabolites were characterized by comparing their product ion spectra to that of the corresponding parent drug. Typical fragmentation patterns of discodermolide showed cleavage at i) the C-C bond adjacent to the C11-hydroxyl group (C10-C11) to give the fragments at *m/z* 352, *m/z* 334 ($-H_2O$) and *m/z* 225 ($-H_2O$), and ii) the C-C bond adjacent to the 17-hydroxyl group (C17-C18) to give the fragments at *m/z* 411 and 393 ($-H_2O$) (Table 3.1 and Figure 3.3A). The ion of *m/z* 393 fragmented further in MS^3 spectrum (Fig. 3.3B) by cleavage of C-C bond near 7-hydroxyl group (C7-C8) to form the *m/z* 171 ion. The lactone ring of the ion of *m/z* 393 was fragmented in MS^3 experiments by cleavage of C1-O bond and C4-C5 bond to form the *m/z* 279 ion, and/or by cleavage of C1-O bond and C3-C4 bond following by loss of water to form the *m/z* 291 ion. These two fragments in the MS^3 experiments proved important in the identification of the structures of metabolites. The proposed fragmentation pattern is shown in Figure 3.4.

Table 3.1 Results of LC-MS/MS analysis of the metabolites of (+)-discodermolide.

Metabolite	***m/z***	**Major Fragment Ions in MS^2 Spectra, *m/z***
Discodermolide	594	393, 334
M1	628	610, 592, 567, 549, 531, 513, 411, 393, 385, 368, 225
M2	628	610, 592, 567, 549, 531, 513, 411, 393, 385, 368, 225
M3	610	592, 574, 549, 409, 391, 368, 350, 337, 307,289, 271, 225
M4	610	592, 574, 549, 531, 513, 409, 391, 350, 337, 322 ,289, 261
M5	610	592, 574, 549, 531, 513, 495, 409, 391, 350, 337, 307,289
M6	610	592, 574, 549, 531, 513, 495, 393, 350, 337, 307,289
M7	610	592, 574, 549, 531, 513, 409, 350, 307,289
M8	592	391, 334

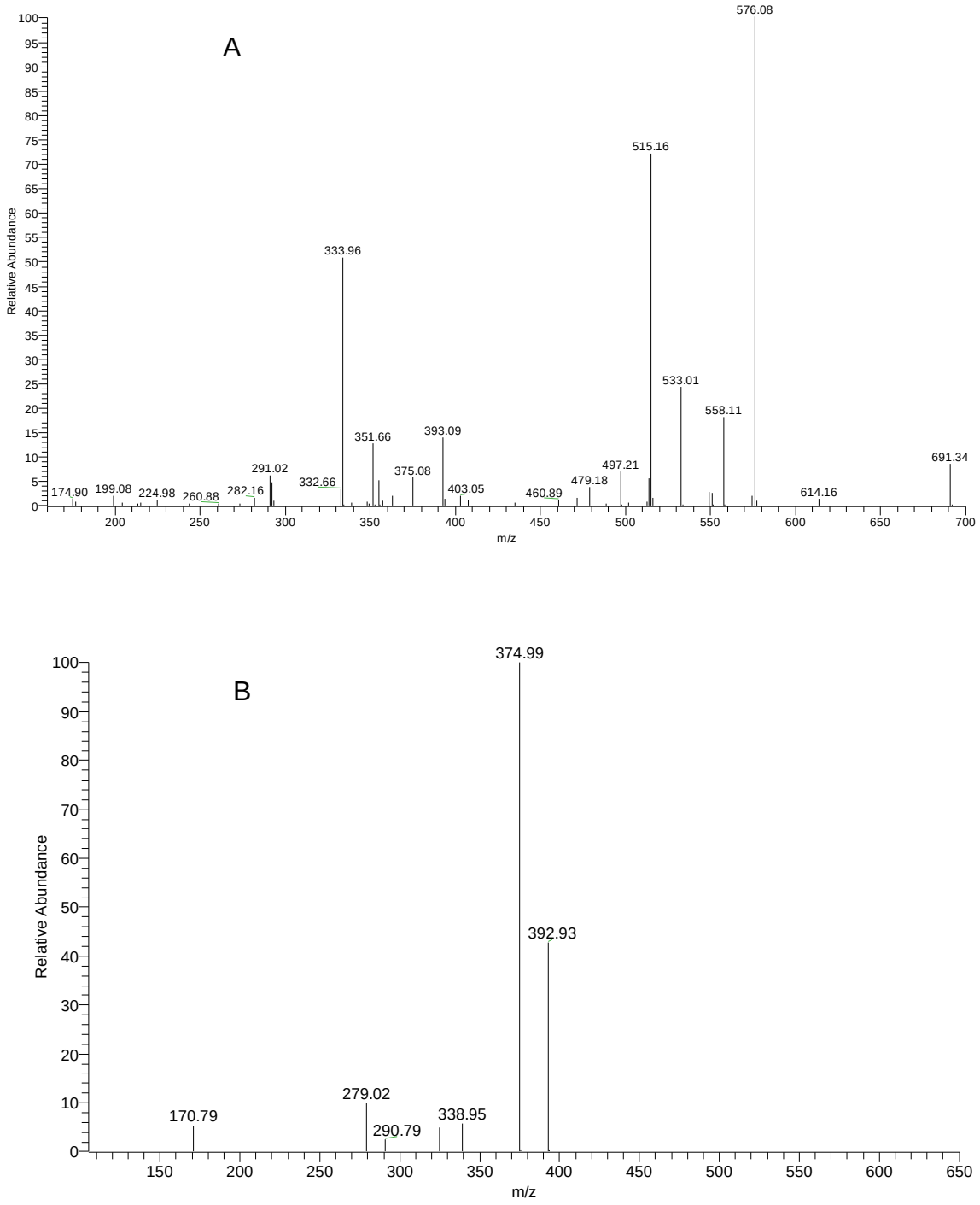

Figure 3.2 Ion trap MS^2 (A) and MS^3 (*m/z* 594→*m/z* 393) (B) product ion spectra of discodermolide.

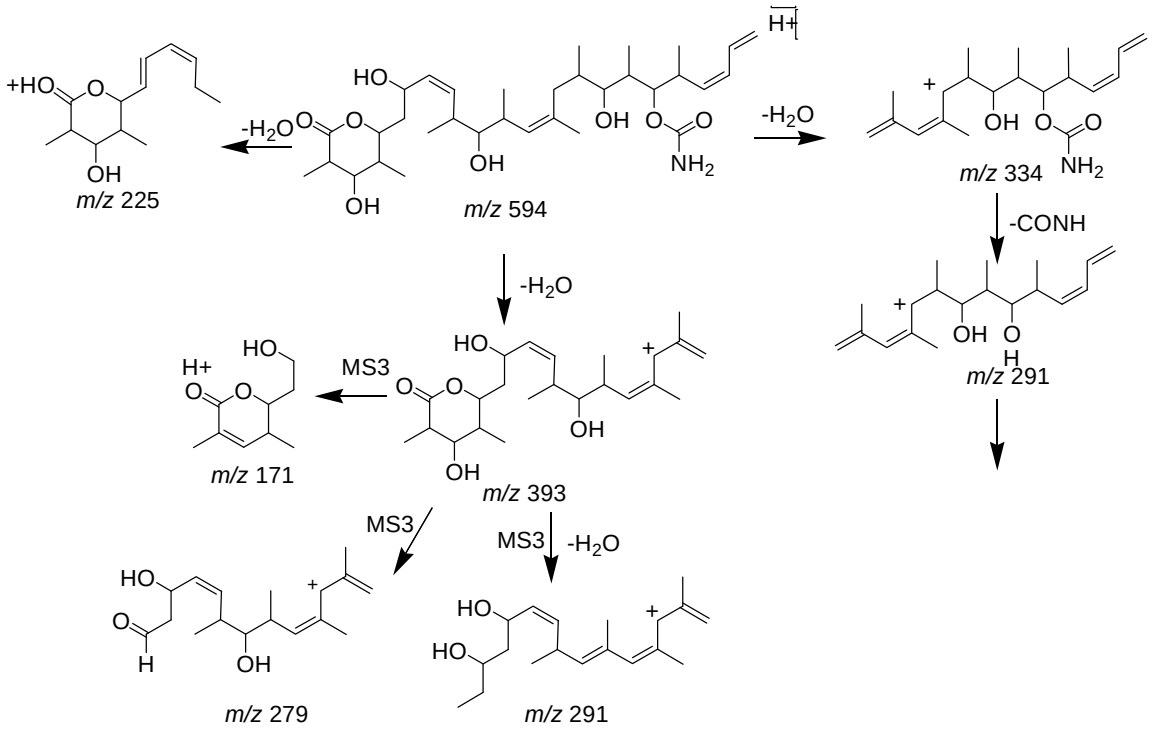

Figure 3.3 Tandem mass spectrometry fragmentation pathways of the $[M+H]^+$ ion of discodermolide.

Metabolite M8. Metabolite M8 produced a protonated molecular ion at *m/z* 592.3848, which corresponded to a net loss of two hydrogen atoms from discodermolide. This biotransformation may be the direct dehydrogenation or the monooxidation followed by a loss of water molecule. In addition, the retention time of M8 was longer than that of the parent compound, indicating that M8 was of lower polarity. The MS^2 product ion spectrum of M8 contained abundant ions of *m/z* 391 and *m/z* 334 (Figure 3.5A), which suggested that the right (carbamate-containing) side and middle portion of the molecule were unchanged, and that dehydrogenation took place on the left (delta lactone-containing) side. In contrast to parent drug, the cleavage of the C1-O bond and C4-C5 bond was not observed in the MS^3 spectrum of the *m/z* 391 ion (Figure 3.5B), but cleavage of C1-O and C3-C4 were detected. The cleavage of C1-O and C3-C4 followed by a loss of water formed the ion at *m/z* 271 in this MS^3 spectrum, indicating that the dehydrogenation might have occurred at C4-C5. Loss of two water molecules was relatively facile from the *m/z* 391 ion (in the related MS^3 spectrum of discodermolide, only one of the hydroxyl groups was eliminated through loss of water). This suggested the presence of double bond at C4-C5 so that loss of an additional water molecule from the 7-hydroxy group would form a conjugated system that would delocalize and stabilize the positive charge on the *m/z* 271 ion. Another important diagnostic fragment was recorded at *m/z* 169 with high abundance compared with the fragment at *m/z* 171 from discodermolide product ion at *m/z* 393 in MS^3 spectrum. It is proposed that the *m/z* 169 ion originated from homolytic cleavage of the C7-C8 bond followed by loss of water and stabilization by the resulting conjugated system (Figure 3.6). Based on these considerations, M8 was assigned as C4-C5 dehydrodiscodermolide.

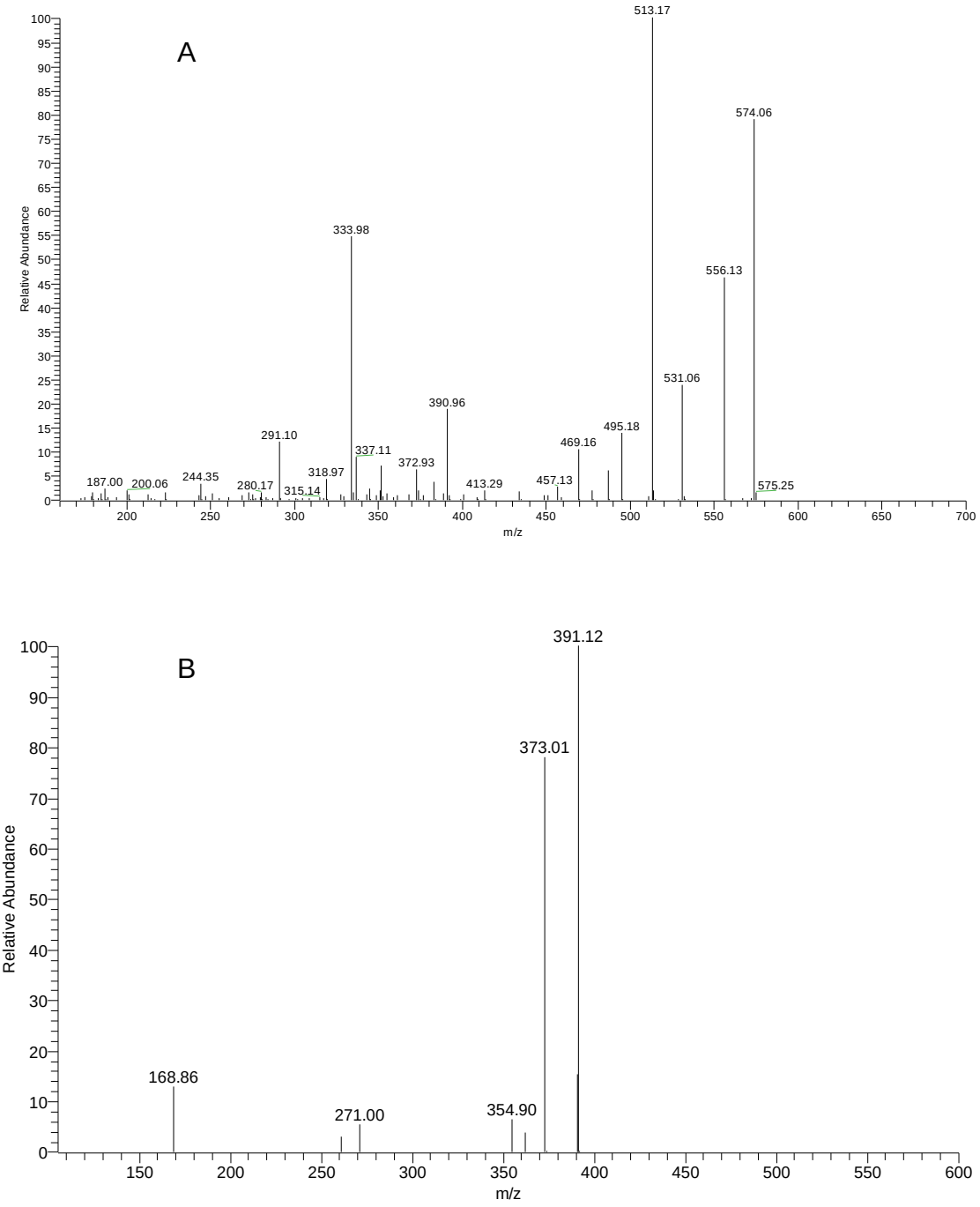

Figure 3.4 Ion trap MS^2 (A) and MS^3 (*m/z* 592→*m/z* 391) (B) product ion spectra of metabolite 8 (M8).

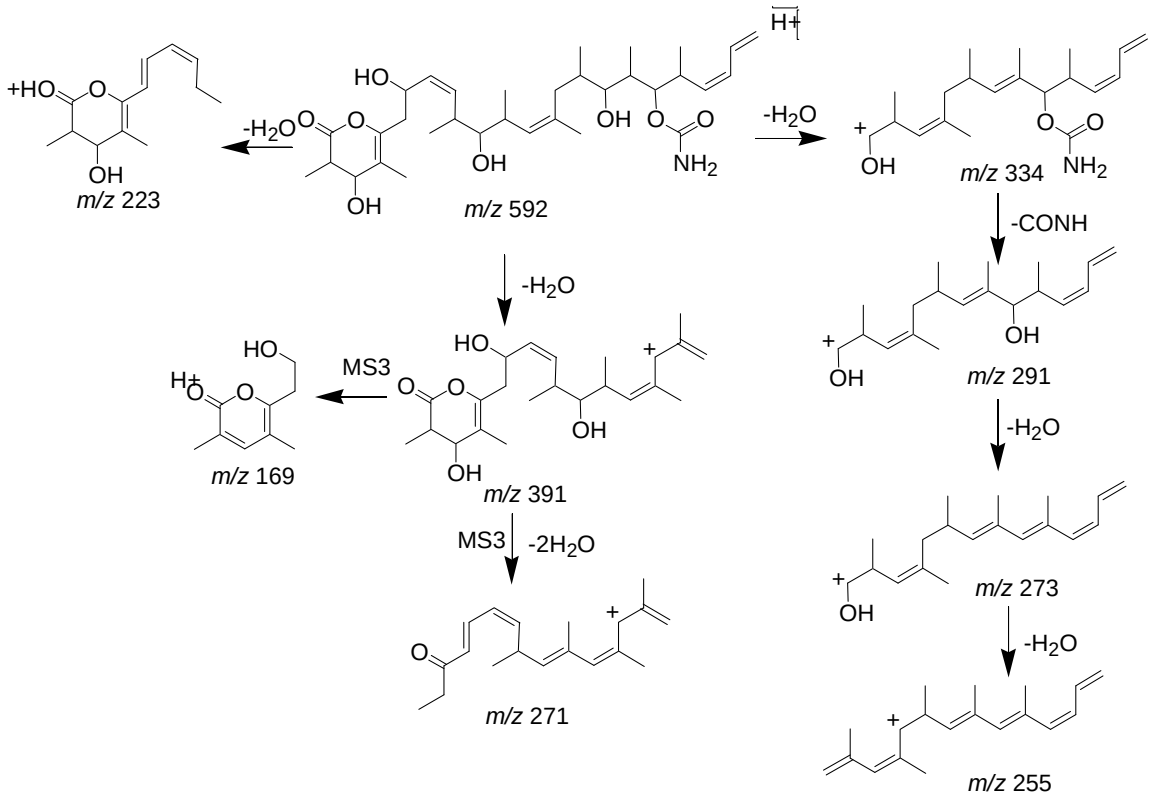

Figure 3.5 Tandem mass spectrometry fragmentation pathways of the $[M+H]^+$ ion of M8.

Metabolite M1. Metabolite M1 yielded an $[M+H]^+$ ion at *m/z* 628. The observed accurate mass for M1 was *m/z* 628.4010, which corresponded to a product of monooxygenation plus hydrolysis with an elemental composition of $C_{33}H_{57}NO_{10}$. M1 yielded fragmentation patterns similar to those of the parent compound , The fragmentogram is shown in Figure 3.7A. The cleavage occurred at the C10-C11 and C17-C18 bonds. These fragment ions were detected at *m/z* 368 and *m/z* 393, which suggested that oxidation took place on the right side of the molecule instead of left side and in the middle (proposed fragmentation patterns are shown in Figure 3.8). Metabolite M1 also yielded a fragment ion at *m/z* 549, which correspond to the loss of two H_2O and one CONH (549 = 628–36–43) (Figure 3.7A and Table 3.1). Further fragmentation of the ion at *m/z* 549 of M1 in an MS^3 spectrum gave the most informative fragment ion at *m/z* 485. This ion corresponded to a loss of CO and two water molecules (485 = 549–36–28) (Figure 3.7B). This indication of the presence of a CO group strongly suggested that oxidation occurred on the terminal double bond of the right side (C23-C24) to form 23,24-dihydroxydiscodermolide, the structure assigned to M1.

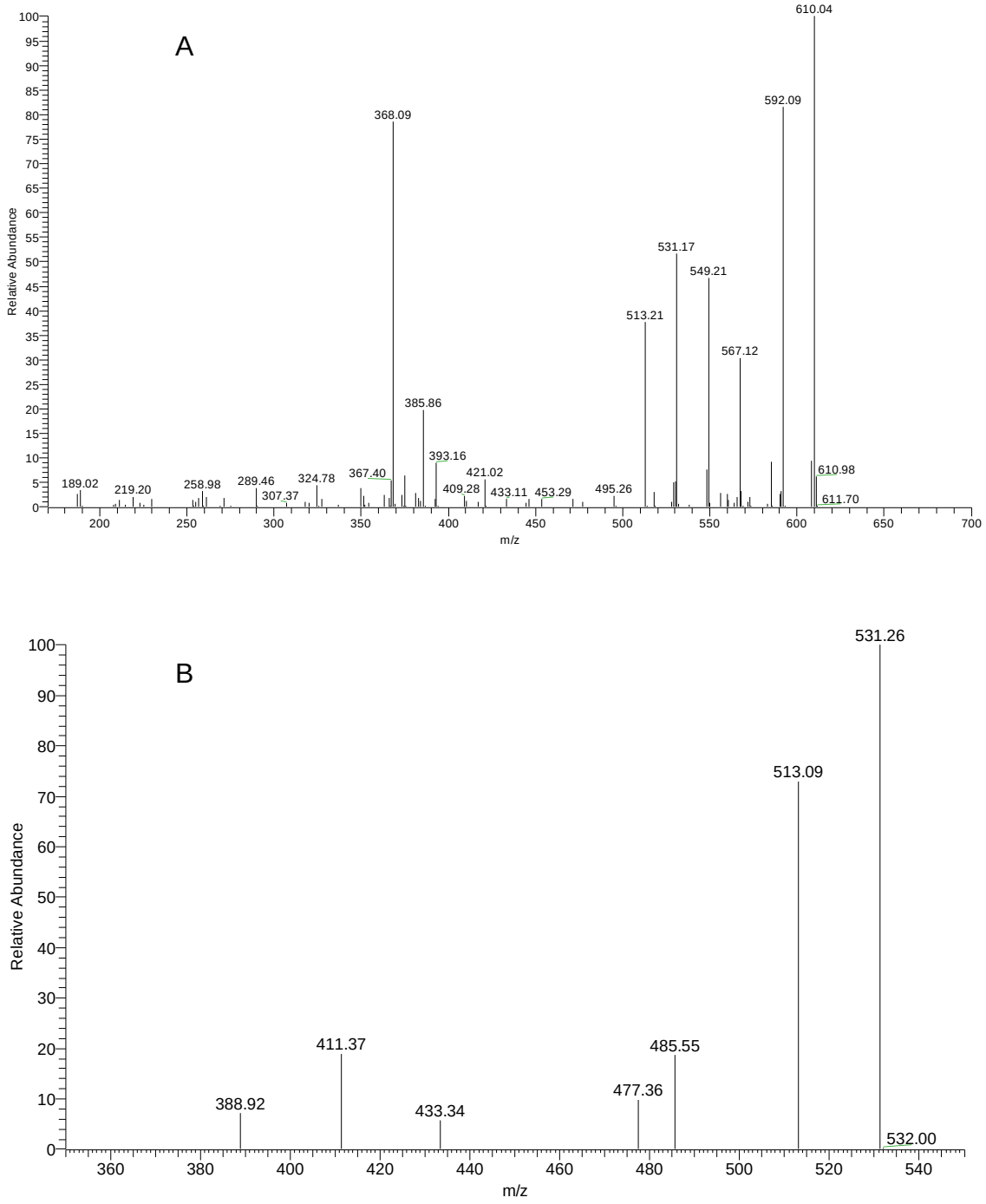

Figure 3.6 Ion trap MS^2 (A) and MS^3 (*m/z* 628→*m/z* 549) (B) product ion spectra of metabolite 1 (M1).

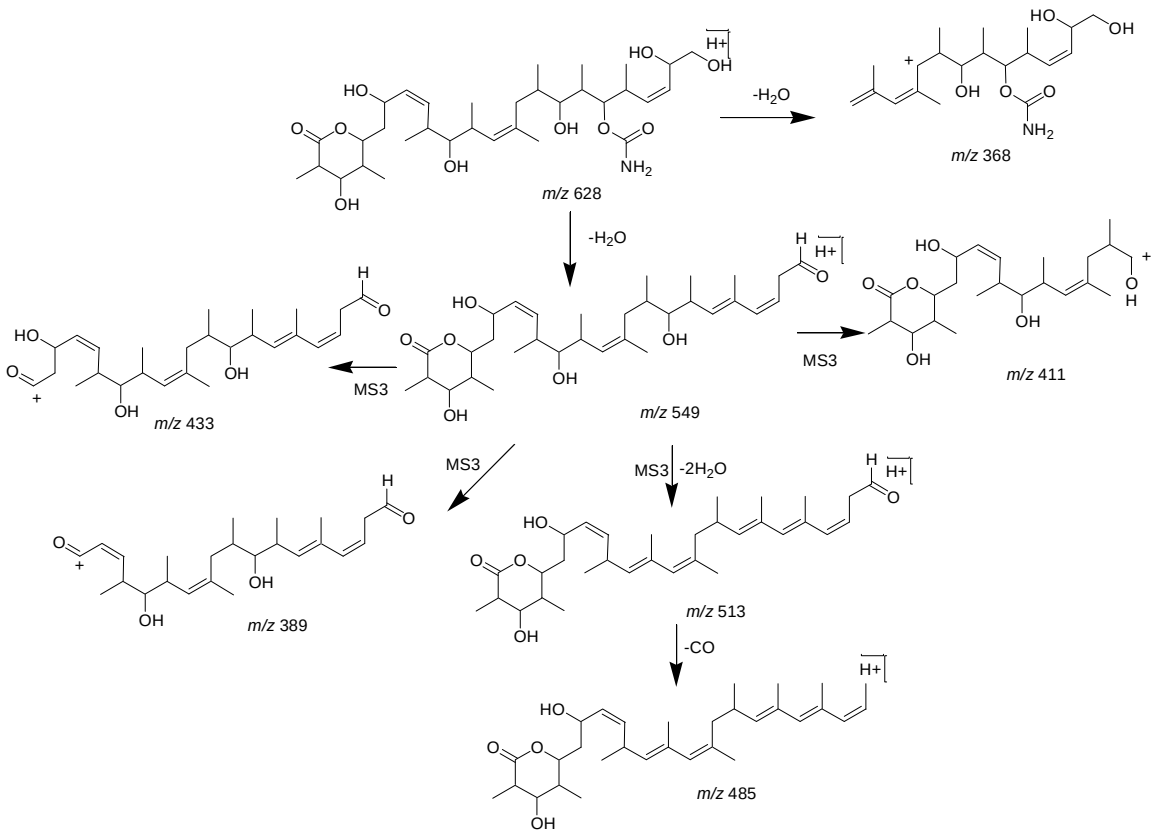

Figure 3.7 Tandem mass spectrometry fragmentation pathways of the $[M+H]^+$ ion of M1.

Metabolite M2. Metabolite M2 also yielded an $[M+H]^+$ ion at *m/z* 628. The observed accurate mass for M2 was *m/z* 628.3999, also corresponding to a product of monooxygenation plus hydrolysis with an elemental composition of $C_{33}H_{57}NO_{10}$. M2 yielded fragmentation patterns similar to the parent compound (Figure 3.9A and Table 3.1). In the MS/MS spectrum, cleavage was, like M1, at the C10-C11 and C17-C18 bonds to give ions at *m/z* 368 and *m/z* 393, again suggesting that oxidation took place on the right side of the molecule (proposed fragmentation patterns are shown in Figure 3.10). M2 also showed the fragment ion at *m/z* 549 (loss of two H_2O and one CONH) (Figure 3.9A and Table 3.1). However, the MS^3 spectrum (Figure 9B) of the ion at *m/z* 549 did not show the same diagnostic ion as seen in M1. Therefore, most possible dihydroxylation positions for M2 were deemed to be at C21 and C22 (Figure 3.10).

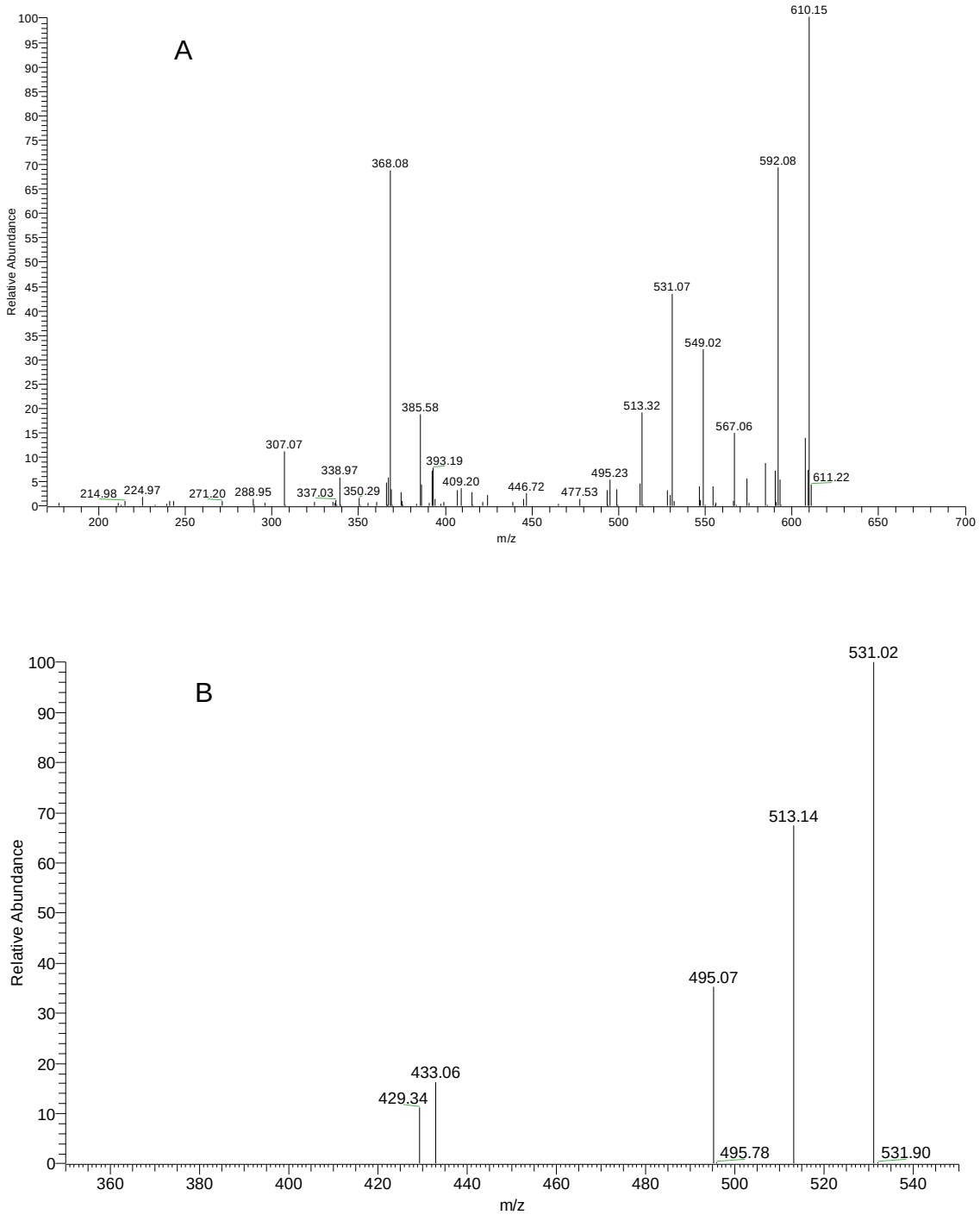

Figure 3.8 Ion trap MS^2 (A) and MS^3 (*m/z* 628→*m/z* 549) (B) product ion spectra of metabolite 2 (M2).

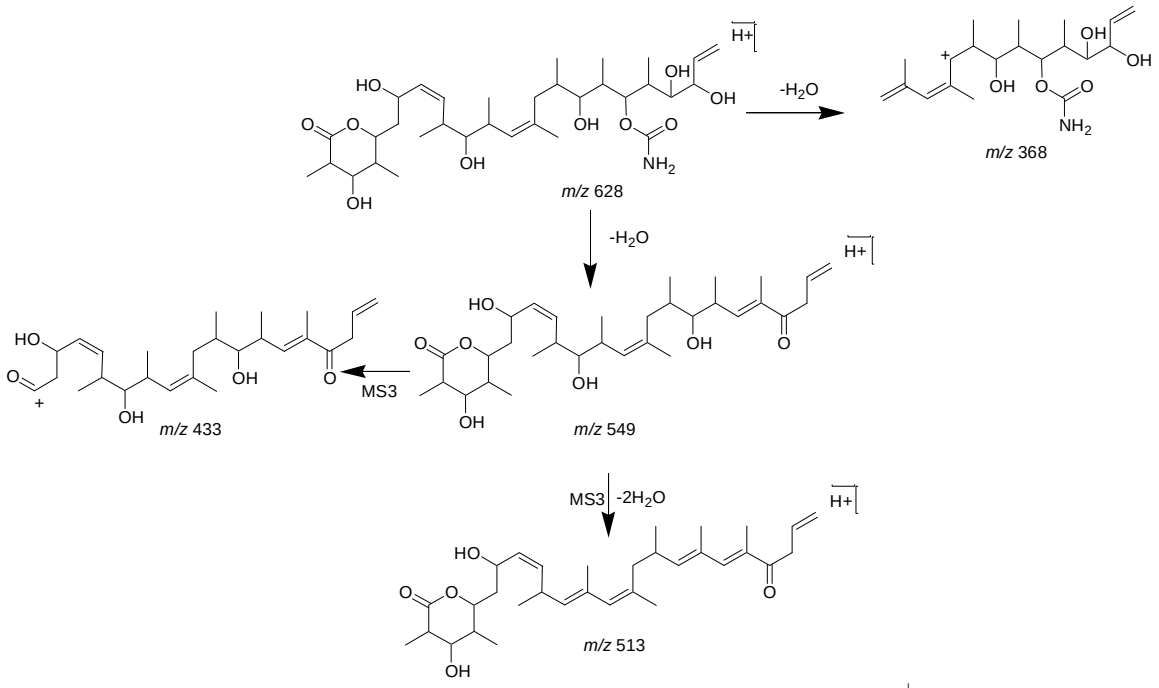

Figure 3.9 Tandem mass spectrometry fragmentation pathways of the $[M+H]^+$ ion of M2.

Metabolite M3. Metabolite M3 eluted after the dihydroxylation products. This metabolite showed a protonated molecular ion at *m/z* 610. The observed accurate mass of M3 was at *m/z* 610.3917, corresponding to a monooxygenation product with an elemental composition of $C_{33}H_{55}NO_9$.

M3 yielded MS/MS fragment ions of *m/z* 391 and *m/z* 350 (Figure 3.11A and Table 3.1), indicating that oxidation occurred in the middle portion of discodermolide (Figure 3.12). The most informative fragment ions in the MS^3 spectrum of *m/z* 350 were detected at *m/z* 320, 241 and 161 (Figure 3.11B). These corresponded to a loss of formaldehyde (HCHO) from the *m/z* 350, 271 and 191 ions (Figure 3.12). The ion at *m/z* 271 was produced by loss of one CONH group and two water molecules from the *m/z* 350 ion. The ion at *m/z* 191 was produced by the cleavage of C19-C20 bond followed by loss of one CONH group and two water molecules. This loss indicated the presence of a CH_2OH group and strongly suggested that oxidation occurred on the terminal methyl groups near C13-C14 to produce 14-(1'-hydroxy)discodermolide (see Figure 3.12).

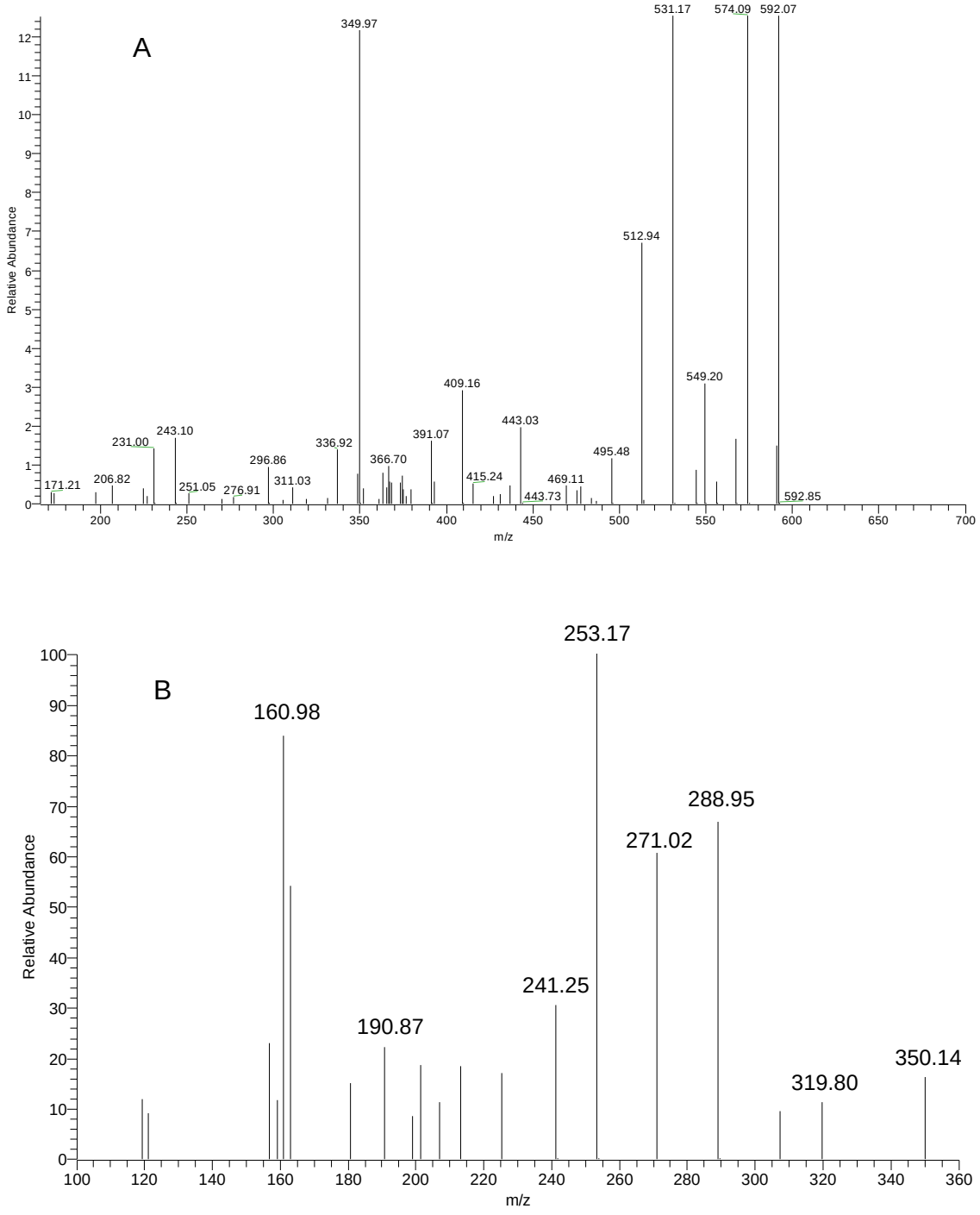

Figure 3.10 Ion trap MS^2 (A) and MS^3 (*m/z* 610→*m/z* 350) (B) product ion spectra of M3.

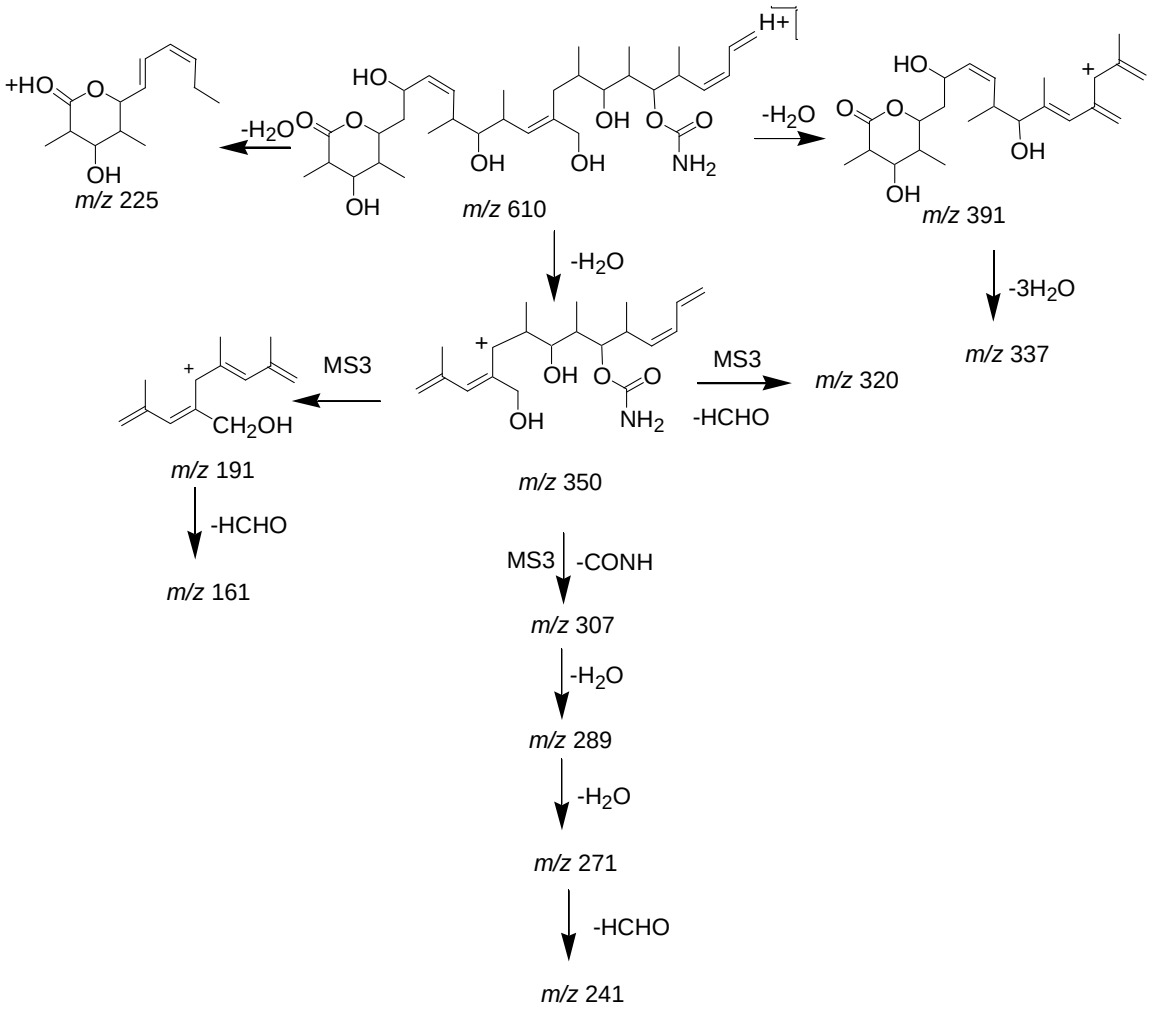

Figure 3.11 Tandem mass spectrometry fragmentation pathways of the $[M+H]^+$ ion of M3.

Metabolite M4. M4 eluted after M3. This metabolite gave an $[M+H]^+$ ion at *m/z* 610 and an accurate mass of *m/z* 610.3926, corresponding to a monooxygenation product with an elemental composition of $C_{33}H_{55}NO_9$.

The abundant M4 fragment ions of *m/z* 391 and 350 indicated that oxidation occurred in the middle portion of discodermolide. The product ion mass spectrum of M4 also showed unusual fragments at *m/z* 322 and 261. The most probable structure for M4 is 12-hydroxydiscodermolide. Based on this structure, the fragment ion at *m/z* 322 can be explained to arise by homolytic cleavage of the C11-C12 bond, initiated by a positive charge located on the C12 hydroxyl group. The fragment ion at *m/z* 261 would therefore have arisen from additional loss of the CONH group and a water molecule (Figure 3.14).

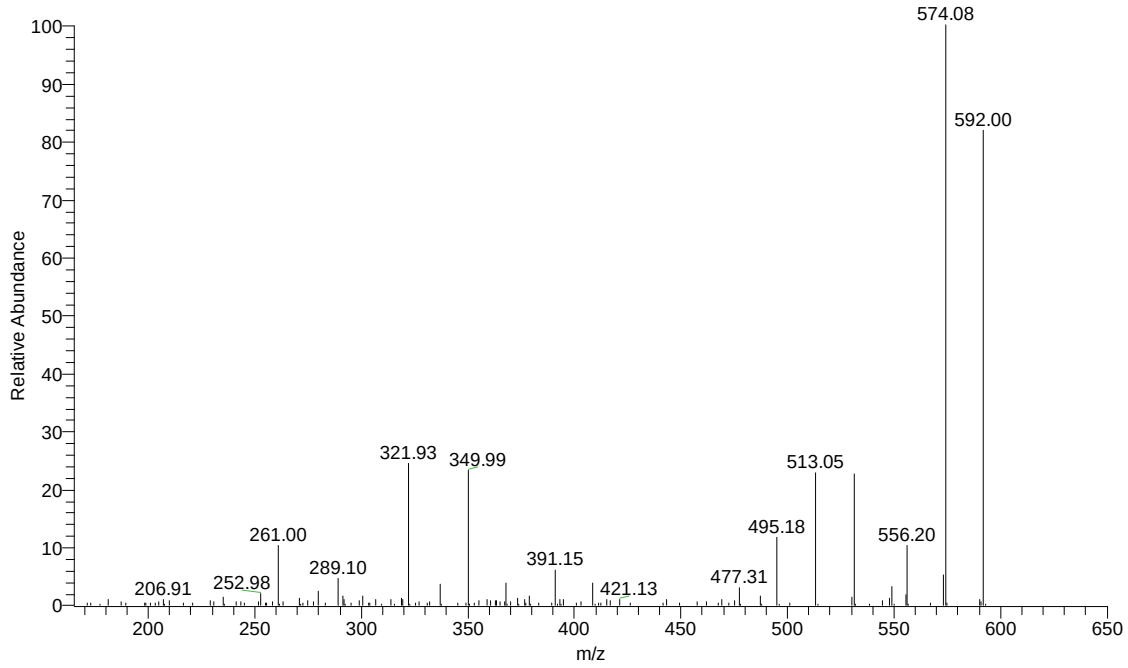

Figure 3.12 Ion trap MS^2 product ion spectra of M4.

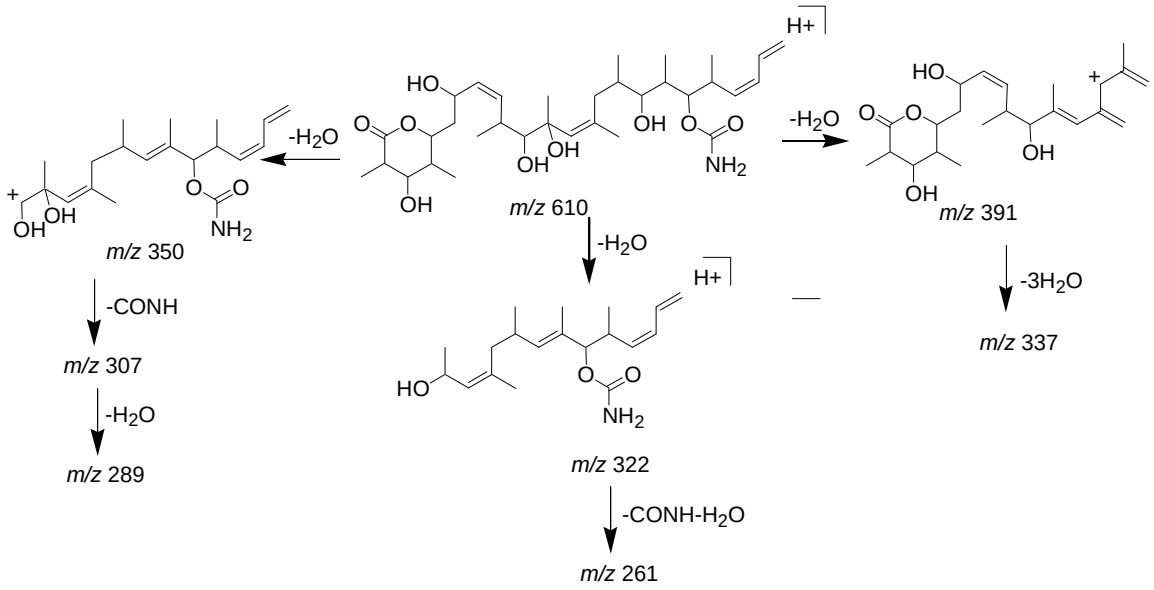

Figure 3.13 Tandem mass spectrometry fragmentation pathways of the $[M+H]^+$ ion of M4.

Metabolite M5. Metabolite M5 eluted after M4, also gave an $[M+H]^+$ ion at *m/z* 610, and an accurate mass determination of *m/z* 610.3912, which corresponded to a monooxygenation product with an elemental composition of $C_{33}H_{55}NO_9$.

The product ion spectrum of M5 was dominated by the fragment ions at *m/z* 391 and 350 (Figure 3.15A and Table 3.1), and suggesting that oxidation occurred in the middle portion of discodermolide. A unique fragment ion at *m/z* 322 was detected in MS^3 spectrum of the ion at *m/z* 350 (Figure 3.15B), corresponding to the loss of a CO moiety. This implied the presence of a formaldehyde group on the *m/z* 350 ion. Another interesting feature in the MS^3 spectrum of *m/z* 350 was the ion at *m/z* 259, which corresponded to the loss of one CONH group, one water molecule and formaldehyde (HCHO). This loss indicated the presence of a CH_2OH group and suggested the metabolic oxidation occurred on a terminal methyl group. Since the C14 methyl is the only methyl group near the double bond in the middle portion, and oxidation at this position was already assigned to M3, it is therfore highly possible that M5 was oxygenated on the C12 methyl group. The double bond between C13 and C14 might have migrated to C12-C13. Based on this structure, the fragment ion at *m/z* 322 can be explained by the loss of a CO moiety from the formaldehyde group on the ion at *m/z* 350 (see the structure in Figure 3.16). The reason of formation of a formaldehyde group on the ion at *m/z* 350 after the cleavage of C10-C11 bond would be due to the lack of a hydrogen on C12, and therefore the loss of water after cleavage of C10-C11 could not occur.

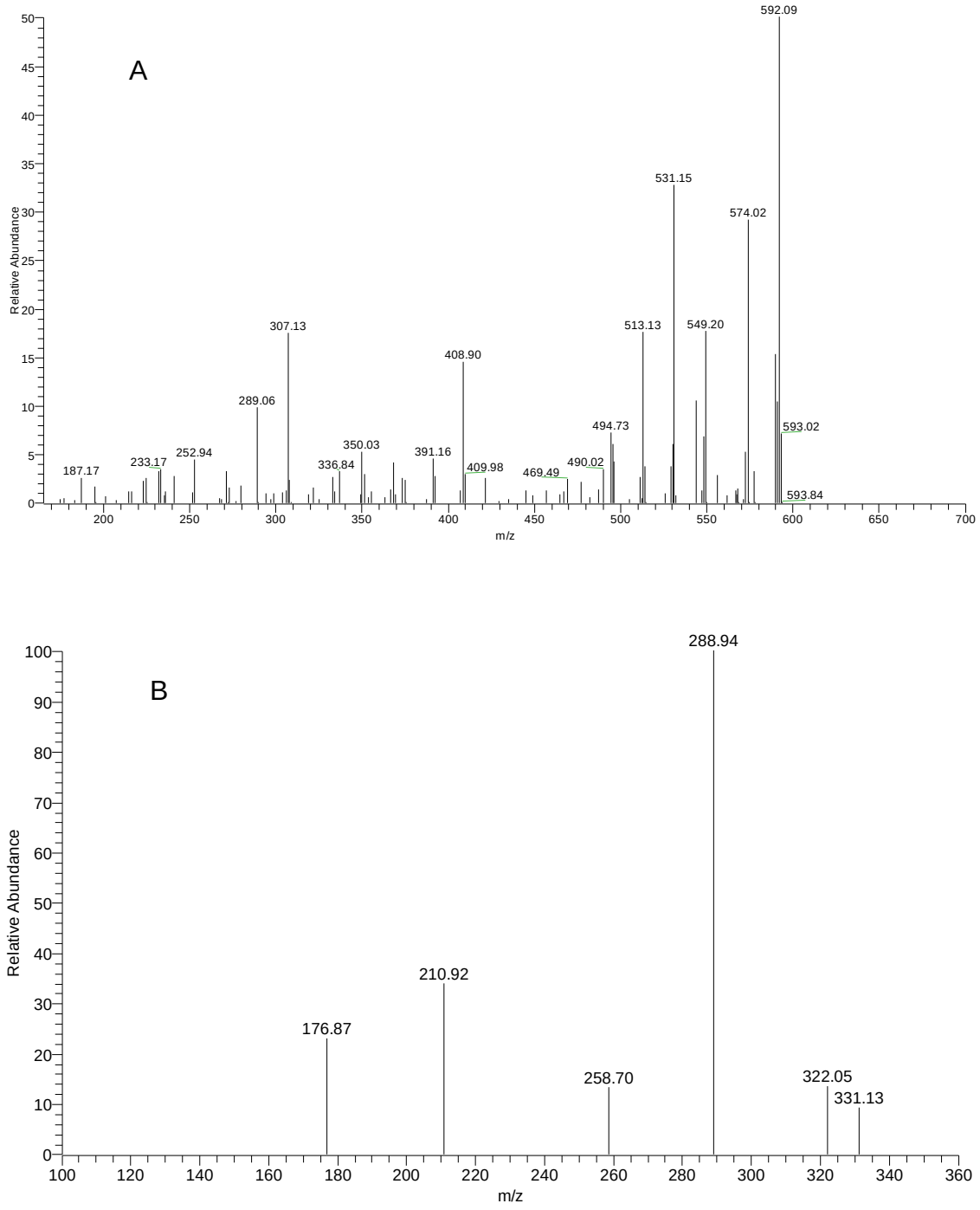

Figure 3.14 Ion trap MS^2 (A) and MS^3 (*m/z* 610→*m/z* 350) (B) product ion spectra of M5.

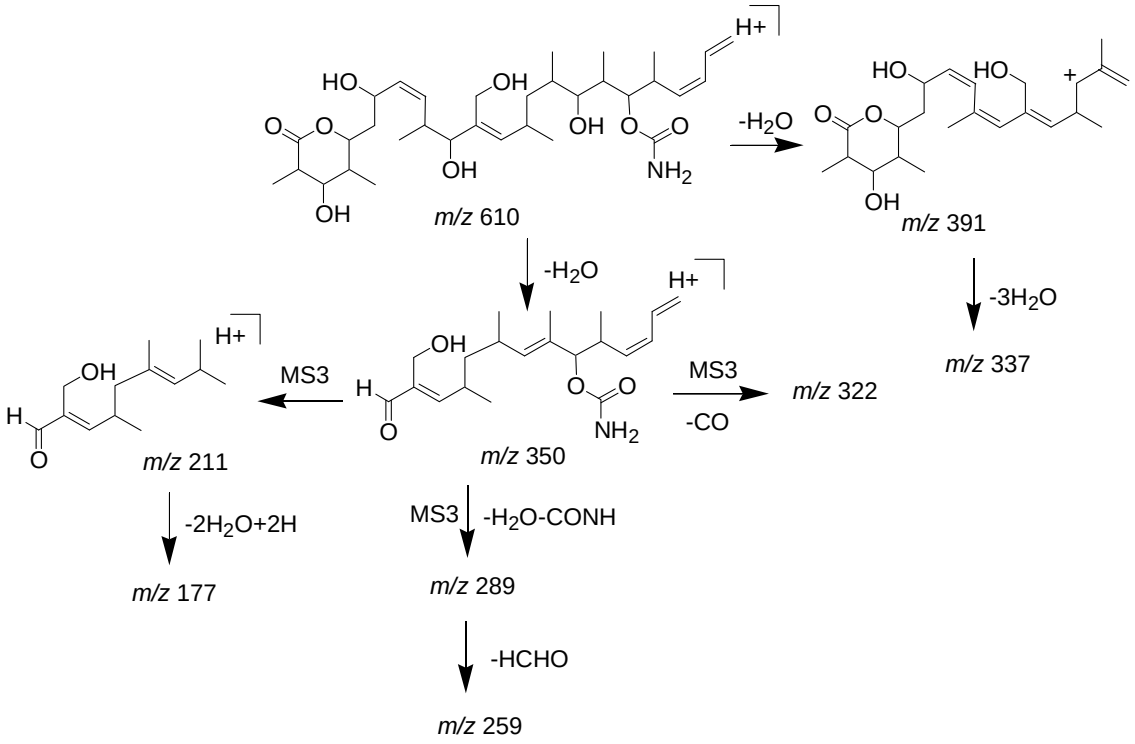

Figure 3.15 Tandem mass spectrometry fragmentation pathways of the $[M+H]^+$ ion of M5.

Metabolite M6. Metabolite M6 eluted after M5. Like M3-M5, its $[M+H]^+$ appeared at *m/z* 610. The accurate mass determination of M6 gave *m/z* 610.3919, again corresponding to a monooxygenation product with an elemental composition of $C_{33}H_{55}NO_9$.

The MS/MS spectrum of M6 showed fragment ions at *m/z* 393 and 350 (Figure 3.17A and Table 3.1), suggesting that oxidation took place in the right side of discodermolide. Further fragmentation of the ion at *m/z* 350 (Figure 3.17B) gave the most informative fragment ion at *m/z* 320, which indicated a loss of formaldehyde from *m/z* 350. The loss of HCHO strongly suggested that metabolic oxidation occurred on the only terminal methyl group in the right side of discodermolide, the methyl at C21. The most likely structure consistent with the formation of the ion at *m/z* 320 includes migration of the double bond of the right side (Figure 3.18). This double bond migration would also generate another terminal methyl group at C24. Therefore, the possibility that the hydroxyl group was added on the terminal methyl group on C24 after double bond migration cannot be excluded.

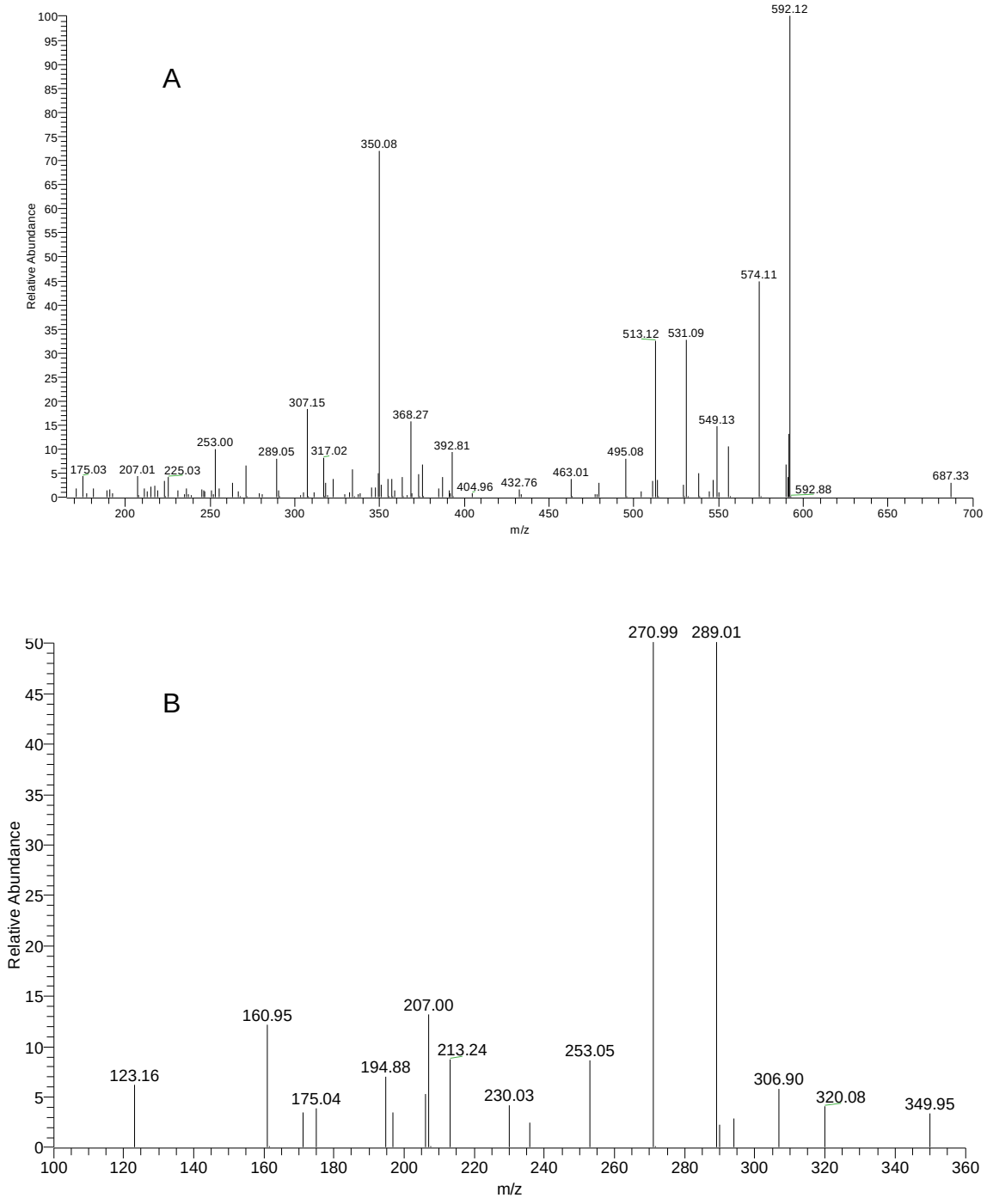

Figure 3.16 Ion trap MS^2 (A) and MS^3 (*m/z* 610→*m/z* 350) (B) product ion spectra of M6.

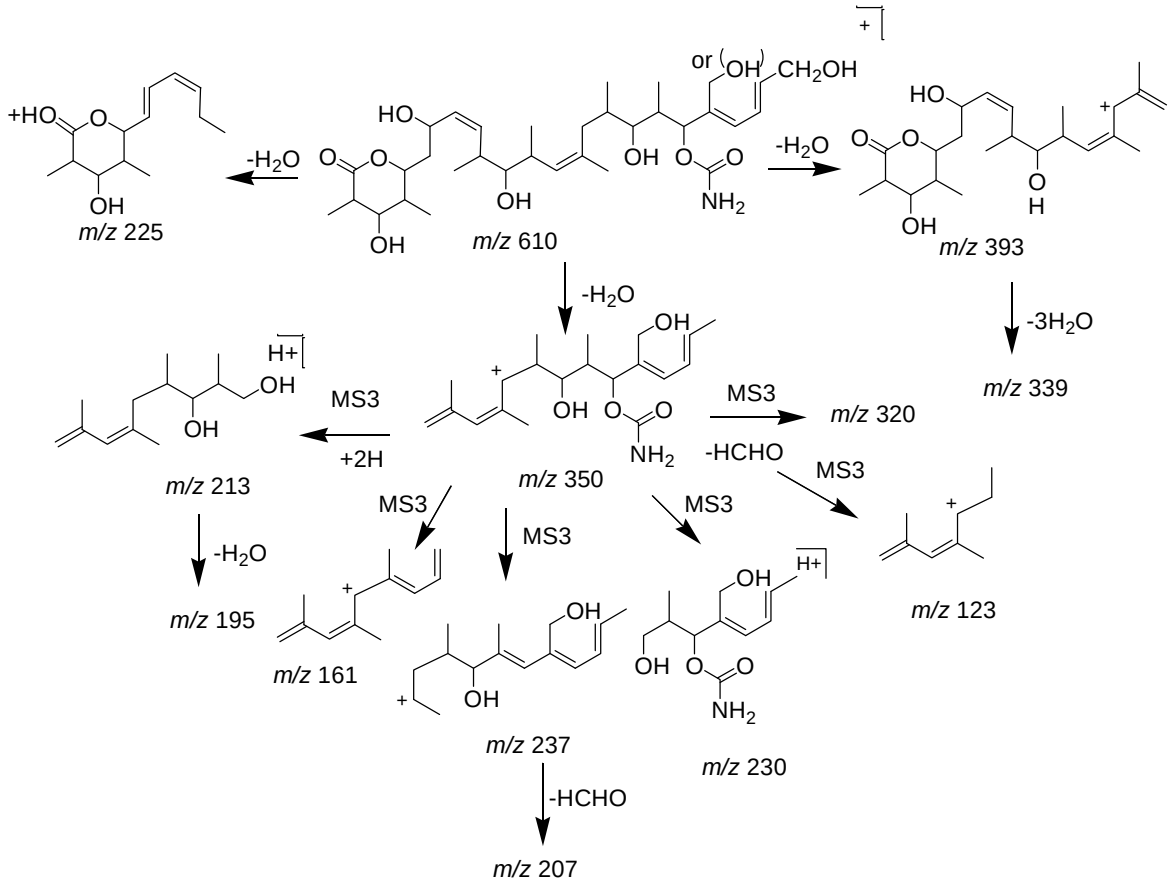

Figure 3.17 Tandem mass spectrometry fragmentation pathways of the $[M+H]^+$ ion of M6.

Metabolite M7. The metabolite M7 eluted after M6 but before the parent compound and M8. Like M3-M6, its protonated molecular ion appeared at *m/z* 610 and the accurate mass determination yielded *m/z* 610.3922. This was another monooxygenation metabolite with the composition $C_{33}H_{55}NO_9$.

The MS^2 spectrum of M7 showed fragment ions at *m/z* 391 and *m/z* 350 (Figure 3.19A and Table 3.1), indicating that oxygenation occurred in the middle portion of discodermolide. At this point, all the highly possible sites for monooxygenation in the middle portion, except C15, had been assigned. Further fragmentation of the ion at *m/z* 350 (Figure 3.19B) produced an interesting ion at *m/z* 272. The even nature of this ion implied the presence of an odd number of nitrogen atoms, i.e., one. The fragment ion at *m/z* 272 was thus likely generated by the cleavage of the C14-C15 bond near the metabolically added hydroxyl group. Therefore, the most probable structure of M7 is 15-hydroxydiscodermolide (Figure 3.20).

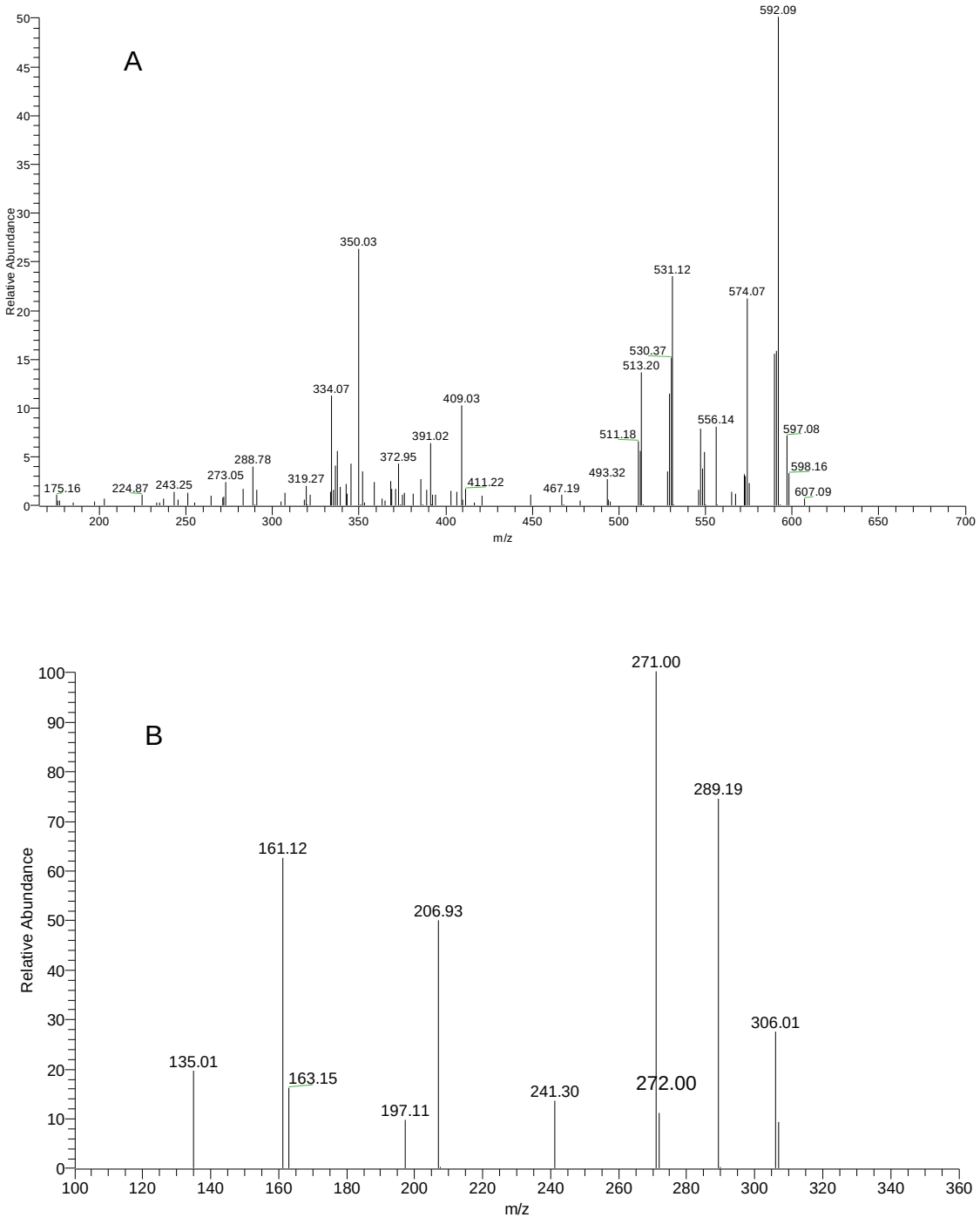

Figure 3.18 Ion trap MS^2 (A) and MS^3 (*m/z* 610→*m/z* 350) (B) product ion spectra of M7.

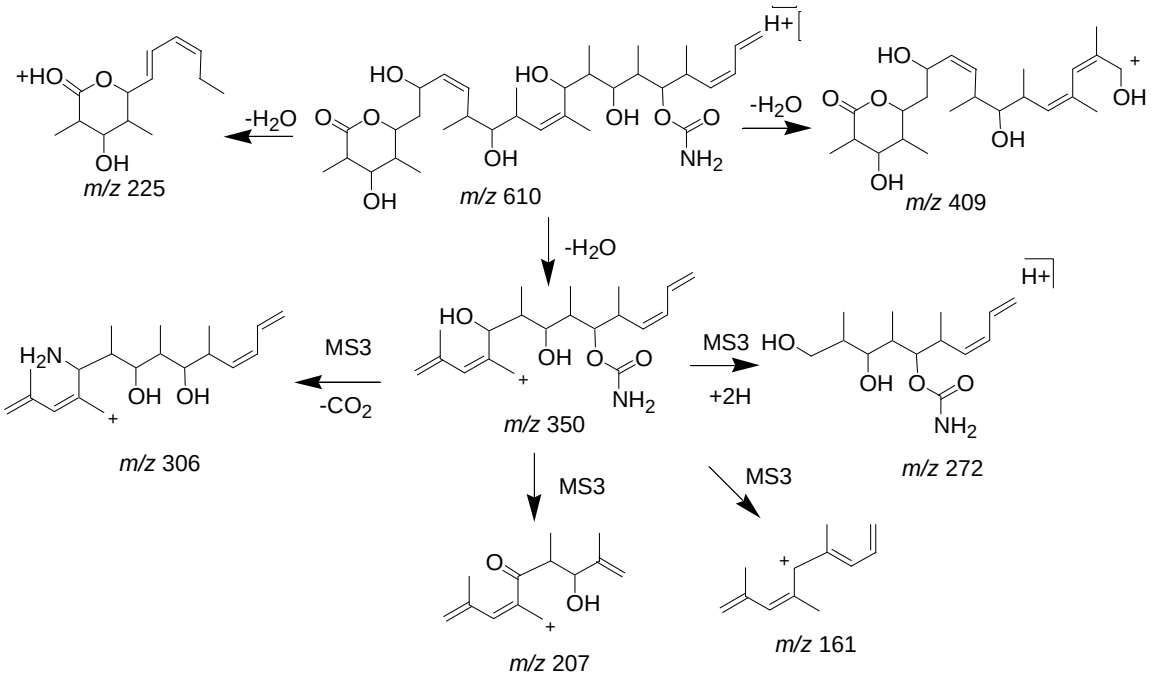

Figure 3.19 Tandem mass spectrometry fragmentation pathways of the $[M+H]^+$ ion of M7.

3.4 DISCUSSION

Although discodermolide has been under development as an anticancer drug for many years, nothing has been reported regarding its metabolism. Discodermolide was selected for study here due to some features that will have an impact on clinical development, such as potential toxicity and its reported rapid clearance rate from plasma in a preliminary ADME study (Mita C, et al., 2003). The present experiments showed that discodermolide is susceptible to biotransformation *in vitro* by human liver microsomes, and the appearance of multiple metabolites resulting from monoxygenation supported the hypothesis that the compound is metabolized by cytochromes P450. The data show the metabolic soft spots in the molecule, which may be responsible for its high clearance. Furthermore, the numerous metabolites might be a source of toxicity.

The LC-MS/MS results yielded useful information about the fragmentation patterns of the metabolites and the parent drug, particularly the ions at *m/z* 350 and 393. However these ions alone were not enough to identify the structures of metabolites. MS^3 spectra were therefore generated in a 3D ion trap as an additional tool to identify the structures of metabolites.

Human liver microsomes converted discodermolide into at least eight metabolites (summarized in Figure 3.21).

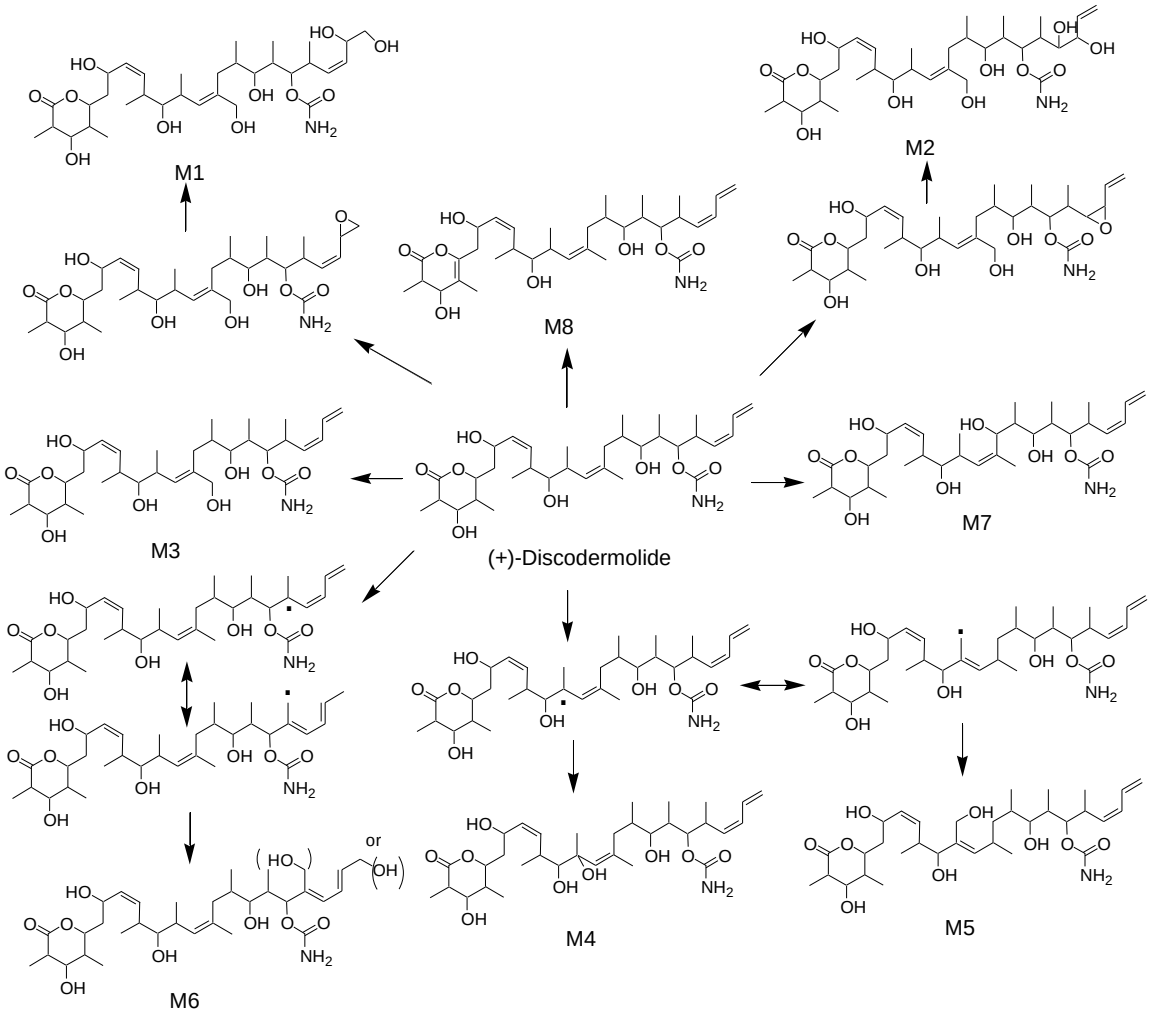

Figure 3.20 Proposed biotransformation pathways of (+)-discodermolide by pooled human liver microsomes**.**

These metabolites were either dehydrogenation or oxygenation products of discodermolide. The epoxidation of the diene moiety in the right side of discodermolide was followed by hydrolysis of the oxirane to give metabolites M1 and M2. The predominance of this metabolic pathway is not surprising given steric consideration for the attack to this site. Because of the *Z*-double bonds and substituent pattern particularly in the middle portion of the molecule, discodermolide is known to adopt a 'tilde' or 'corkscrew' shape, both in solution and in the crystal form (Sanchez-Pedregal VM et al., 2006). This leaves the diene group of discodermolide

as the most exposed and thus accessible to the attack by CYP450 enzymes. This finding might be significant in terms of compound optimization, since the terminal diene system does not contribute significantly to the biological activity of discodermolide (Smith et al., 2005). Substitution of terminal diene group with saturated carbon systems would increase metabolic stability of the compound without sacrificing the biological activity. Previous SAR studies have showed that an analogue of discodermolide with an unsaturated latone ring has slightly higher potency than parent drug (Smith et al., 2005). Here it was found that discodermolide could be dehydrogenated at C4-C5 to form metabolite M8. Based on the chemical structures of M1, M2 and M8, It is proposed that an analogue of discodermolide, which may have higher metabolic stability, should be prepared. The structure of this molecule is shown in Figure 3.22.

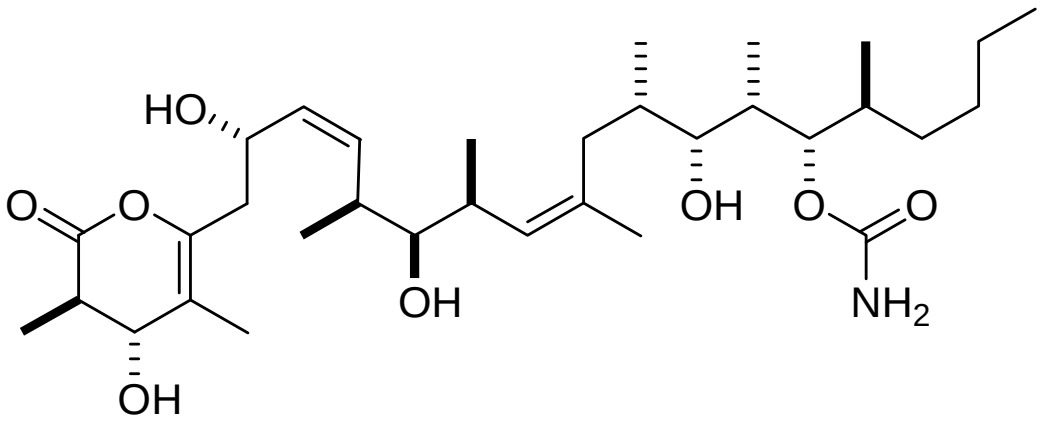

Figure 3.21 Structure of an analogue of discodermolide proposed for synthesis based on the metabolism of the parent drug..

Another interesting observation was the detection of double bond migration of C13-C14 and C21-C22 in metabolites M5 and M6. These migrations might be caused by the delocalization

of the unpaired electrons of radicals generated by CYP450 enzyme onto the other carbons of the allylic system.

3.5 ACKNOWLEDGMENT

Supported in part by grants from the NIH (CA078039) and the DoD (TATRC USAMRMC 04145001).

4.0 METABOLISM OF (–)-DICTYOSTATIN IN POOLED HUMAN LIVER MICROSOMES

4.1 INTRODUCTION

As outlined in the previous chapter, the microtubule system is an important target for cancer therapy as evidenced by the clinical success of the taxanes, so the search continues for agents that cause microtubule stabilization. (–)-Dictyostatin is a unique 22-membered macrocyclic lactone (Figure 4.1).

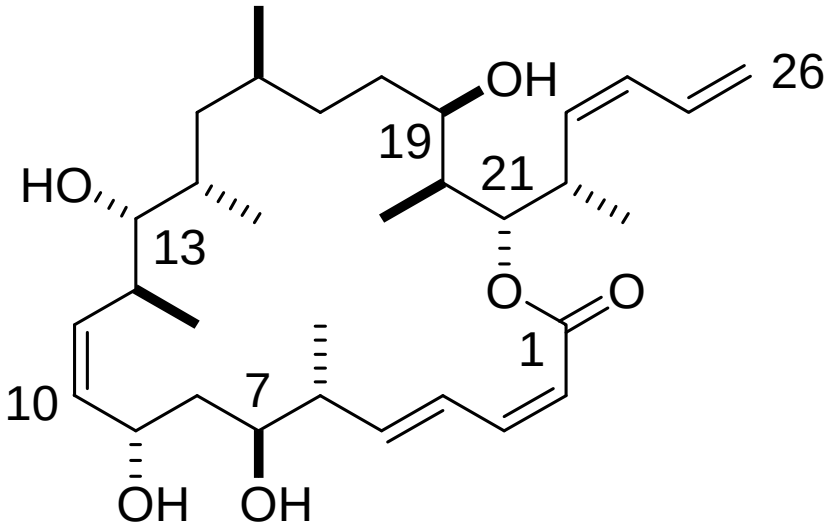

Figure 4.1 The chemical structure of (−)-dictyostatin

It was first isolated from a Republic of Maldives marine sponge in the genus *Spongia* in extremely low yield (3.4×10^{-7}%) in 1994 and was found to strongly inhibit the cell growth of murine P388 lymphocytic leukemia cells (Pettit GR, et al., 1994). In 2003, dictyostatin was identified as a highly active microtubule stabilizing agent in an extract from a *Lithistida* sponge of the family *Corallistidae* collected off the north cost of Jamaica. Dictyostatin was found to arrest cells in the G2/M phase and to induce the polymerization of tubulin in vitro. Dictyostatin was also highly potent against two paclitaxel-resistant human cancer cell lines overexpressing P-glycoprotein (Isbrucker RA, et al., 2003). This data makes dictyostatin a promising compound for further study.

Because of the low availability from natural sources, the full evaluation of dictyostatin was difficult. The relative stereochemistry of dictyostatin was determined by high field NMR and molecular modeling in 2004 (Paterson I, et al., 2004). Total syntheses of (–)-dictyostatin were simultaneously reported by Paterson (Paterson I et al., 2004) and Curran (Shin Y, et al., 2004), and later by Phillips (O'Neil GW, et al., 2006) and Ramachandran (Ramachandran PV, et al., 2007). These total syntheses allowed evaluation of dictyostatin's therapeutic potential.

Nothing is known about the metabolism of (–)-dictyostatin. Because of the extensive metabolism of the closely related compound (+)-discodermolide reported in the previous chapter, as well as the clinical failure of the agent, the in vitro biotransformation of synthetic (–)-dictyostatin in pooled human liver microsomes was examined. The hypothesis was that dictyostatin would also be a substrate for cytochromes P450, but that its cyclic structure might limit, as compared to discodermolide, the number of metabolites formed. The metabolites of dictyostatin were identified using liquid chromatogram ion trap mass spectrometry and are reported here.

4.2 MATERIALS AND METHODS

Chemicals. Dictyostatin was synthesized by Prof. Dennis Curran's group at the University of Pittsburgh (Shin Y et al., 2004). All other chemicals were purchased from Sigma-Aldrich (St.Louis, MO). HPLC grade acetonitrile and water were purchased from Burdick & Jackson (Muskegon, MI).

Human Liver Microsomes. Pooled human liver microsomes were purchased from BD Gentest (Wobum, MA). The cytochrome P450 content was 0.33 nmol/mg of protein.

Microsomal Incubations. A typical incubation mixture (0.5mL) contained 0.2mg/mL of microsomal protein, 10 μM dictyostatin, and 100 mM phosphate buffer, pH7.4. The reaction was initiated by adding of NADPH regeneration system (BD Bioscience, San Jose, CA), which included 1.3 mM $NADP^+$, 3.3 mM glucose-6-phosphate, 0.4 U/mL glucose-6-phosphate dehydrogenase, and 3.3 mM magnesium chloride. The incubation was carried out for 15 min at 37 ºC and was stopped by addition of 0.5 mL of cold acetonitrile to precipitate proteins. Control reactions contained all the components except microsomal protein or no $NADP^+$ was added.

HPLC. Reverse phase HPLC separations were carried out using a prepacked Pico Frit C18 column (7.5 μm x 10 cm, New Objectives, Inc.). The column was eluted with 0.1% formic acid in water (solvent A) and 0.1% formic acid in acetonitrile (solvent B). The initial condition was 35% solvent B. The gradient as follows: isocratic 35% B for 5 min, linear gradient from 35% to 70% B over 10 min, isocratic at 70% B for 5 min, linear gradient from 70% to 95% B over 1 min, then isocratic at 95% B for 4 min. The flow rate was 155 μL/min. The injection volume was 1 μL.

LC-MS/MS Analysis. A Thermo Electron LCQ Deca XP Plus mass spectrometer with a nanospray source (Thermo Electron Corporation) was used for MS/MS analysis of dictyostatin

metabolites. Positive ions were monitored. Spray voltage was set at 1.43 kV, capillary temperature was 180 ºC and the capillary voltage was 40 V. Activation energy for fragmentation was set at 30%.

4.3 RESULTS

Metabolite Identification. Pooled human liver microsomes with a cytochrome P450 content of 0.33 nmol/mg of protein were diluted to 0.2 mg/mL in 100 mM phosphate buffer containing 10 μM (–)-dictyostatin and reactions were initiated at 37 ^{o}C with a glucose-6-phosphate dehydrogenase-based NADPH regenerating system. Final reaction volumes were 0.5 mL. Reactions were allowed to proceed for 15 min and proteins were precipitated by addition of ice-cold acetonitrile

The total ion chromatogram and the extracted ion chromatograms for the positive ion nanospray LC-MS/MS analysis of of 10 μM (–)-dictyostatin incubated with active pooled human liver microsomes is shown in Figure 4.2A. Control incubations without microsomal protein or without NADP(H) showed no degradation and oxygenation of the parent molecule (Figure 4.2B). Six major metabolites were detected, all as their protonated molecular ions. The corresponding product ion mass spectra obtained using the ion trap and the proposed fragmentation pathways for (–)-dictyostatin and its metabolites are listed in Table 4.1 and depicted in Figures 4.3-4.18. Detailed discussions of each are given below.

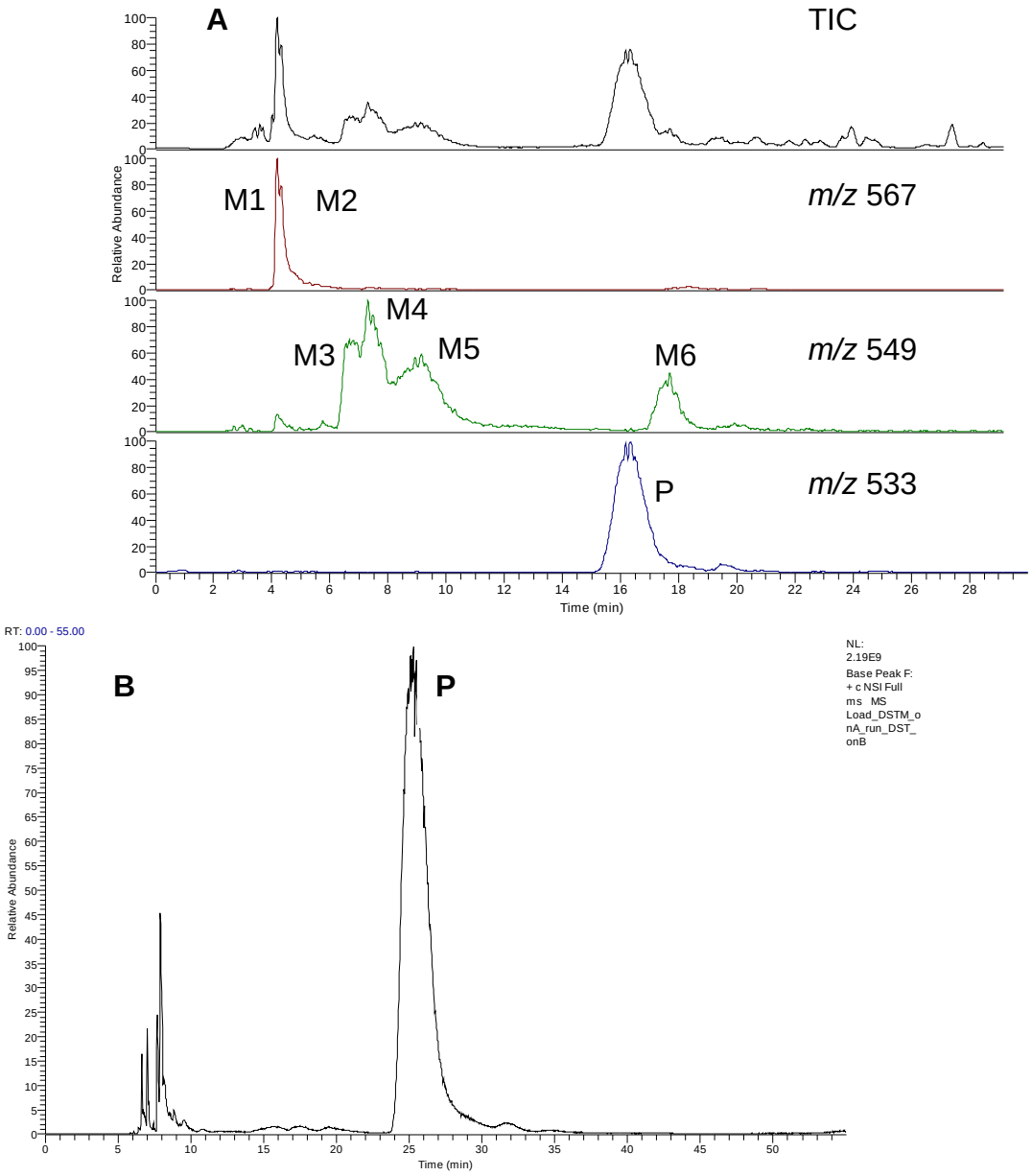

Figure 4.2 (A) Positive ion LC-MS total ion and extracted ion chromatograms of 10 µM (–)-dictyostatin after incubation with pooled human liver microsomes at 37ºC for 15min with NADPH. (B) Total ion chromatogram of incubation without NADPH.

Table 4.1 Mass spectrometric data for (-)-dictyostatin and its metabolites.

Metabolite	$[M+H]^+$ *m/z*	Major Fragment Ions in MS^2 Spectra
Dictyostatin	533	453, 415, 393, 375, 357, 339, 329, 279, 261, 243
M1	567	513, 483, 477, 471, 449, 433, 419, 375, 339, 295, 277
M2	567	477, 471, 431, 421, 375, 339, 295, 277, 259
M3	549	495, 465, 431, 413, 391, 355, 295, 277, 265
M4	549	469, 413, 391, 373, 359, 331, 295, 277, 259, 241
M5	549	451, 393, 375, 359, 295, 277, 265
M6	549	469, 409, 391, 309, 291, 279

Dictyostatin. The major fragmentation pathway for the parent molecule (–)-dictyostatin was the cleavage of the C1-O bond of the macrocyclic lactone ring, followed either by the cleavage of the C12-C13 bond near the C13-hydroxyl to give the fragment ion at *m/z* 279 or by the cleavage of C19-C20 bond near the C19-hydroxyl to give the fragment ion at *m/z* 393 (Figure 4.3). As the reader will see later in this chapter, this pathway proved very useful for the determination of the sites of metabolic transformation on (–)-dictyostatin. The loss of water molecules from the *m/z* 393 fragment ion gave rise to the *m/z* 375, *m/z* 357, and *m/z* 339 ions. Likewise, the loss of the water molecules from the *m/z* 279 fragment ion gave rise to the *m/z* 261 and *m/z* 243 ions. The loss of a CO moiety from the *m/z* 357 ion gave the *m/z* 329 ion. Other minor fragmentation pathways included the cleavage of the C21-C22 bond to give the *m/z* 453 product ion, and the cleavage of the C8-C9 and C12-C13 bonds to give *m/z* 415 product ion. The proposed fragmentation pathways of (–)-dictyostatin are shown in Figure 4.4.

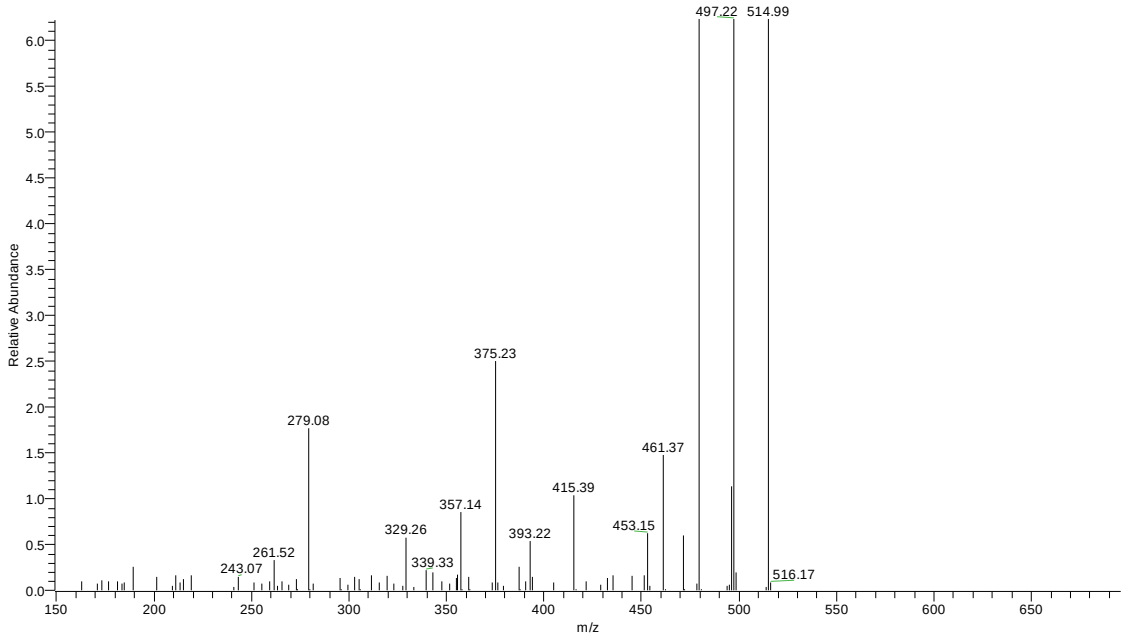

Figure 4.3 Positive ion nanospray MS/MS product ion mass spectrum of the protonated molecular ion of (–)-dictyostatin.

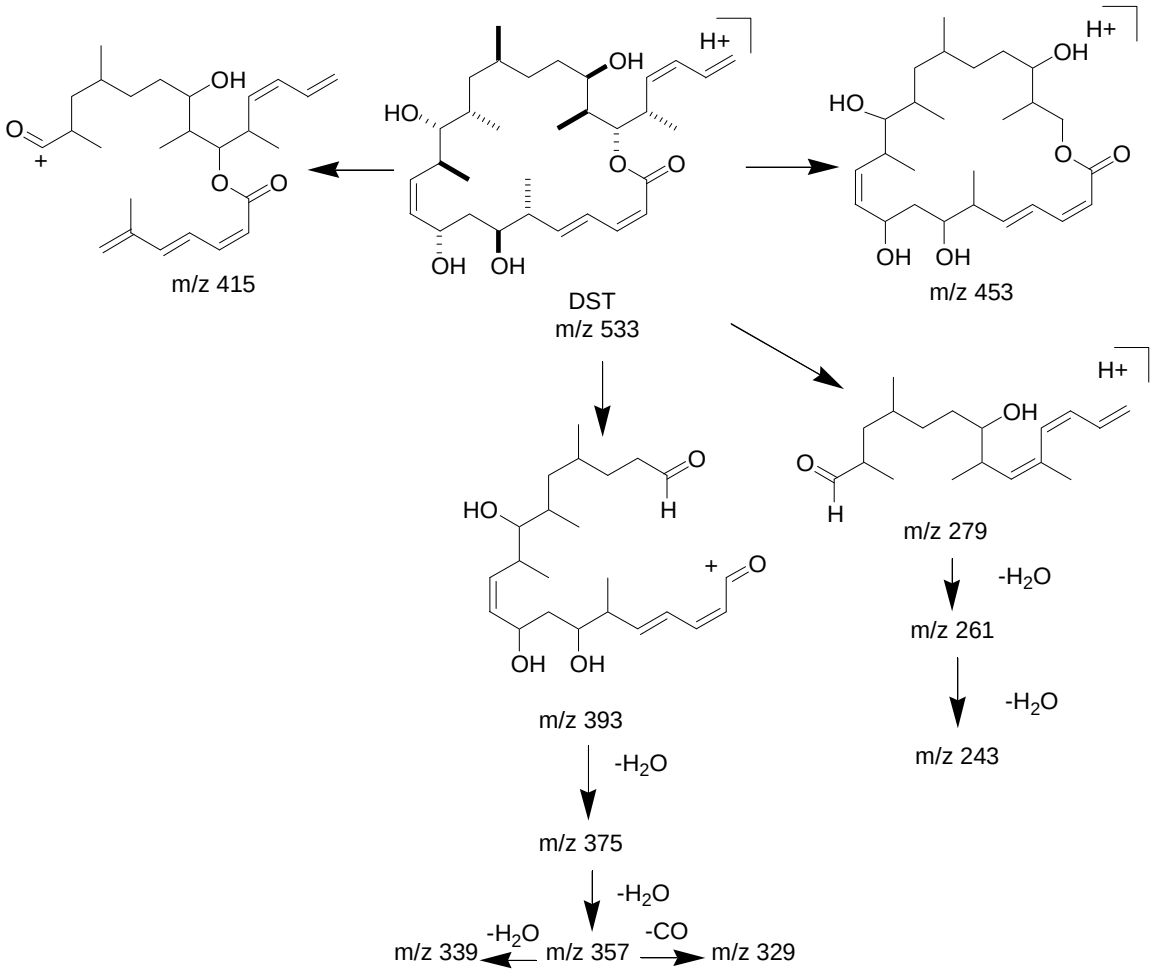

Figure 4.4 Tandem mass spectrometry MS/MS fragmentation pathways of the protonated molecular ion of (–)-dictyostatin.

Metabolite M1. Metabolite M1 was the first eluting peak during the reverse phase nanoflow LC separation. This relatively high polarity implied M1 to be the most hydrophilic metabolite. The $[M+H]^+$ ion of M1 appeared at *m/z* 567, making the mass difference between the parent compound and M1 +34 Da, which corresponded to monooxidation (+16 Da) plus hydrolysis (+18 Da). The MS/MS spectrum of M1 is shown in Figure 4.5. Abundant fragment ions were detected at *m/z* 295 and *m/z* 375, the latter corresponding to the loss of water from the *m/z* 393 ion. The loss of two water molecules from *m/z* 375 gave the ion at *m/z* 339 and the loss of one water molecule from *m/z* 295 gave the ion at *m/z* 277. Recall that the ion at *m/z* 375 was also detected in the MS/MS spectra of (–)-dictyostatin. The 16 Da difference between the ion at *m/z* 295 in the MS^2 spectrum of M1 and the *m/z* 279 ion in the MS^2 spectrum of (-)-dictyostatin suggested that the oxidation took place somewhere between C19 and C26, and that the macrolactone ester bond had hydrolyzed (see the proposed fragmentation pathway in Figure 4.6). Elimination of three water molecules from the protonated molecular ion gave rise to *m/z* 513; subsequent neutral loss of 30 Da from this ion produced *m/z* 483, which corresponds to a formaldehyde moiety. Collectively, this fragmentation pattern suggested that M1 is dictyostatin hydroxylated on a terminal methyl group. In addition, neutral loss of 30 Da from *m/z* 449 to give *m/z* 419 was observed. The *m/z* 449 corresponds to the loss of five water molecules and a CO moiety from the protonated molecular ion of M1. The ion at *m/z* 471 and *m/z* 433 were also observed in the MS/MS spectrum of M1, corresponding to the cleavage of the C21-C22 bond and the cleavage of C21-C22 followed by elimination of two water molecules and two hydrogen atoms, respectively. This suggested that the hydroxylation did not take place on the C19, C20 or C21 carbons. It is possible that M1 was generated by hydroxylation of the methyl group on C22 followed by the hydrolysis of the lactone ring after double bond migration. Such a double bond

migration would also generate another terminal methyl group on C25, so the possibility that the hydroxylation occurred at this position can not be excluded. Based on the results, the structure of M1 was assigned as the lactone hydrolyzed version of the parent molecule also hydroxylated at either the C22 methyl group or at the C25 after double bond migration.

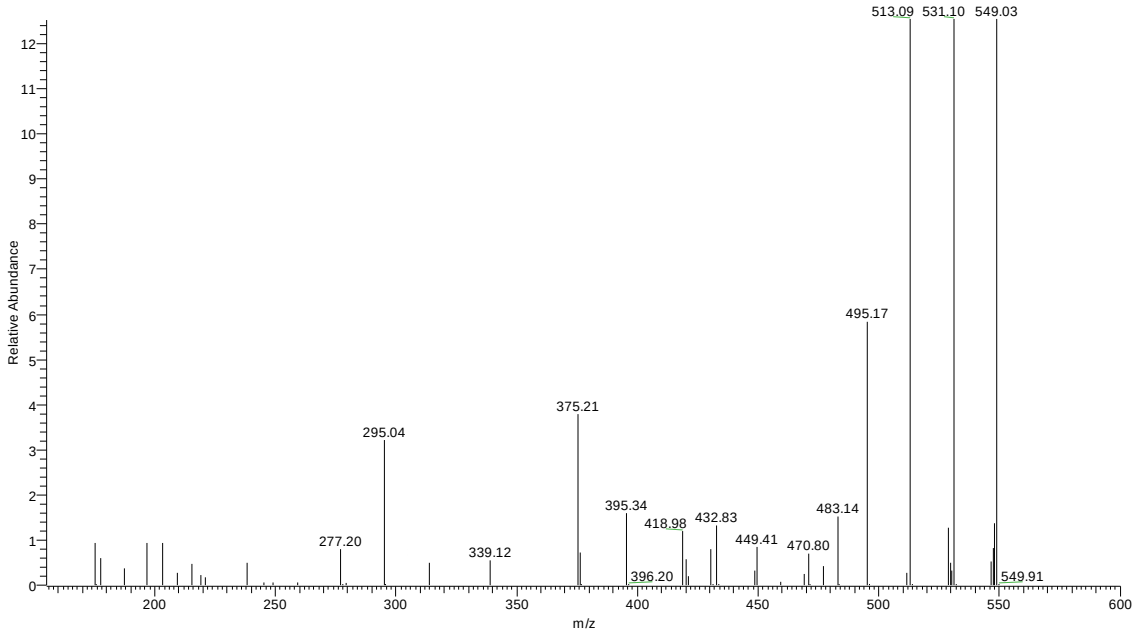

Figure 4.5 MS^2 spectrum of the protonated molecular ion (*m/z* 567) of metabolite M1.

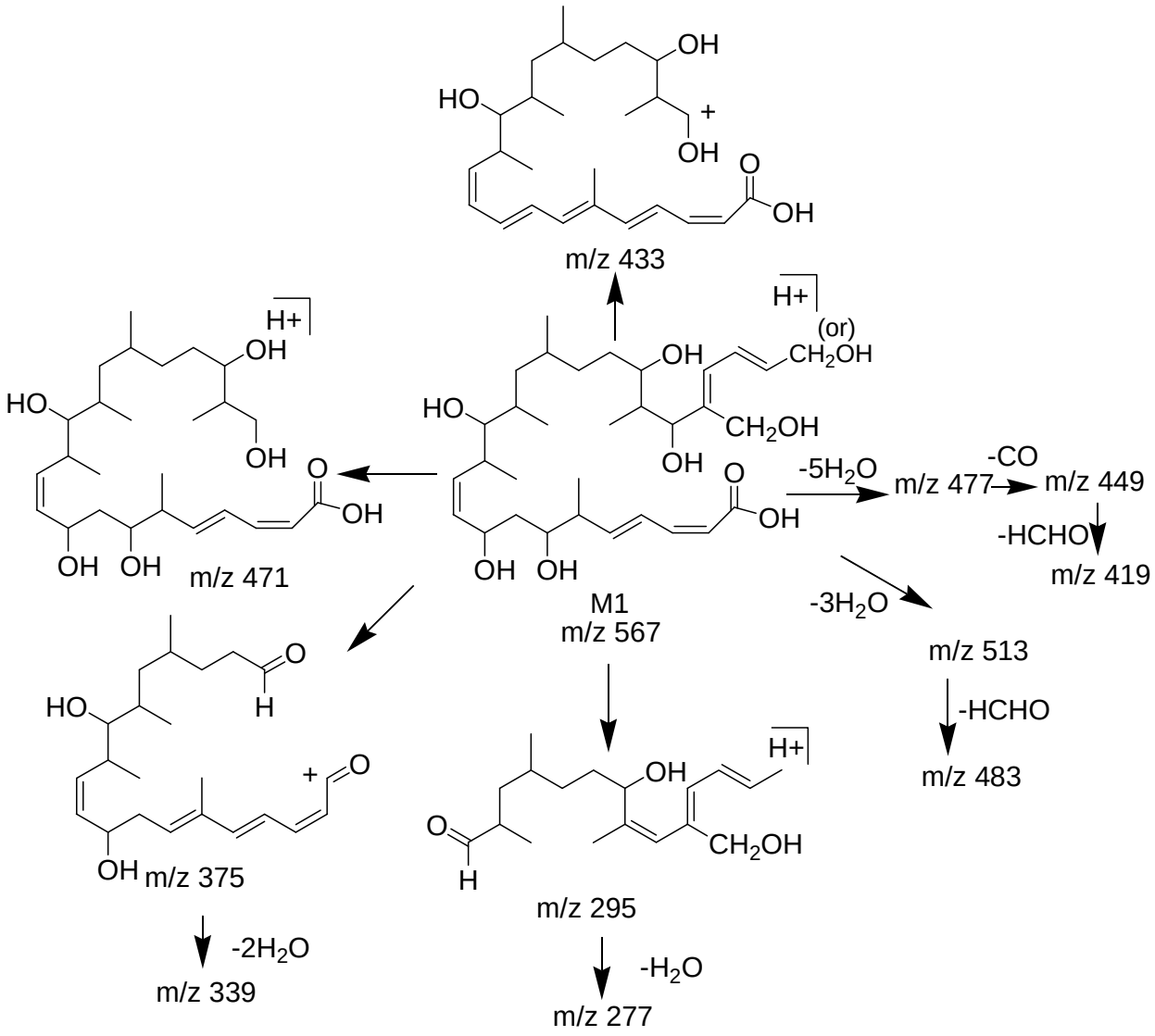

Figure 4.6 MS/MS fragmentation pathways of the protonated molecular ion of M1.

Metabolite M2. M2 eluted after M1. The retention times of M1 and M2 were close to each other. The $[M+H]^+$ ion of M2 was the same as that of M1, *m/z* 567 indicating that M2 was also a hydroxylated macrolactone hydrolysis product of (–)-dictyostatin. The mass spectral fragmentation pattern of M2 was very analogous to that of M1. Dissociation of the $[M+H]^+$ at *m/z* 567 produced two major fragment ions at *m/z* 375 and *m/z* 295 (see Figure 4.7), suggesting that the oxidation took place between C19 and C26 and that the ester bond was hydrolyzed (see the proposed fragmentation pathway in Figure 4.8). The neutral loss of five water molecules from the protonated molecular ion of M2 produced the *m/z* 477 ion, and the subsequent loss of one water molecule and one CO moiety gave rise to the *m/z* 431 ion. The loss of water molecules from *m/z* 295 generated the *m/z* 277 and *m/z* 259 ions. The ion at *m/z* 471, also detected in the MS/MS spectrum of M1, was observed. This informative fragment ion narrowed down the possible hydroxylation site to the C22-C26 region. No ions corresponding to the loss of formaldehyde were observed in the MS/MS spectrum of M2, suggesting that the oxygenation did not occur on the terminal methyl group of (–)-dictyostatin. A moderately abundant signal at *m/z* 421 was detected in the MS/MS spectrum of M2. This ion was unique in all MS/MS spectra of all metabolites of (–)-dictyostatin, plus was not observed in the MS/MS spectra from the parent molecule. It is highly possible that the hydroxyl group of M2 resides on C22. The cleavage of C22-C23 afforded the most important diagnostic ion at *m/z* 421. This assignment is supported by the relatively similar HPLC retention time of M2, which was only slightly less polar than the apparently closely related M1.

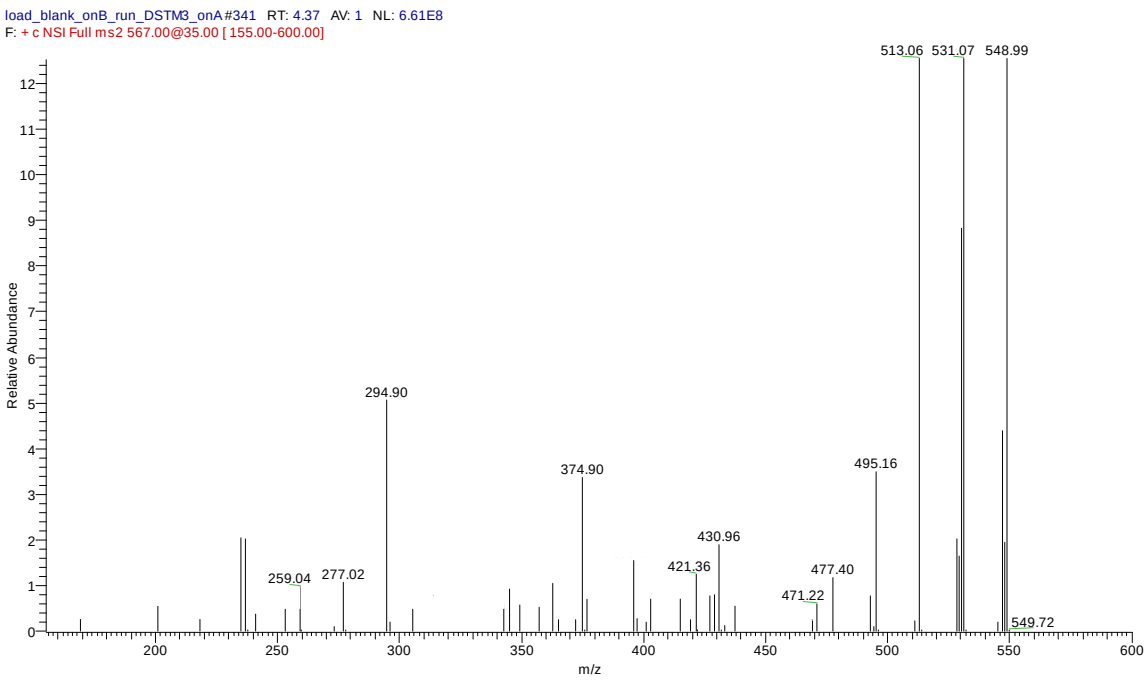

Figure 4.7 MS^2 spectrum of the protonated molecular ion (*m/z* 567) of metabolite M2.

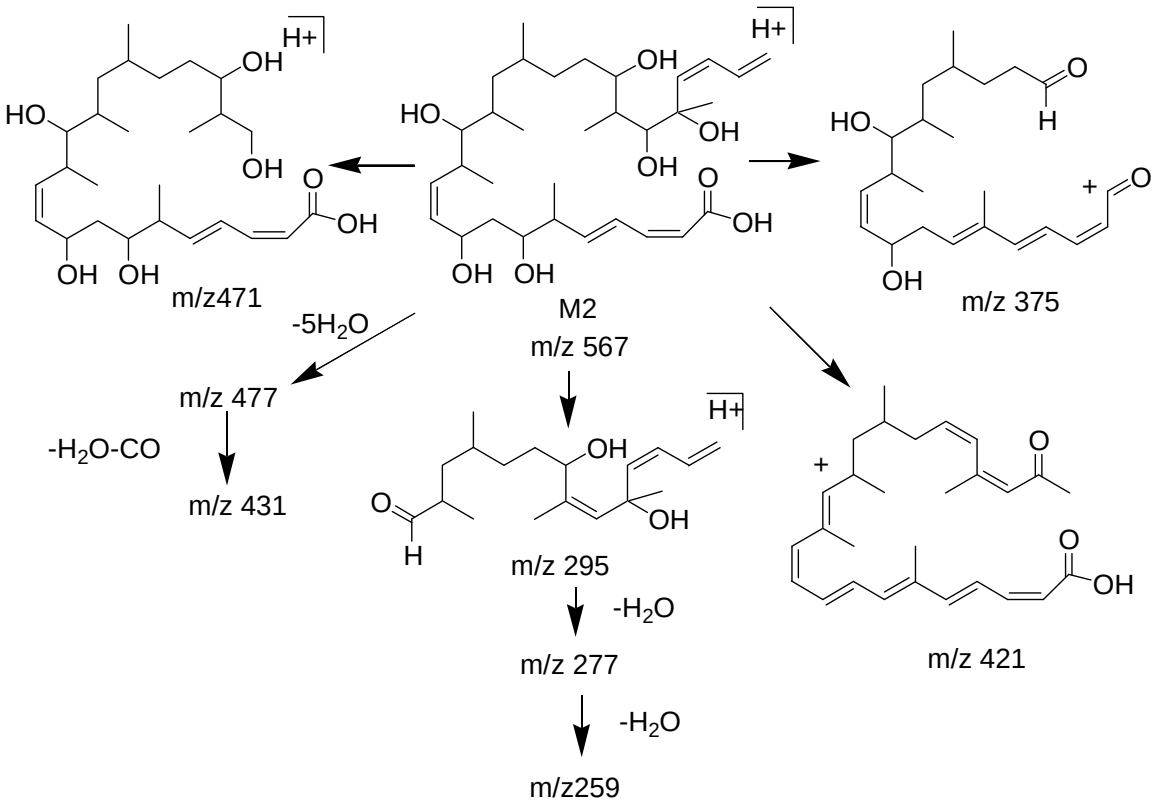

Figure 4.8 MS/MS fragmentation pathways of the protonated molecular ion of M2

Metabolite M3. M3 eluted after M2 and gave rise to the $[M+H]^+$ ion detected at *m/z* 549. The $[M+H]^+$ ion for M3 was 16 Da higher than that of (–)-dictyostatin, indicating M3 to be a monooxygenation metabolite. The MS/MS spectrum of M3 is presented in Figure 4.9. The fragment ion at *m/z* 295 corresponded to the cleavage of the C1-O and C12-C13 bonds and loss of a water molecule (see Figure 10). Elimination of another water molecule gave rise to the ion at *m/z* 277. Compared to the MS/MS spectrum of the parent compound, the ion at *m/z* 295 was 16 Da higher than (–)-dictyostatin's *m/z* 279 ion, which was presumed to be produced by the same cleavage. This implied that the oxygenation took place between C19-C26. The cleavage of the C9-C10 and C12-C13 bonds gave rise to the product ion at *m/z* 431, and subsequent loss of H_2O afforded the ion at *m/z* 413. The *m/z* 415 ion, presumed to be produced by the similar fragmentation pattern observed in the MS/MS spectrum of (–)-dictyostatin (Figure 4.3) was 16 Da higher than that from the parent molecule. This confirmed that the oxygenation occurred between C19 and C26. The loss of three H_2O produced the ion at *m/z* 495. The two most informative ions were observed at *m/z* 265 and *m/z* 465, which correspond, respectively, to the elimination of formaldehyde from the ions at *m/z* 295 and *m/z* 495. This strongly suggests that the hydroxylation occurred at one of the terminal methyl groups between C19 and C26. As with M1, it is possible that M3 was the hydroxyl derivative on 22-methyl group of (–)-dictyostatin after double bond migration. Double bond migration also generates another terminal methyl group on C25, a possibility that can not be excluded. The ion at *m/z* 393, produced by the cleavage of C1-O and C19-C20, was not detected in the MS/MS spectrum of M3. Instead, an ion at *m/z* 391 was observed. This ion can be explained by the cleavage of C21-O and C19-C20 and

elimination of H_2O. The reason why the fragmentation took place between C21-O instead of C1-O is possibly due to the influence of the migrated double bond.

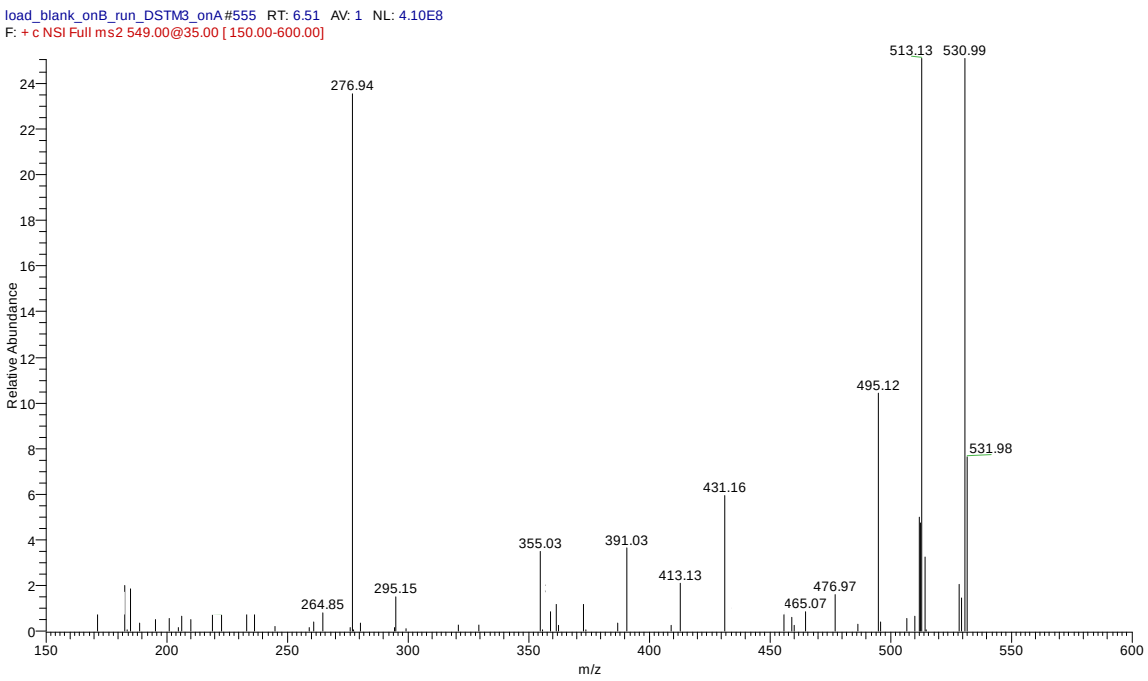

Figure 4.9 MS^2 spectrum of the protonated molecular ion (*m/z* 549) of metabolite M3.

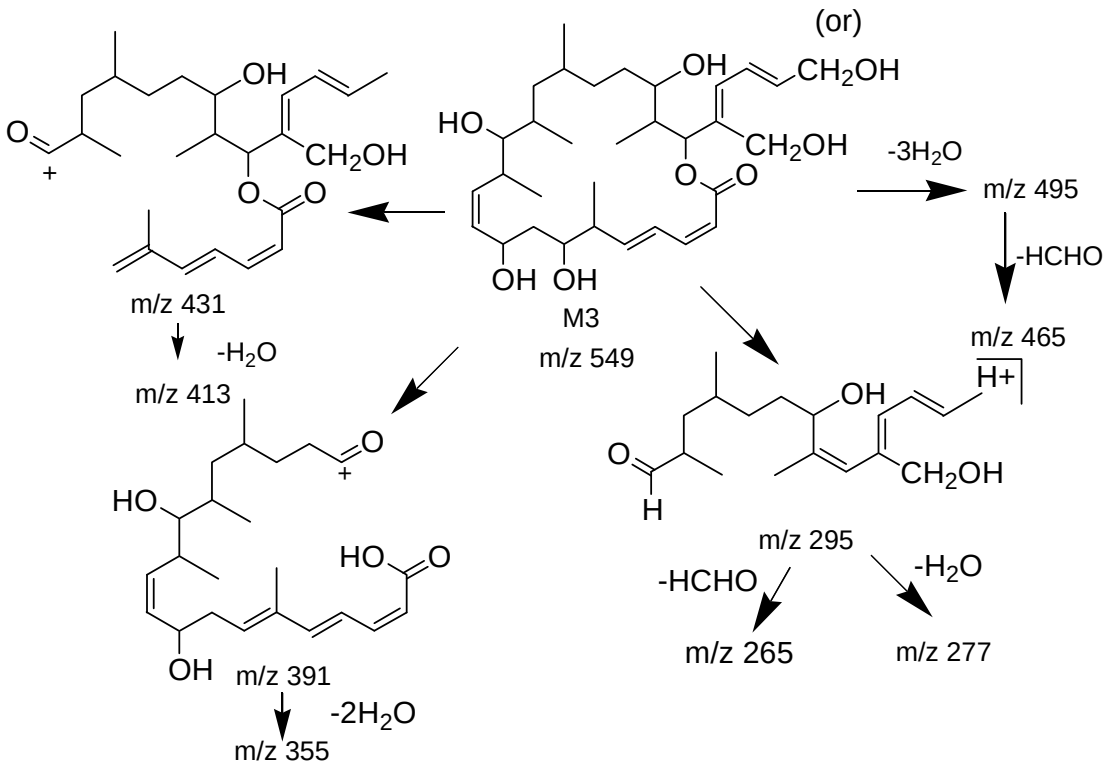

Figure 4.10 Tandem mass spectrometry fragmentation pathways of the protonated molecular ion of M3.

Metabolite M4. Metabolite M4 eluted after M3. The $[M+H]^+$ ion of M4 was observed at *m/z* 549, and the mass difference between M4 and the parent compound was 16 Da, indicating that M4 was a monooxygenation derivative. The fragmentation pattern of M4 was similar to that of M3 (see Figure 4.12). The MS/MS spectrum of M4 (Figure 4.11) exhibited two major fragment ions. One was at *m/z* 295, which corresponded to the cleavage of C12-C13 and C1-O. Subsequent elimination of H_2O from the *m/z* 295 ion gave rise to the *m/z* 277, *m/z* 259, and *m/z* 241 ions. The *m/z* 295 ion was 16 Da higher than the *m/z* 279 ion observed in the MS/MS spectrum of (–)-dictyostatin. This indicated that the oxygenation took place between C13-C26. The cleavage of C9-C10 and C12-C13 followed by the loss of water produced the ion at *m/z* 413.The same fragmentation pattern of the parent compound generated the ion at *m/z* 415. In addition, an intense signal was observed at *m/z* 469, 16 Da higher than the *m/z* 453 ion, produced by the cleavage C21-C22 as mentioned before, observed in the MS/MS spectrum of the parent compound. This difference indicated that the hydroxylation did not occur between C21 and C26. Therefore, the position of hydroxylation was between C13 and C20. It is highly possible that the hydroxylation took place on C20, which is more electrophilic than C13-C19. Therefore, M4 is proposed to be the 20-hydroxyl derivative of (–)-dictyostatin. The ion detected at *m/z* 359 confirms the structure. It corresponds to the cleavage of C1-O, C21-C22 and C6-C7. Subsequent elimination of CO gave rise to the ion of *m/z* 331. The typical fragment ion at *m/z* 393 was not observed in the MS/MS spectrum of M4. Instead, an ion at *m/z* 391 was detected. It can be explained by the cleavage of C21-O and C19-C20 and loss of H_2O. The reason why the ion was cleaved in C21-O but not in C1-O may be the same as for M3. Hydroxylation C20 would influence the cleavage of C21 and C19.

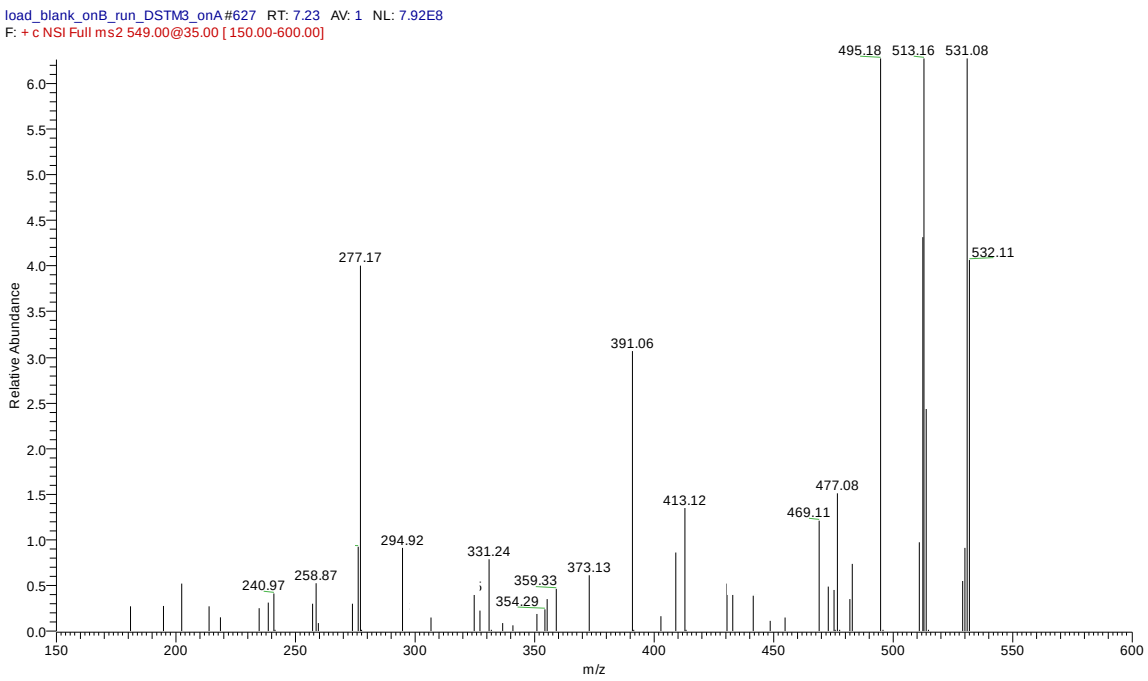

Figure 4.11 MS^2 spectrum of the protonated molecular ion (*m/z* 549) of metabolite M4.

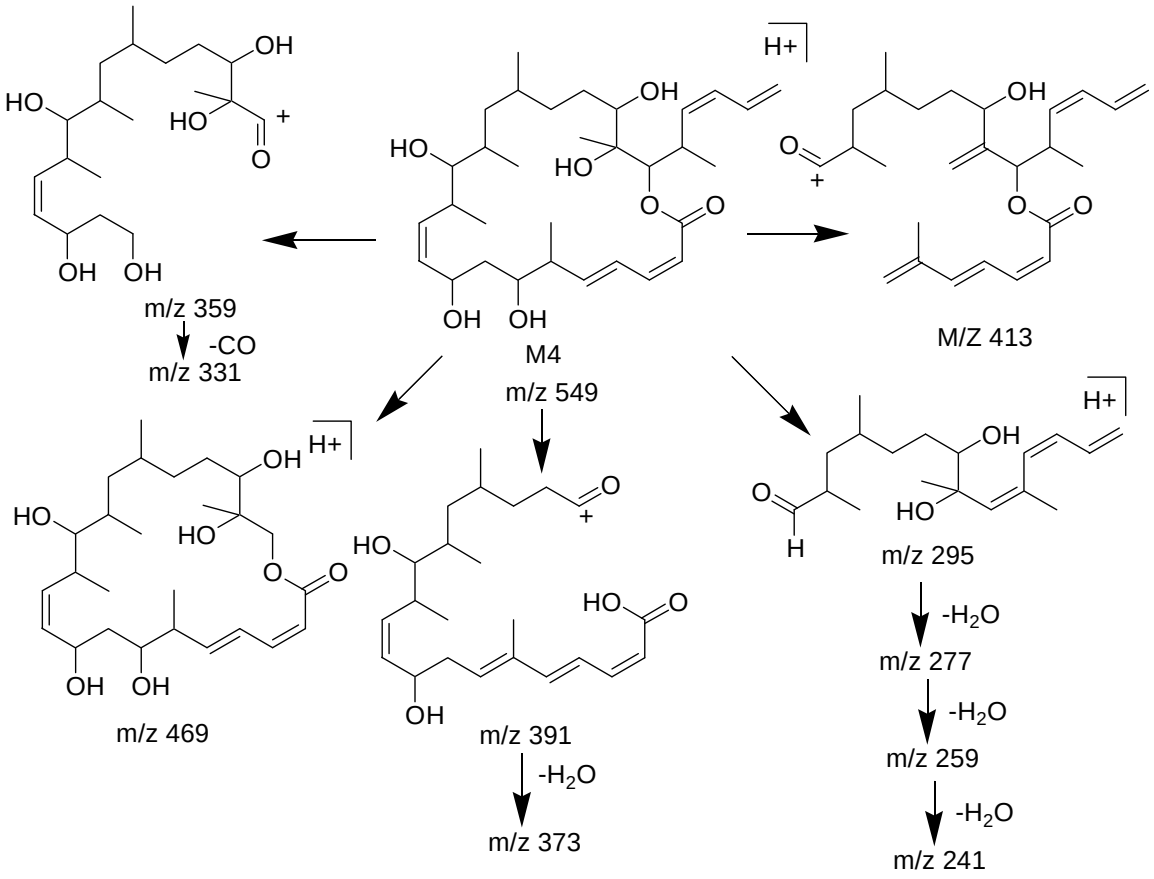

Figure 4.12 Tandem mass spectrometry fragmentation pathways of the protonated molecular ion of M4.

Metabolite M5. M5 eluted after M4 but before the parent compound. The $[M+H]^+$ ion of M5 was observed at *m/z* 549, 16 Da higher than that of parent compound, suggesting M5 to be a monooxgenation product of (–)-dictyostatin. Major fragment ions were detected at *m/z* 295, *m/z* 393, *m/z* 451, *m/z* 359 and *m/z* 309 (Figure 4.13). The ion at *m/z* 393 was produced by the cleavage of C1-O and C19-C20, also observed in the MS/MS spectrum of parent compound, indicating that the hydroxylation took place between C20-C26. Further loss of H_2O from *m/z* 393 gave the fragment ion at *m/z* 375. The appearance of the ion at *m/z* 295 supported the conclusion that the metabolism occurred between C20-C26. The ion at *m/z* 295 was generated by the cleavage of C12-C13 and C1-O, and the loss of a water molecule. The cleavage of C21-C22 and further loss of a water molecule gave rise to another important diagnostic ion at *m/z* 451. This observation suggested that the hydroxylation did not take place on between C21-C26, but rather on C21 itself or its methyl substituent. Hydroxylation of C21 has already been assigned to M4; therefore it is highly likely that M5 is hydoxylated on the terminal methyl group on C21. Subsequent loss of formaldehyde from the ion at *m/z* 295 gave rise to the most informative ion, at *m/z* 265, which strongly supports the structural assignment given to M5. The ion at *m/z* 359 was observed in MS/MS spectrum of M5, corresponding to the cleavage of C1-O, C21-C22 and C6-C7. The cleavage of C20-C21 and C6-C7 gave rise to the fragment ion at *m/z* 309. All these fragment ions were consistent with the assigned structure of M5 (see proposed fragmentation pathways in Figure 4.14).

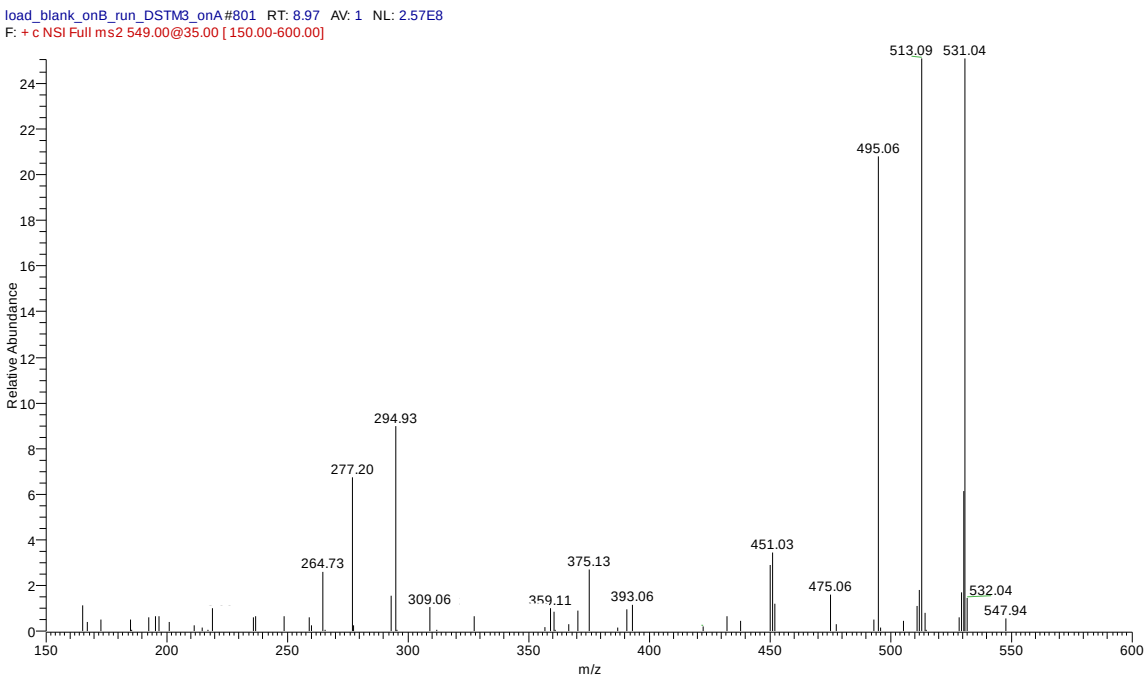

Figure 4.13 MS^2 spectrum of the protonated molecular ion (*m/z* 549) of metabolite M5.

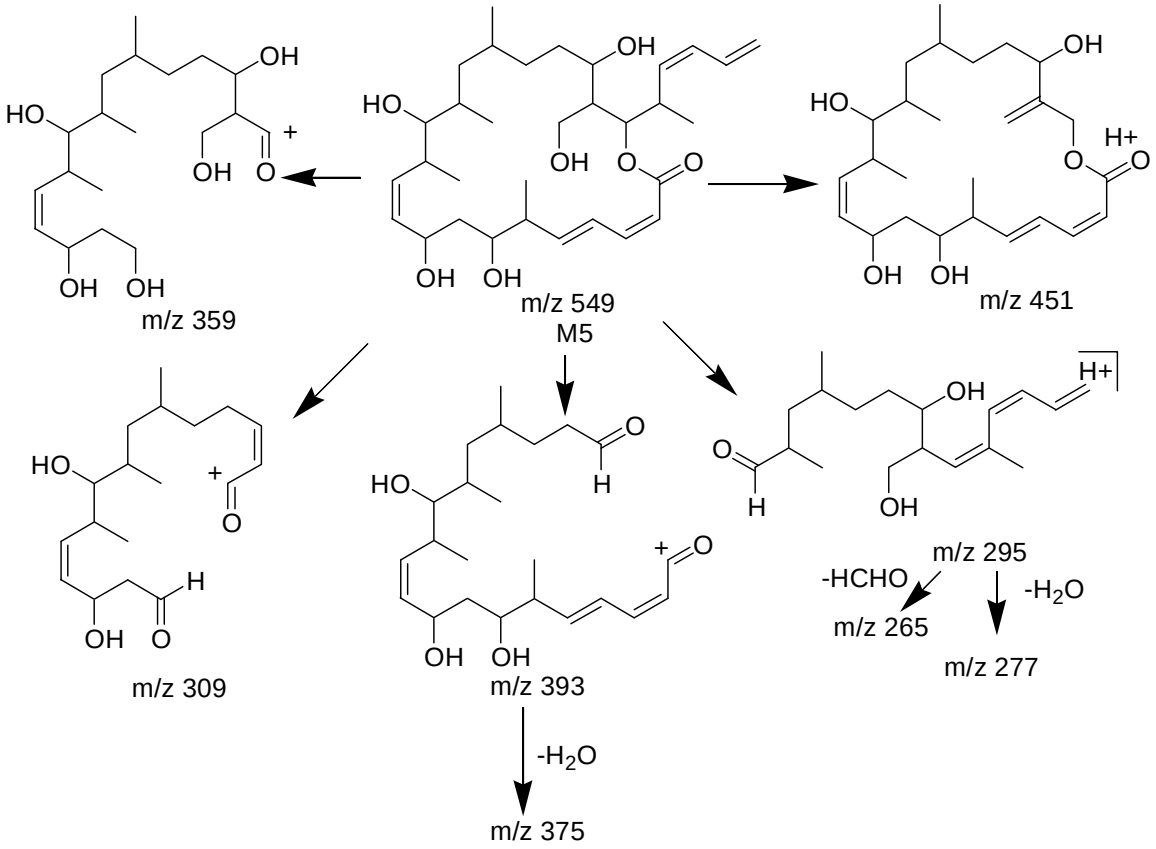

Figure 4.14 Tandem mass spectrometry fragmentation pathways of the protonated molecular ion of M5.

Metabolite M6. M6 was the only metabolite to elute after the parent compound. This indicated a lower polarity of M6 compared to the parent compound. M6 gave an $[M+H]^+$ ion at *m/z* 549, 16 Da higher than the parent compound, suggesting M6 to be a monooxygenation product. The lower polarity than the parent compound suggested that this was not a simple hydoxylation product. The MS/MS spectrum of M6 showed a product ion at *m/z* 279 (Figure 4.15), which corresponded to the cleavage of the C12-C13 and C1-O bonds and elimination of a water molecule. This implied that the oxidation did not take place between C13 and C26. The cleavage of the C1-O and C19-C20 bonds gave rise to the typical fragment ion at *m/z* 409, 16 Da units higher than that of parent compound. Further elimination of water from *m/z* 409 gave rise to the *m/z* 391 ion, suggesting that the oxidation occurred on a carbon between C1 and C12. The cleavage of the C21-C22 bond produced the ion at *m/z* 469. The most important diagnostic ion in the MS/MS spectrum of M6 was the high intensity ion observed at *m/z* 309. Further elimination of water from *m/z* 309 gave rise to the ion at *m/z* 291. This unusual ion at *m/z* 309 was structurally significant. Its existence implied the oxidation took place on a carbon between C6 and C12. It is therefore highly possible that M6 was generated by the epoxidation of the C10-C11 double bond followed by intramolecular attack by the C7-hydroxyl group to give a tetrahydrofuran derivative (see proposed biotransformation pathways of dictyostatin in Figure 4.17). The high intensity of the ion at *m/z* 309 can be explained by the stable furan ring formed after the cleavage of the C6-C7 and C20-C21 bonds followed by the loss of water molecules (Figure 4.16).

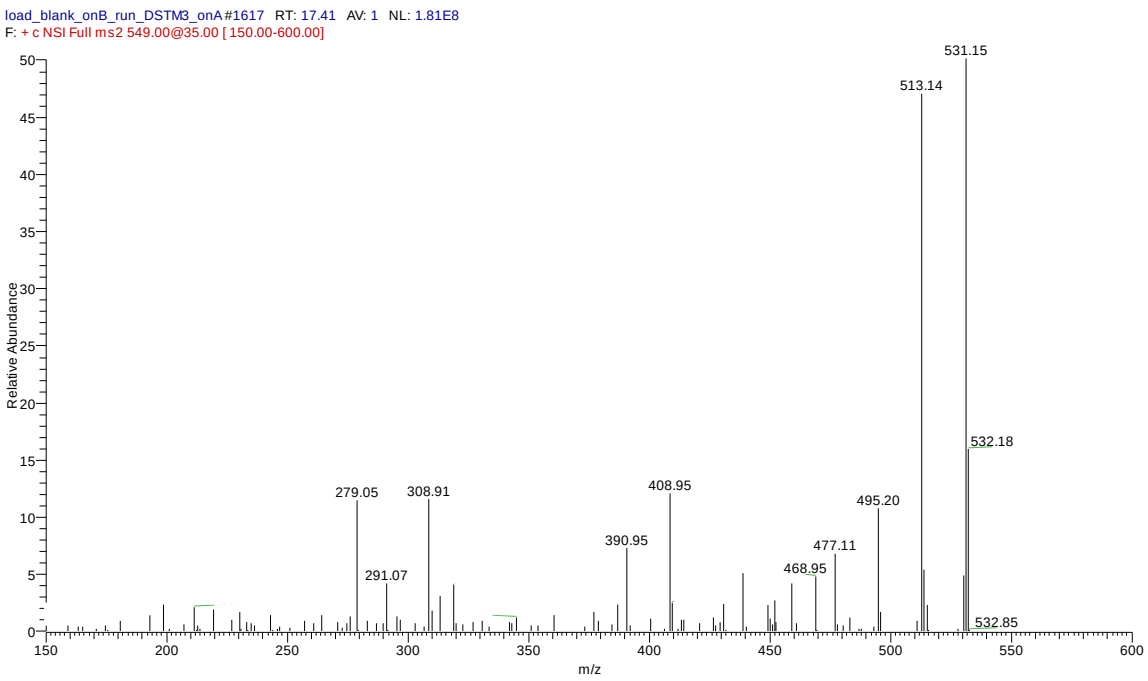

Figure 4.15 MS^2 spectrum of the protonated molecular ion (*m/z* 549) of metabolite M6.

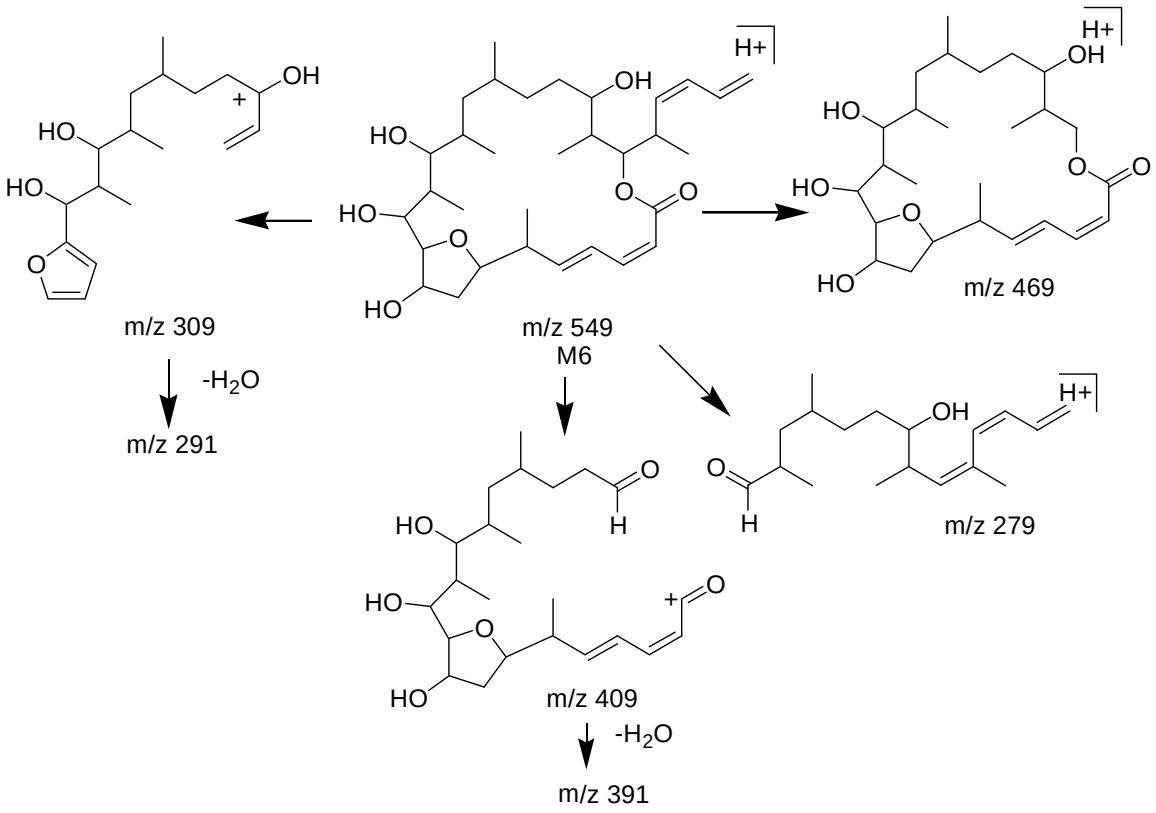

Figure 4.16 Tandem mass spectrometry fragmentation pathways of the protonated molecular ion of M6.

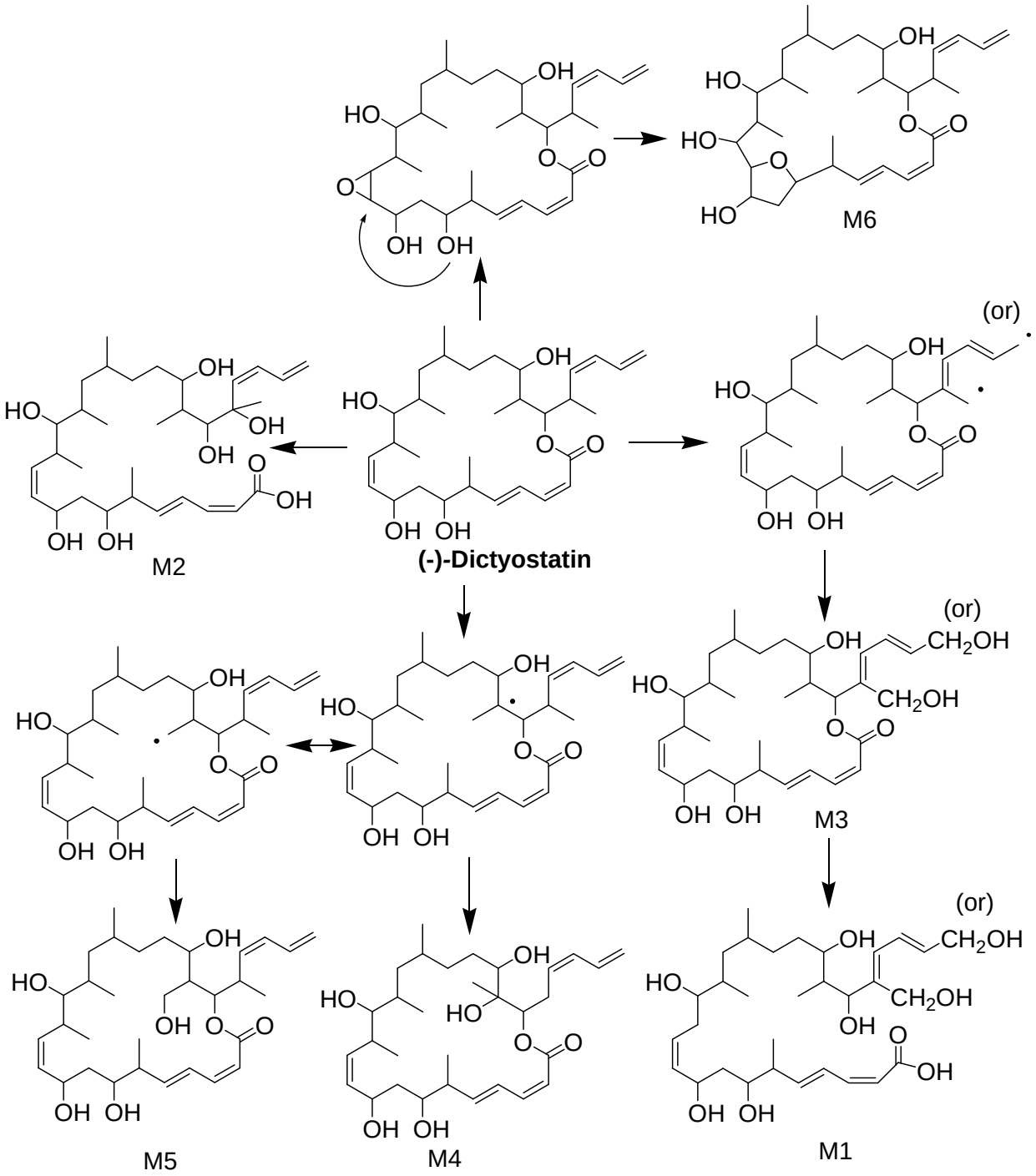

Figure 4.17 Metabolic pathways of (–)-dictyostatin catalyzed by pooled human liver microsomes.

4.4 DISCUSSION

The results presented here show that pooled human liver microsomes convert (–)-dictyostatin into at least six metabolites. The proposed biotransformation scheme is summarized in Figure 4.17. The structures of the identified metabolites indicate that macrolactone ring opening, which appears to proceed via hydrolysis of the lactone ester bond, is one of the main metabolic routes for (–)-dictyostatin. This was indeed due to microsomal enzymes, as ring opening did not occur when the microsomes were not in an activated state. Another main metabolic route is the oxygenation of the C20-C26 subunit. The epoxidation of the C10-C11 double bond following the attack of oxygen atom on C7 also leads to the unusual metabolite M6.

Oxygenation on C20-C26. Most of the metabolites of (–)-dictyostatin were identified to have a hydroxyl group on C20-C26, with or without lactone ring opening, by MS/MS experiments using 3D ion trap mass spectrometer. These oxidation products of C20-C26 were also the most abundant human liver microsomal metabolites of (–)-dictyostatin. Among these, hydroxylation of the terminal methyl group on C22 was an interesting pathway. The hydroxylation of the terminal methyl group on C22 formed the metabolite M1. The hydrolysis of the lactone ring of M3 led to the formation of metabolite M1. These two metabolites also showed evidence of double bond migration. These products were formed most likely due to the delocalization of the unpaired electron from C22 to the terminal methyl group of C22. This electron delocalization generated a radical on the terminal methyl group either on C22 or on C25. The unpaired electron on the terminal methyl group would be expected to be more stable than the unpaired electron on C22, and the steric hindrance for oxygen rebound from cytochrome P450 is much lower than that of C22. Therefore, the radical formed by double bond migration gave the most favorable electronic and steric considerations for the site of attack. This is a common type

of transformation observed in other allylic systems (Fischer IU, *et al*., 1990). Another interesting observation was the formation of metabolites M4 and M5. Metabolite M4 was the hydroxylation product on C20 formed through the classical hydrogen abstraction/oxygen-rebound mechanism. The two oxygen atoms on C21 and C19 provide an electron withdrawing influence on C20, making the hydrogen atom on C20 acidic and relatively easier to be abstracted by CYP enzymes. The following oxygen rebound onto C20 gave rise to the metabolite M4. However, the unpaired electron on C20 was likely not stable because of the two electron withdrawing groups on C19 and C21, and this unpaired electron was likely delocalized onto the terminal methyl group on C20. The radical structure formed by this delocalization was the favorable structure in terms of electronic and steric considerations. The following oxygen rebound generated the metabolite M5.

To help explain these results, the physical-chemical properties of (–)-dictyostatin and its metabolites were calculated by Cerius^2 (Accelrys, Inc). A summary of these parameters are shown in Table 4.2.

Table 4.2 Calculated parameters of (–)-dictyostatin and its metabolites

	ALogP98	**Dipole-mag**	**H bond accep**	**H bond donor**
(–)-dictyostatin	5.36	4.413	6	4
M1	3.87	10.146	8	7
M2	3.81	8.364	8	7
M3	4.48	6.003	7	5
M4	4.55	4.986	7	5
M5	4.37	3.027	7	5
M6	4.51	5.562	7	4

The calculated logP values for M1 and M2 suggested that these two metabolites have higher aqueous partitioning than the parent compound and other metabolites. Although the logP

values of M1 and M2 were close to each other, the dipole moment of M1 was higher than that of M2. Therefore, M1 eluted from the C18 column earlier than M2. The logP value of M3 was lower than that of M4, and the dipole moment of M3 was higher than that of M4, so there is no surprise that the retention time of M4 was longer than that of M3. The logP value of M5 was lower than those of M3 and M4; however, the dipole moment of M5 was much lower than those of M3 and M4. Meanwhile, the hydroxyl group on the terminal methyl group of C20 might form an intramolecular hydrogen bond with the oxygen atom on carbonyl group and decrease the H bond acceptor and donor properties of M5. Based on these considerations, the retention of M5 was later than those of M3 and M4.

Formation of the metabolite M6. Another type of metabolic reaction seen with (–)-dictyostatin was expoxidation of the double bond on C10-C11. This metabolic pathway was found to be the major route for the structurally related microtubule stabilizer (+)-discodermolide (Chapter 3). Although no intact epoxide metabolite was observed in the incubation mixture with human liver microsomes, the cyclization derivative of (–)-dictyostatin was envisioned to be formed by the attack on the epoxide moiety by the neighboring hydroxyl group on C7. Attack of this hydroxyl oxygen, depending upon which of the two carbons atoms in the oxirane ring is attacked, could lead to either a five- or a six-membered ring. However, only the relatively more stable five-membered ring system was observed. The epoxide intermediate could pose a toxicity risk as oxiranes are a potential target of endogenous nucleophiles. Although the calculated logP value and dipole moment of M6 was not too low, the later retention time of M6 might be explained by the formation of multiple intra-molecular hydrogen bonds amongst the hydroxyl groups on C9, C11 and C13. These multiple intra-molecular hydrogen bonds dramatically decrease the number of potential H bond-acceptor and -donor sites in M6.

Biotransformation pathways of (–)-dictyostatin and (+)-discodermolide. Based on their several structural similarities, (+)-discodermolide and (–)-dictyostatin likely interact with tubulin in the same or very similar ways. Previous studies show that the conformation of discodermolide as determined from NMR data when the molecule is incubated with tubulin is closely related to the solution structure of dictyostatin in water (Sanchez-Pedregal VM, *et al*., 2006). This result strongly implies that the interaction of these two compounds with CYP enzymes might also have common features. Not surprisingly, oxygenation products near the terminal diene group of discodermolide and the side chain diene group of dictyostatin were detected in these two compounds, and double bond migration took place on the diene groups of both of these compounds. Saturation of the diene group may increase the metabolic stability of dictyostatin, and a structure proposed for future synthesis is shown in Figure 4.18.

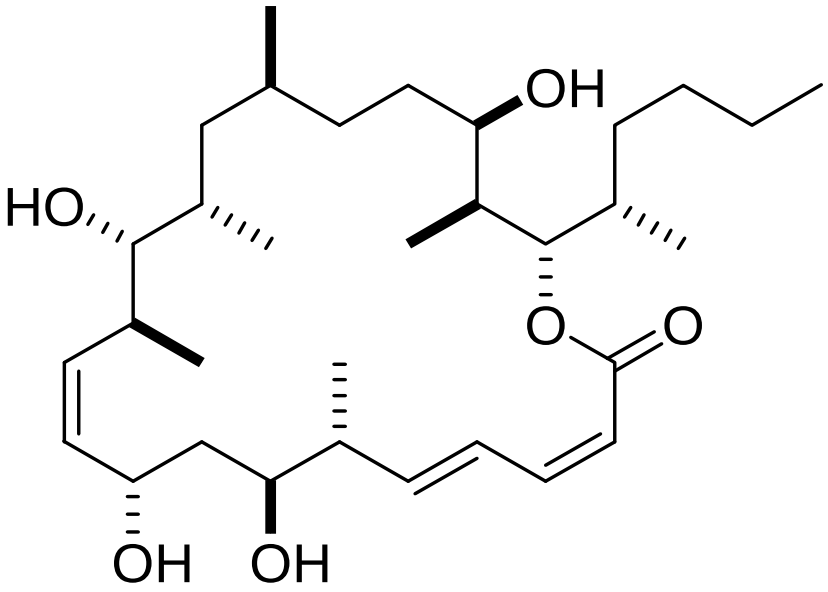

Figure 4.18 Proposed structure of an analogue of dictyostatin to be synthesized.

4.5 ACKNOWLEDGMENT

Supported in part by grants from the NIH (CA078039) and the DoD (TATRC USAMRMC 04145001).

5.0 METABOLIC STABILITY STUDIES OF (+)-DISCODERMOLIDE AND (-)-DICTYOSTATIN

5.1 INTRODUCTION

Historically, drugs have been discovered with much assistance from serendipity and luck. Recent advances in chemistry, molecular biology and computational chemistry have provided the means for rapid attainment of chemical diversity and both virtual and real high-throughput screening against biological targets (Burkhard P, 1999; Shuker SB, 1996; Kiyama R, 1999; Broach JR, 1996; Fernandes PB, 1998; Silverman L, 1998). Although high-throughput screening has substantially accelerated the drug discovery process, more than 40% of drug candidates fail during clinical trials because of unfavorable drug metabolism and pharmacokinetic properties (Brennan MB, 2000; Prentis RA, 1988; Cunningham MJ, 2000). Hence, evaluation of metabolic and pharmacokinetic properties in the drug discovery stage has been recognized as an important tool to enhance the success rates in clinic trial. In the present study, a metabolic stability screening approach (Obach RS, 1997) was used to determine the *in vitro* half-lives of the microtubule stabilizers (+)-discodermolide and (–)-dictyostatin. These half-life values were also converted to the *in vitro* CL_{int}' using a published forumula (Obach RS, 1999).

Discodermolide and dictyostatin are potent microtubule stabilizing agents from marine sponges. Both are promising candidates to be anticancer drugs. However, the pharmacokinetic

profile of discodermolide is less than desirable, and the studies described in Chapters 3 and 4 show that these two compounds are extensively metabolized by human liver microsomes. One of the objectives in this study was to determine the extent of metabolic biotransformation of these two compounds by hepatic metabolism enzymes. Therefore, one can decide whether it is worth modifying the chemical structures of these two compounds to improve their metabolism and pharmacokinetic properties.

5.2 MATERIALS AND METHODS

Chemicals. The compounds used as internal standards, NC2-165 [(1*S*,2*S*,3*R*,8*S*,9*R*,10*S*)-3,9-dihydroxy-14-(4*S*-hydroxy-3*R*,5*R*-dimethyl-6-oxotetrahydropyran-2*S*-yl)-1-isopropyl-2,8,10-trimethyltetradeca-6*Z*,11*Z*-dienyl carbamate] and WHJ-360 [(7*R*,8*S*,10*R*,13*S*,14*R*,15*S*,20*R*,21*S*,22*S*)-8,10,14,20-tetrahydroxy-7,13,15,21-tetramethyl-22-(1*S*-methylpenta-2*Z*,4-dienyl)oxacyclodocosa-3*Z*,5*E*,11*Z*,16*Z*-tetraen-2-one], prepared and reported elsewhere (Choy N, 2003; Jung, W-H, 2007), were obtained from Prof. Dennis Curran.

Microsomal Incubations. Pooled human liver microsomal incubations were repeated three times for each data point. Incubation mixtures (0.5 mL) contained 0.5 mg/mL of microsomal protein, 1 μM discodermolide or dictyostatin, and 100 mM phosphate buffer pH 7.4. The reaction was initiated by adding an NADPH regeneration system (BD Bioscience, San Jose, CA) that included 1.3 mM NADP+, 3.3 mM glucose-6-phosphate, 0.4 U/mL glucose-6-phosphate dehydrogenase, and 3.3 mM magnesium chloride. The incubation was carried out at

37 ºC. Aliquots (50 µL) were removed at different time points (0, 2, 4, 8 and 10 min) and the reaction was stopped in each aliquot by addition of 50 µL of cold methanol containing the respective internal standard (for discodermolide, the internal standard was 0.5 µM NC2-165; for dictyostatin, the internal standard was 0.05 µM WHJ360). Precipitated proteins were pelleted by centrifugation and the supernatant was used for analysis. Controls were the incubation without microsomal protein or without NADPH.

LC-MS/MS analysis. The LC-MS/MS experiments were performed on a Thermo Finnigan TSQ Quantum Ultra triple quadrupole system. The spray voltage used was 3.8 kV and the scan mode was positive selective reaction monitoring (SRM) mode. The parameters of the mass spectrometer were optimized for each compound (Table 5.1). Separation was performed on a C18 YMC ODS-AQ (2.0 mm × 150 mm) column. The flow rate was 200 µL/min and the injection volume was 10 µL. Mobile phase A was water containing 0.1% formic acid, and mobile phase B was acetonitrile containing 0.1% formic acid. The gradients used for discodermolide and dictyostatin are given in Table 5.2. The retention times observed for discodermolide and its internal standard, NC2-165, were 4.19 min and 4.64 min, respectively. The retention times observed for dictyostatin and its internal standard, WHJ360, were 5.77 min and 5.71 min, respectively.

Table 5.1 Mass spectrometry conditions for discodermolide and dictyostatin in this analysis.

	Capillary Temperature	**MS/MS (*m/z*)**	**Collision Energy**
Discodermolide	300°C	594.000→334.074	15V
NC2-165	300°C	512.000→415.256	15V
Dictyostatin	320°C	533.000→497.173	16V
WHJ360	320°C	517.000→481.251	16V

Table 5.2 HPLC gradients for for discodermolide and dictyostatin in this analysis.

	Discodermolide		**Dictyostatin**	
Gradient	**A**	**B**	**A**	**B**
0 min	85%	15%	80%	20%
4 min	10%	90%	10%	90%
6 min	10%	90%	10%	90%
6.1 min	85%	15%	80%	20%
11 min	85%	15%	80%	20%

A: 0.1% formic acid/H2O

B: 0.1% formic acid/ACN

Retention times: Discodermolide, 4.19 min; NC2-165, 4.64 min

Dictyostatin, 5.77 min; WHJ360, 5.71 min

5.3 RESULTS

LC-MS/MS analysis using a triple quadrupole mass analyzer system is a powerful, and the most widely accepted, instrumental arrangement to perform mass spectrometric quantitative analyses. The high sensitivity and selectivity of such instruments allows for the quantitation of compounds present at low concentration in biological matrices. In the present case, the highest concentration of the compounds was 1 μM in a human liver microsomal reaction mixture. For this metabolic stability study, the triple quadrupole system was considered to be the best available tool.

For quantitative purposes, the analogues of discodermolide and dictyostatin, NC2-165 and WHJ360, were respectively used as the internal standards for these two drugs because of their respective similarities to the compounds of interest. The chemical structures of discodermolide and its internal standard, NC2-16, are shown in Figure 5.1, and the chemical structures of dictyostatin and WHJ-360 are shown in Figure 5.2. Figures 5.3 and 5.4 show these similarities in that the retention times of discodermolide and NC2-165 as well as those of dictyostatin and WHJ360.

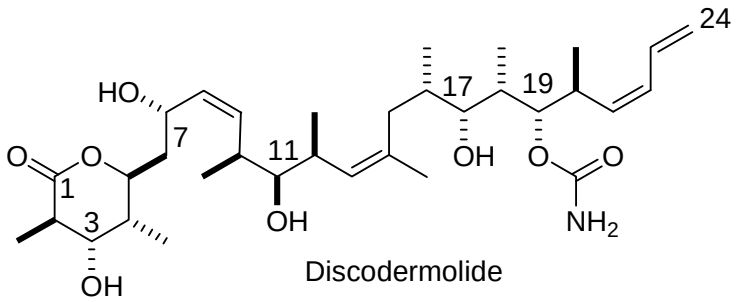

Discodermolide

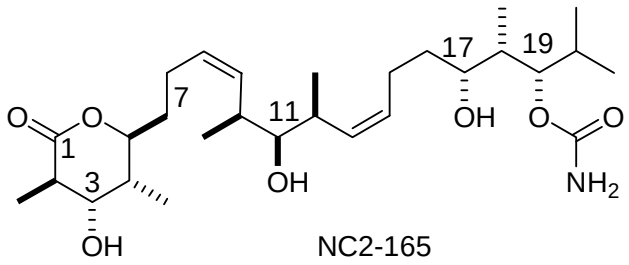

NC2-165

Figure 5.1 Chemical structures of discodermolide and NC2-165.

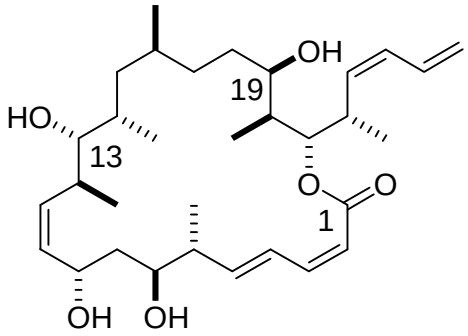

(–)-Dictyostatin

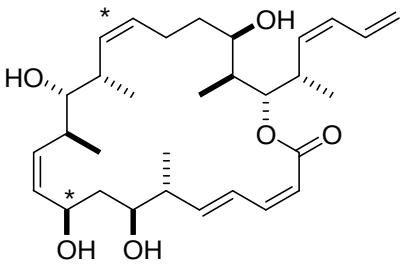

WHJ360

Figure 5.2 Chemical structures of dictyostatin and WHJ360.

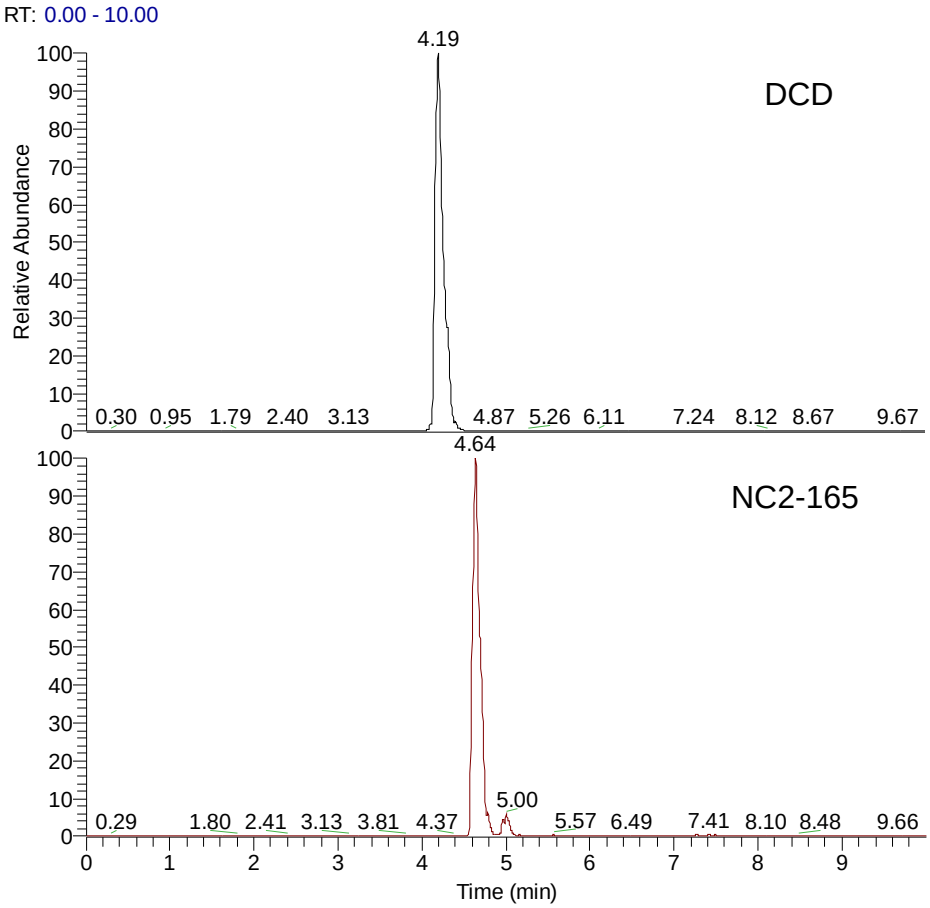

Figure 5.3 HPLC chromatograms of discodermolide (DCD) and its internal standard NC2-165.

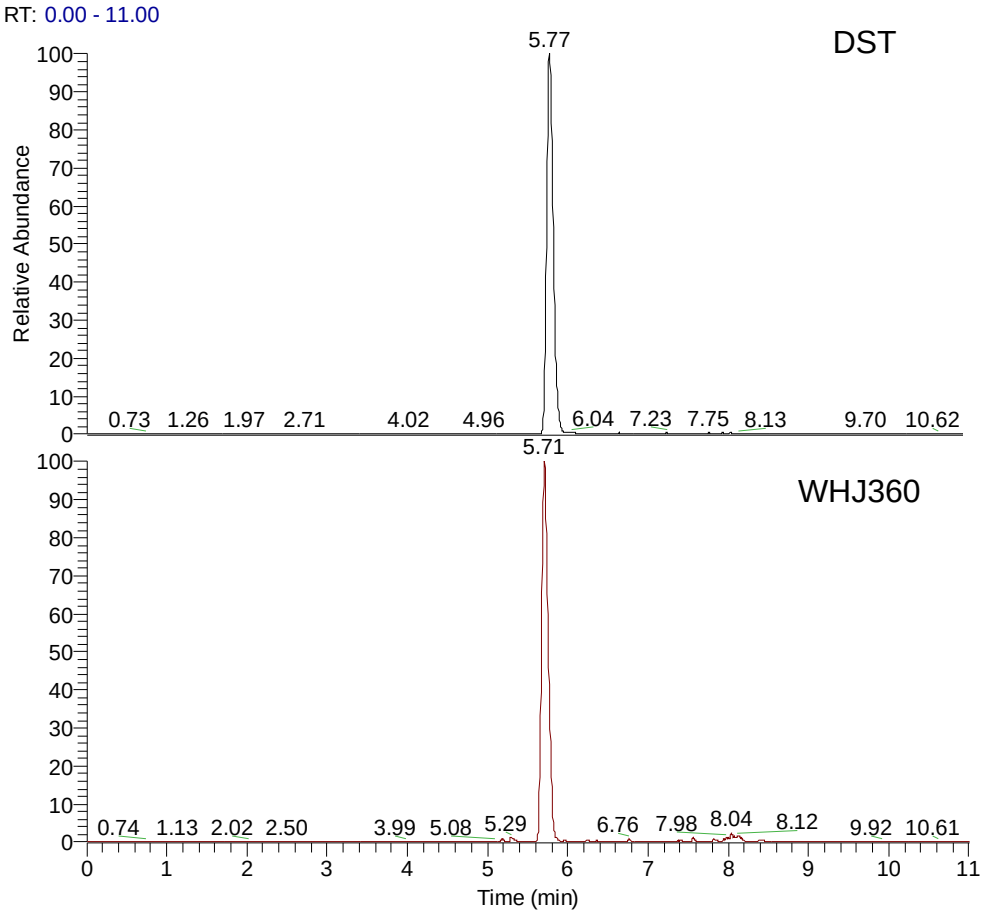

Figure 5.4 HPLC chromatograms of dictyostatin (DST) and its internal standard WHJ360.

The metabolic stability profiles for discodermolide and dictyostatin are shown in Figures 5.5 and 5.7, respectively. The x-axis shows time of incubation and the y-axis the percentage of parent drug remaining compared with the analyte/internal standard peak area ratio at t = 0 (assigning t = 0 as 100%). The k values for discodermolide and dictyostatin were determined by linear regression (Figures 5.6 and 5.8). The calculated k values for the two drugs are shown in Table 5.3.

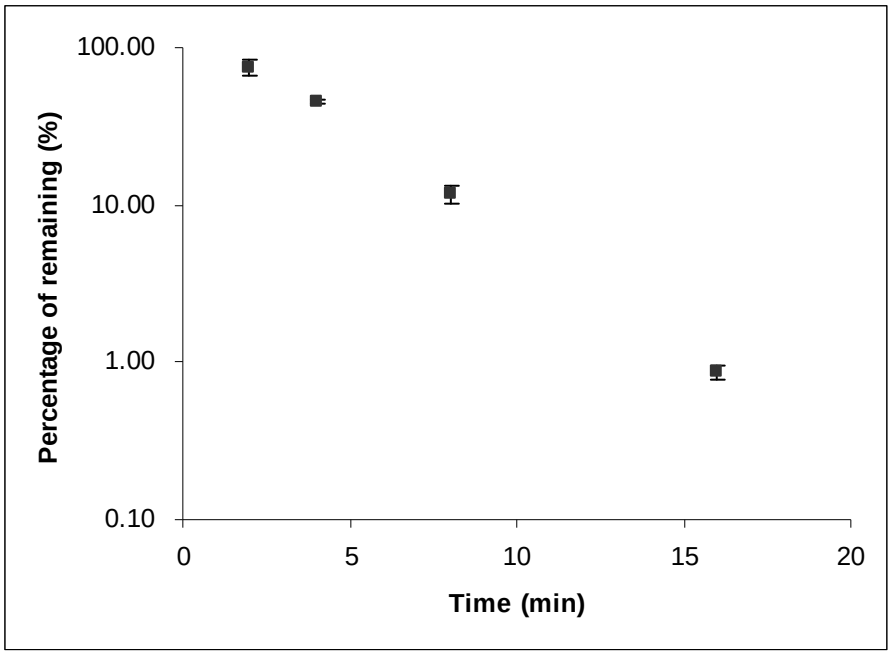

Figure 5.5 Metabolic stability profile for discodermolide (n = 3).

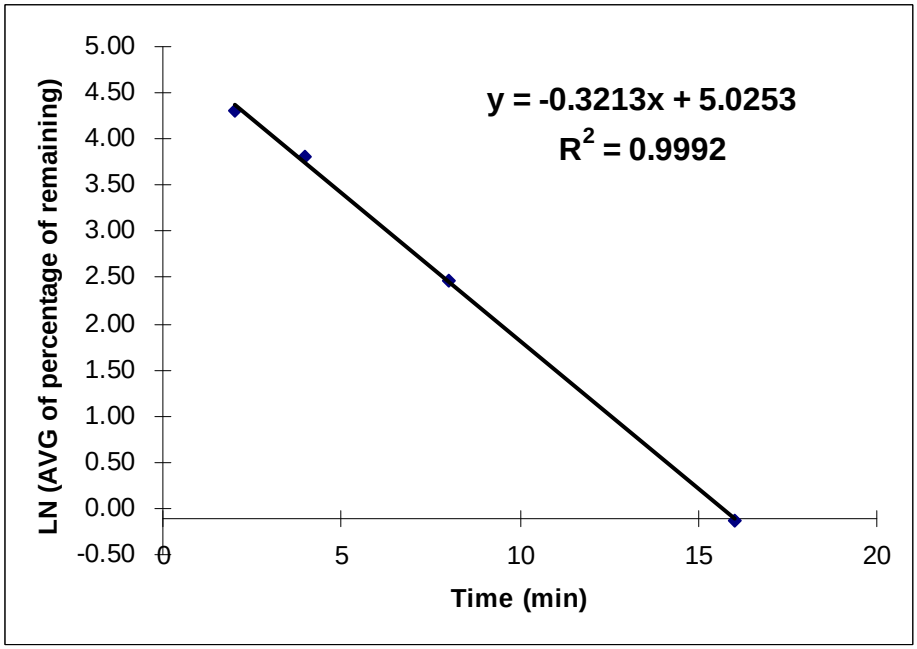

Figure 5.5 Determination of the slope (-k) of the linear regression from ln percentage remaining versus incubation time relationship for discodermolide.

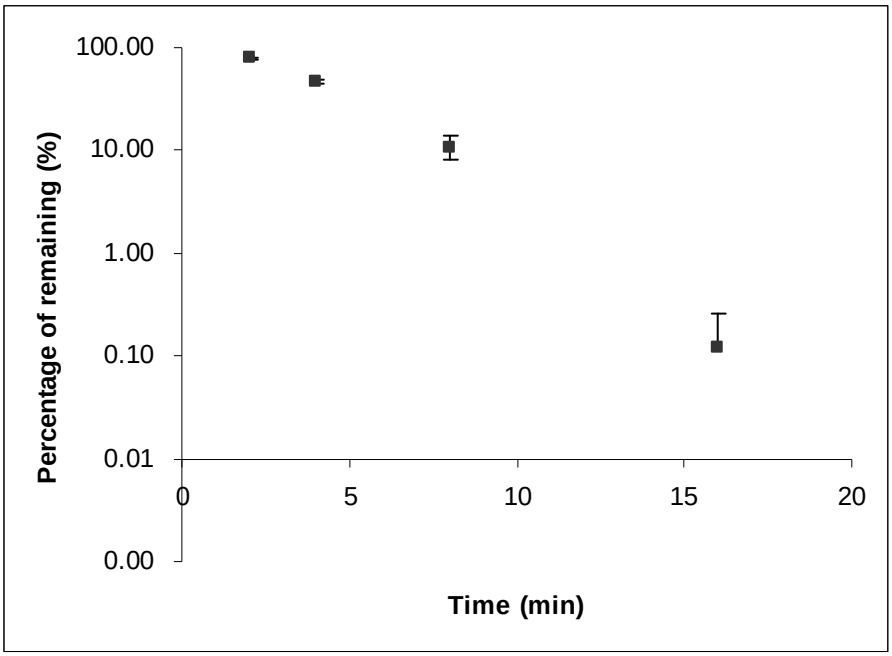

Figure 5.7 Metabolic stability profile for dictyostatin (n = 3).

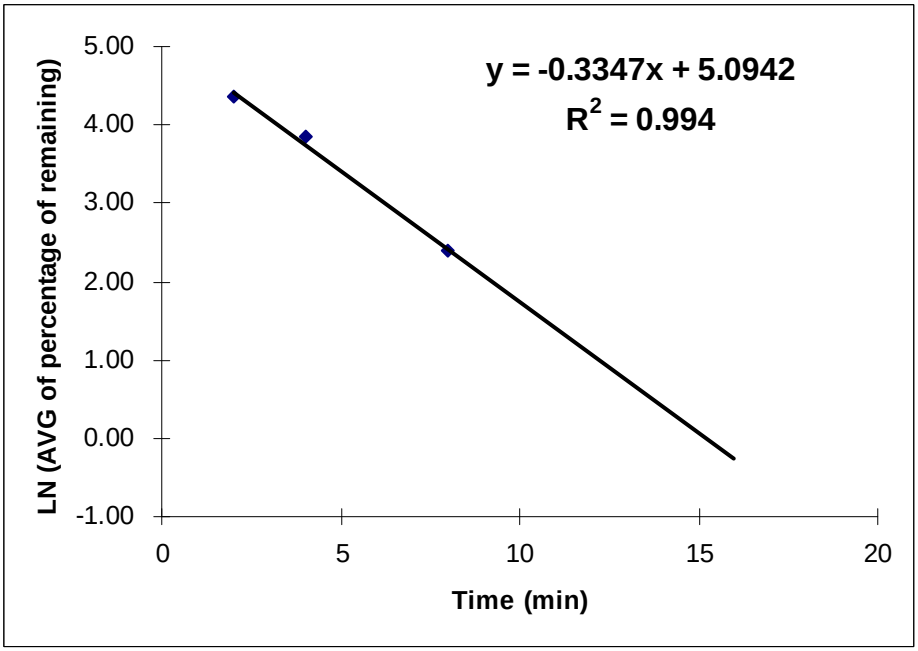

Figure 5.6 Determination of the slope (-k) of the linear regression from ln percentage remaining versus incubation time relationship for dictyostatin.

Table 5.3 Summary of parameters for metabolic stabilities of discodermolide and dictyostatin.

	Discodermolide	**Dictyostatin**
K (min^{-1})	0.321	0.335
$T_{1/2}$ (min)	2.2	2.1
CL_{int}' (ml/min/kg)	396	378

These k values were converted to *in vitro* half lives $t_{1/2}$ (Table 5.3). The $t_{1/2}$ values were calculated using the slope value k as follows:

$t_{1/2} = -0.693/k$

The short half lives of discodermolide and dictyostatin indicated that their *in vivo* clearance might be high. The intrinsic clearance (CL_{int}') was calculated using the following formula (Obach RS, 1999):

CL_{int}'= (0.693/*in vitro* $t_{1/2}$)*(mL of incubation/mg of microsomal protein)*(45 mg microsomes/g liver)*(20 g liver/kg body weight)

5.4 DISCUSSION

The metabolic transformation of drugs represents one of the major pathways by which they are cleared from the body. Metabolic transformation usually includes two phases, Phase I and Phase II transformation. The purpose of metabolic transformation is to increase the polarity of xenobiotics, including drugs, and enhance their clearance from the body. Oxidation, reduction and hydrolysis reactions belong to Phase I category of metabolic reactions. In the drug discovery stage, it is impossible to obtain metabolic transformation information from humans. Also and unfortunately, studies from laboratory animals do not always accurately reflect what happens in human beings, partially because of the differences in drug-metabolism enzymes. Hence, the use of *in vitro* drug metabolizing systems to predict *in vivo* pharmacokinetic behavior has become an increasingly accepted part of drug discovery (Houston JB, 1994; Houston JB, 1997). The enzymes that metabolize drugs are distributed amongst the different organs and tissues, such as liver, intestine, kidney, lung and brain. Since the human liver is the major organ of drug metabolism in man, human liver-derived systems are the primary models used for studying drug metabolism. These systems include recombinant forms of the enzymes found in the liver, primary human hepatocytes, immortalized human hepatic carcinoma cell lines, liver slices, and human liver microsomes. Among these systems, the liver microsomal system is the most commonly chosen due to its several conveniences, particularly long shelf life (in a –80 ^{o}C freezer or liquid nitrogen storage). Human liver microsomes can not only be used predict the metabolic stability of a compound in humans, but also the body clearance, if the prediction meets the following assumptions: 1) metabolic clearance is the major pathway of total body clearance and the liver is the major organ of clearance; 2) oxidative metabolic transformation is the major route compared to other metabolic pathways such as Phase II metabolism; and 3) the rates of

metabolism and enzyme activities *in vitro* reflect those found *in vivo*. Usually, intrinsic clearance is obtained using kinetic data in the forms derived from the Michaelis-Menten equations (i.e., Vm/Km). However, such enzyme kinetic data is not always available in the discovery stage, especially in early points of the process because metabolite standards are not generally available. One of the simplest methods to predict human clearance is the *in vitro* half-life method used here (Obach RS, 1997). The *in vitro* $t_{1/2}$ approach is based on two assumptions, that: 1) the apparent Km is far above the concentration of substrates used; and 2) there is no substrate inhibition or mechanism-based inhibition.

The objective of this work in this chapter was to establish the metabolic stability screening method to select compounds with relatively low clearance for further development in microtubule stabilizing drug discovery. The second objective, as described in previous chapters, was to find the metabolic soft spots on discodermolide and dictyostatin so that future analogues could be designed with improved pharmacokinetic properties. The results indicate that discodermolide and dictyostatin are compounds that should have high hepatic clearance, and show that the compounds are extensively metabolized by human liver microsomes. Modification of these two compounds by substitution of metabolically stable groups that do not negatively alter their biological activity may be a promising strategy to find potent anticancer drugs with the acceptable pharmacokinetic properties.

5.5 ACKNOWLEDGMENT

Supported in part by grants from the NIH (CA078039) and the DoD (TATRC USAMRMC 04145001).

6.0 SUMMARY

Drug metabolism is an interdisciplinary science that involves the diverse research areas of chemistry, biochemistry, toxicology and analytical chemistry. Recently, the recognition of metabolic liabilities of drugs has attracted attention, moving the field closer to the starting points in drug discovery and development. In most cases, drug metabolism results in more hydrophilic metabolites without biological activity that are more easily cleared from body, and are regarded as detoxification pathways. Sometimes biotransformation of the parent drugs can, however, lead to the formation of reactive metabolites, which represent an underlying mechanism that gives rise to adverse drug reactions. Most of these bioactivation reactions can be attributed to cytochrome P450 enzymes, but, as seen in Chapter 1, some other oxidative enzymes such as myeloperoxidase can give rise to reactive metabolites.

The possible mechanism(s) by which etoposide causes secondary leukemias have been studied for many years, yet the true answers to this mystery are still unclear. In this dissertation, a chemically reactive metabolite, etoposide *ortho*-quinone, was detected in HL60 cells. This reactive metabolite can react with the endogenous antioxidative barrier, glutathione, non-enzymatically. The experiments demonstrated that the formation of the GSH adduct of etoposide *ortho*-quinone in HL60 cells was myeloperoxidase-dependent. The characterization of the GSH adduct of etoposide *ortho*-quinone in HL60 cells was performed using a 3D ion trap LC-MS instrument. This adduct was synthesized using normoisotopic materials. Comparison of the mass

spectra gave confidence regarding the structure of the adduct. The adduct was also synthesized in stable isotope-labeled form for use as an isotope dilution mass spectrometric internal standard.The ability to detect, characterize, and quantify the GSH adduct in intact HL60 cells was demonstrated with these tools. These studies and the stable isotope labeled adduct will be important for future investigations of the mechanism(s) of etoposide-associated secondary leukemias and for estimating the risk of treatment-related secondary leukemias. Future studies will likely focus on developing an understanding of the role of etoposide metabolites in the myeloid leukemogenic process that is frequently associated with the clinical use of this antineoplastic agent. In this study, H_2O_2 was added to HL60 cells, found to increase the rate and extend of the reaction of etoposide with MPO. An alternative way to increase the concentration of H_2O_2 in HL60 cells would be to use an inhibitor of catalase, such as 3-Aminotriazole.

In the early stages of drug discovery and development, it is important to identify metabolic soft spots on lead compounds. Low metabolic stability is a warning sign to medicinal chemists that they should modify their chemical structures in order to reduce metabolic rate as early as possible. Discodermolide and dictyostatin are two potent microtubule stabilizing agents derived from marine sponges. Although they have tremendous biological potency in vitro, they are extensively metabolized by CYP enzymes, which is interpreted here as being of low metabolic stabilities. Eight metabolites of discodermolide were detected after incubation with pooled human liver microsomes. The diene group on discodermolide was identified as a metabolic soft spot. Substitution of the diene group with a saturated system could therefore possibly decrease the metabolic rate and improve the drug's metabolic and pharmacokinetic properties. If potency is retained in such an analogue, the dose needed could therefore also

possibly be reduced and, hopefully, also any toxicities caused by discodermolide. Such analogues have already been reported.

Previous studies have shown that a lactone ring-unsaturated analogue of discodermolide has more biological potency. In the present study, a related lactone ring metabolite of discodermolide was formed by pooled human liver microsomes. An unsaturated lactone ring analogue of discodermolide might be a promising agent, as it would be expected to have higher metabolic stability (and perhaps even efficacy).

At least six metabolites of dictyostatin were formed in the *in vitro* microsomal system. The chemical structures of dictyostatin and discodermolide share many similarities. After the examinations done with discodermolide, it came as no surprise that the exocyclic diene group of dictyostatin was also found to be a metabolic soft spot. As with discodermolide, an analogue with a saturated version of these two double bonds may represent a promising way to increase metabolic stability.

Another goal of this work was to establish a metabolic stability assay in the lab. In order to identify the compounds with optimal drug-like properties, a medicinal chemist should consider not only biological activity and potency, but also metabolic properties. The biotransformation of drug molecules is one of key processes by which drugs are cleared from the body. The liver microsomal system used here is a common experimental tool for the *in vitro* study of metabolic stability because the system is easy to prepare and use. For such studies, however, the requisite analytical instrument is a triple quadrupole LC-MS/MS system. Fortunately, one became available for use near the end of these dissertation studies. The results showed that the metabolic rate of discodermolide and dictyostatin were high *in vitro* and the half lives of these two compounds were within 10 minutes. The result also indicated that chemical

structure modification to discodermolide and dictyostatin should be made in order to improve their metabolic and pharmacokinetic properties.

As mentioned early on in this dissertation, nuclear magnetic resonance (NMR) is often a necessary method to be used to generate more detailed information, especially for stereochemistry. NMR studies were not performed here, however, due to the limited amount of compounds available and the avaibility of a high field NMR spectrometer. Future studies will almost certainly be focused on the elucidation of the stereochemistry of the metabolites of discodermolide and dictyostatin using high field NMR.

The CYP enzymes responsible for the formation of the metabolites of discodermolide and dictyostatin were not determined in this study because neither metabolite standards nor isotopically labeled parent compounds were available. Future steps should be: 1) synthesis of the metabolites of discodermolide and dictyostatin; 2) preparation of stable isotope labeled forms of discodermolide and disctystatin for quantitative studies; and 3) determination, through inhibitor (antibodies and/or competitive inhibitors) studies, of the CYP enzyme(s) responsible for the metabolism.

APPENDIX A

LIST OF ABBREVIATIONS & SPECIALIZED NOMENCLATURE

MPO	Myeloperoxidase
GSH	Glutathione
Topo II	Topoisomerase II
HL60 cells	Human Leukemia 60 cells
SA	Succinylacetone
MLL	Mixed lineage leukemia genes
t-AML	Treatment-related acute myeloid leukemias
MALDI	Matrix-assisted laser dissociation ionization
Q-TOF	Quadrupole-time of flight
ESI	Electrospray ionization
XIC	Extracted ion chromatogram
NMR	Nuclear magnetic resonance spectroscopy
IR	Infrared spectrscopy
CYP450	Cytochrome P450
FMO	Flavin-containing monoxygenase

MAOs	Monoamine oxidases
UGT	UDP-glucuronosyltransferase
P-gp	P-glycoprotein
DCD	Discodermolide
DST	Dictyostatin
CL	Clearance
CLint’	Intrinsic clearance

BIBLIOGRAPHY

Aplan PD, Chervinsky DS, Stanulla M, Burhans WC (1996) Site-specific DNA cleavage within the MLL breakpoint cluster region induced by topoisomerase II inhibitors. *Blood* **87**:2649-2658.

Banks AT, Zimmerman HJ, Ishak KG and Harter JG (1995) Diclofenac-associated hepatotoxicity: analysis of 180 cases reported to the Food and Drug Administration as adverse reactions. *Hepatology* **22**:820–827.

Banoglu E (2000) Current status of the cytosolic sulfotransferases in the metabolic activation of promutagens and procarcinogens. *Curr Drug Metab* **1:**1-30.

Bonierbale E, Valadon P, Pons C, Desfosses B, Dansette PM, and Mansuy D (1999) Opposite behaviors of reactive metabolites of tienilic acid and its isomer toward liver proteins: use of specific anti-tienilic acid-protein adduct antibodies and the possible relationship with different hepatotoxic effects of the two compounds. *Chem Res Toxicol* **12:**286-296.

Bougie D, Johnson ST, Weitekamp LA, and Aster RH (1997) Sensitivity to a metabolite of diclofenac as a cause of acute immune hemolytic anemia. *Blood* **90**:407–413.

Brennan MB (2000) Drug discovery. Filtering out failures early in the pipeline. *Chem Eng News* **5**: 63-73.

Broach JR, Thorner J (1996) High-throughput screening for drug discovery. *Nature* **384**: 14-16.

Brown KE, Brunt EM, Heinecke JW (2001) Immunohistochemical detection of myeloperoxidase and its oxidation products in Kupffer cells of human liver. *Am J Pathol* **159:**2081-2088.

Burkhard P, Hommel U, Sanner M, Walkinshaw MD (1999) The discovery of steroids and other novel FKBP inhibitors using a molecular docking program. *J Mol Biol* **287**: 853-858.

Calderoni A, Cerny T (2001) Taxanes in lung cancer: a review with focus on the European experience. *Crit Rev Oncol Hematol* **38**: 105-127.

Cashman JR (2000) Human flavin-containing monooxygenase: substrate specificity and role in drug metabolism. *Curr Drug Metab* **1:**181-191.

Chen LJ, DeRose EF, Burka LT (2006) Metabolism of furans in vitro: Ipomeanine and 4-ipomeanol. *Chem Res Toxicol* **19:**1320-1329.

Choy H (2001) Taxanes in combined modality therapy for solid tumors. *Crit Rev Oncol Hematol* **37**: 237-247.

Choy N, Shin Y, Nguyen P-Q, Curran DP, Balachandran R, Madiraju C, Day BW (2003) Simplified discodermolide analogs: synthesis and biological evaluation of 4-*epi*-7-dehydroxy-14,16-didemethyl-(+)-discodermolides as microtubule-stabilizing agents. *J Med Chem* **46**: 2846-2864.

Chung MH, Kim HS, Ohtsuka E, Kasai H, Yamamoto F, and Nishimura S (1991) An endonuclease activity in human polymorphonuclear neutrophils that removes 8-hydroxyguanine residues from DNA. *Biochem Biophys Res Commun* **178**:1472-1475.

Clarke JB, Neftel K, Kitteringham NR, Park BK (1991) Detection of antidrug IgG antibodies in patients with adverse drug reactions to amodiaquine. *Int Arch Allergy Appl Immunol* **95:**369-375.

Clarke NJ, Rindgen D, Korfmacher WA, Cox KA (2001)Systematic LC/MS metabolite identification in drug discovery. *Anal Chem* **73**:430A-439A.

Cunningham MJ (2000) Genomics and proteomics: The new millennium of drug discovery and development. *J Pharmacol Toxicol Methods* **44**: 291-300.

Dachtler M, Glaser T, Kohler K, Albert K (2001) Combined HPLC-MS and HPLC-NMR on-line coupling for the separation and determination of lutein and zeaxanthin stereoisomers in spinach and in retina. *Anal Chem* **73**:667-674.

Davies DM (1985) Textbook of adverse drug reactions. Oxford University Press, Oxford.

Davoine C, Douki T, Iacazio G, Montillet JL, Triantaphylides C (2005) Conjugation of keto fatty acids to glutathione in plant tissues. Characterization and quantification by HPLC-tandem mass spectrometry. *Anal Chem* **77**:7366-7372.

Demple B, and Harrison L (1994) Repair of oxidative damage to DNA: Enzymology and biology. *Annu Rev Biochem* **63**:915-948.

Eguchi M, Eguchi-Ishimae M, Greaves M (2005) Molecular pathogenesis of MLL-associated leukemias. *Int J Hematol* **82**:9-20.

Fan Y, Schreiber EM, Giorgianni A, Yalowich JC, Day BW (2006) Myeloperoxidase-catalyzed metabolism of etoposide to its quinone and glutathione adduct forms in HL60 cells. *Chem Res Toxicol* **19:**937-943.

Felix CA (1998) Secondary leukemias induced by topoisomerase-targeted drugs. *Biochim Biophys Acta* **1400**:233-255.

Felix CA (2001) Leukemias related to treatment with DNA topoisomerase II inhibitors. *Med Pediat Oncol* **36**:525-535.

Fernandes PB (1998) Technological advances in high-throughput screening. *Curr Opin Chem Biol* **2**:597-603.

Fischer IU, Von Unruh GE, Dengler HJ. (1990) Metabolism of eugenol in man. *Xenobiotica* **20**: 209-222.

Flechon A, Droz JP (2006) Chemotherapy practices and perspectives in invasive bladder cancer. *Expert Rev Anticancer Ther* **6**:1473-1482.

Francavilla C, Chen W, Kinder FR Jr. (2003) Formal synthesis of (+)-discodermolide. *Org Lett* **5**:1233-1236.

Freeman RW, Uetrecht JP, Woosley RL, Oates JA, Harbison RD (1981) Covalent binding of procainamide *in vitro* and *in vivo* to hepatic protein in mice. *Drug Metab Dispos* **9:**188-192.

Fukushima M, Fukamiya N, Okano M, Nehira T, Tagahara K, Zhang SX, Zhang DC, Tachibana Y, Bastow KF, Lee KH (2000) Cytotoxity of non-alkaloidal taxane diterpenes from Taxus chinensis against a paclitaxel-resistant cell line. *Cancer Lett* **158**:151-154.

Gantchev TG, Hunting DJ (1998) The ortho-quinone metabolite of the anticancer drug etoposide (VP-16) is a potent inhibitor of the topoisomerase II/DNA cleavable complex. *Mol Pharmacol* **53**:422-428.

Giannakakou P, Sackett DL, Kang YK, Zhan Z, Buters JT, Fojo T, and Poruchynsky MS (1997) Paclitaxel-resistant human ovarian cancer cells have mutant β-tubulins that exhibit impaired paclitaxel-driven polymerization. *J Biol Chem* **272**:17118-17125.

Glatt H (2000) Sulfotransferases in the bioactivation of xenobiotics. *Chem Biol Interact* **129:**141-170.

Greaves RRSH, Agarwal A, Patch D, Davies SE, Sherman D, Reynolds N, Rolles K, Davidson BR, and Burroughs AK (2001) Inadvertent diclofenac rechallenge from generic and nongeneric prescribing, leading to liver transplantation for fulminant liver failure. *Eur J Gastroenterol Hepatol* **13**:71-73.

Gong B, Boor PJ (2006) The role of amine oxidases in xenobiotic metabolism. *Expert Opin Drug Metab Toxicol* **2:**559-571.

Gottesman MM, Pastan I, and Ambudkar SV (1996) P-Glycoprotein and multidrug resistance. *Curr Opin Genet Dev* **6**:610-617.

Guengerich FP, Johnson WW, Shimada T, Ueng YF, Yamazaki H, Langouet S. (1998) Activation and detoxication of aflatoxin B1. *Mutat Res* **402**:121-128.

Gunasekera SP, Gunasekera M, Longley RE and Schuttle GK (1990) Discodermolide: a new bioactive polyhydroxylated lactone from the marine sponge Discodermia dissolute. *J Org Chem* **55**:4912.

Haim N, Roman J, Nemec J, and Sinha BK (1986) Peroxidative free radical formation and O-demethylation of etoposide (VP-16) and teniposide (VM-26). *Biochem Biophys Res Commun* **135**:215-220.

Haim N, Nemec J, Roman J, and Sinha BK (1987) Peroxidase-catalyzed metabolism of etoposide (VP-16-213) and covalent binding of reactive intermediates to cellular macromolecules. *Cancer Res* **47**:5835-5840.

Haim N, Nemec J, Roman J, Sinha BK (1987) In vitro metabolism of etoposide (VP-16-213) by liver microsomes and irreversible binding of reactive intermediates to microsomal proteins. *Biochem Pharmacol* **36**:527-536.

Hamel E, Day BW, Miller JH, Jung MK, Northcote PT, Ghosh AK, Curran DP, Cushman M, Nicolaou KC, Paterson I, Sorensen EJ (2006) Synergistic effects of peloruside A and laulimalide with taxoid site drugs, but not with each other, on tubulin assembly. *Mol Pharmacol* **70**:1555-1564.

Harried SS, Lee CP, Yang G, Lee TI, Myles DC (2003) Total synthesis of the potent microtubule-stabilizing agent (+)-discodermolide. *J Org Chem* **68**:6646-6660.

He L, Yang CP, Horwiz SB (2001) Mutation in beta-tubulin map to domains involved in regulation of microtubule stability in epothilone-resistant cell lines.*Mol Cancer Ther* **1**:3-10.

Honore S, Kamath K, Braguer D, Horwitz SB, Wilson L, Briand C, Jordan MA. (2004) Synergistic suppression of microtubule dynamics by discodermolide and paclitaxel in non-small cell lung carcinoma cells. *Cancer Res* **64**:4957-4964.

Houston JB (1994) Utility of *in vitro* drug metabolism data in predicting *in vivo* metabolic clearance. *Biochem Pharmacol* **47**:1469-1479.

Houston JB and Carlile DJ (1997) Prediction of hepatic clearance from microsomes, hepatocytes, and liver slices. *Drug Metab Rev* **29**: 891-922.

Huang GS, Lopez-Barcons L, Freeze BS, Smith AB, Goldberg GL, Horwitz SB and McDaid HM (2006) Potentiation of taxol efficacy by discodermolide in ovarian carcinoma xenograft-bearing mice. *Clin Caner Res* **12**:298-304.

Hung DT, Nerenberg JB, Schreiber SL (1994) Distinct binding and cellular properties of synthetic (+)- and (-)-discodermolides. *Chem Biol* **1**:67-71.

Hung DT, Chen J, Schreiber SL. (1996) (+)-Discodermolide binds to microtubules in stoichiometric ratio to tubulin dimers, blocks taxol binding and results in mitotic arrest. *Chem Biol* **3**:287-293.

Isbrucker RA, Cummins J, Pomponi SA, Longley RE and Wright AE (2003) Tubulin polymerizing activity of dictyostatin-1, a polyketide of marine sponge origin. *Biochem Pharmacol* **66**: 75-82.

Iwahana M, Utoguchi N, Mayumi T, Goryo M, Okada K (1998) Drug resistance and P-glycoprotein expression in endothelial cells of newly formed capillaries induced by tumors. *Anticancer Res* **18**:2977-2980.

Jorga K, Fotteler B, Heizmann P, Gasser R (1999) Metabolism and excretion of tolcapone, a novel inhibitor of catechol-*O*-methyltransferase. *Br J Clin Pharmacol* **48:**513-520.

Josting A, Wiedenmann S, Franklin J, May M, Sieber M, Wolf J, Engert A, and Diehl V (2003) Secondary myeloid leukemia and myelodysplastic syndromes in patients treated for Hodgkin's disease: A report from the German Hodgkin's Lymphoma Study Group. *J Clin Oncol* **21**:3440-3446.

Ju C and Uetrecht JP (1998) Oxidation of a metabolite of indomethacin (Desmethyldeschlorobenzoylindomethacin) to reactive intermediates by activated neutrophils, hypochlorous acid, and the myeloperoxidase system. *Drug Metab Dispos* **26**: 676–680.

Jung, W-H, Harrison C, Shin, Y, Fournier, J-H, Balachandran R, Raccor BS, Sikorski RP, Vogt A, Curran DP, Day BW (2007) Total synthesis and biological evaluation of C16 analogs of (–)-dictyostatin. *J Med Chem*, accepted with revisions.

Kagan VE, Yalowich JC, Day BW, Goldman R, Gantchev TG, and Stoyanovsky DA (1994) Ascorbate is the primary reductant of the phenoxyl radical of etoposide in the presence of thiols both in cell homogenates and in model systems. *Biochemistry* **33**:9651-9660.

Kagan VE, and Tyurina YY (1998) Recycling and redox cycling of phenolic antioxidants. *Ann NY Acad Sci* **854**:425-434.

Kagan VE, Kuzmenko AI, Tyurina YY, Shvedova AA, Matsura T, and Yalowich JC (2001) Pro-oxidant and antioxidant mechanisms of etoposide in HL-60 cells: Role of myeloperoxidase. *Cancer Res* **61**:7777-7784.

Kagan VE, Yalowich JC, Borisenko GG, Tyurina YY, Tyurin VA, Thampatty P, Fabisiak JP (1999) Mechanism-based chemopreventive strategies against etoposide-induced acute myeloid leukemia: free radical/antioxidant approach. *Mol Pharmacol* **56:**494-506.

Kamel AM, Munson B (2004) Collisionally-induced dissociation of purine antiviral agents: mechanisms of ion formation using gas phase hydrogen/deuterium exchange and electrospray ionization tandem mass spectrometry. *Eur J Mass Spectrom* **10**:239-257.

Kaplowitz N (2004) Drug-induced liver injury. *Clin Infect Dis 1* **Suppl 2:**S44-48.

Karasavvas N, Carcamo JM, Stratis G, and Golde DW (2005) Vitamin C protects HL60 and U266 cells from arsenic toxicity. *Blood* **105**:4004-4012.

Khayat D,Antoine EC, Coeffic D (2000) Taxol in the management of cancers of the breast and the ovary. *Cancer Invest* **18**: 242-60.

Kingma PS, Greider CA, and Osheroff N (1997) Spontaneous DNA lesions poison human topoisomerase IIα and stimulate cleavage proximal to leukemic 11q23 chromosomal breakpoints. *Biochemistry* **36**:5934-5939.

Kingma PS, and Osheroff N (1997) Apurinic sites are position-specific topoisomerase II poisons. *J Biol Chem* **272**:1148-1155.

Kiyama R, Tamura Y, Watanabe F, Tsuzuki H, Ohtani M, Yodo M (1999) Homology modeling of gelatinase catalytic domains and docking simulations of novel sulfonamide inhibitors. *J Med Chem* **42**: 1723-1738.

Kola I, Landis J (2004) Can the pharmaceutical industry reduce attrition rates? *Nat Rev Drug Discov* **3:**711-715.

Kostiainen R, Kotiaho T, Kuuranne T, Auriola S (2003) Liquid chromatography/atmospheric pressure ionization-mass spectrometry in drug metabolism studies. *J Mass Spectrom* **38**:357-372.

Kowalski RJ, Giannakakou P, Gunasekera SP, Longley RE, Day BW, Hamel E (1997) The microtubule-stabilizing agent discodermolide competitively inhibits the binding of paclitaxel (Taxol) to tubulin polymers, enhance tubulin nucleation reactions more potently than paclitaxel, and inhibits the growth of paclitaxel-resistant cells. *Mol Pharmacol* **52**:613-622.

Lasser KE, Allen PD, Woolhandler SJ, himmelstein DU, wolfel SM, and Bor DH (2002)Timing of new black box warnings and withdrawals for prescription medications. *J Am Med Assoc* **287:**2215-2220.

Libura J, Slater DJ, Felix CA, and Richardson C (2005) Therapy-related acute myeloid leukemia-like MLL rearrangements are induced by etoposide in primary human CD34+ cells and remain stable after clonal expansion. *Blood* **105**:2124-2131.

Lindon JC, Nicholson JK, Sidelmann UG, Wilson ID (1997) Directly coupled HPLC-NMR and its application to drug metabolism. *Drug Metab Rev* **29**:705-746.

Litman T, Druley TE, Stein WD, and Bates SE. (2001) From MDR to MXR: new understanding of multidrug resistance systems, their properties and clinical significance. *Cell Mol Life Sci* **58**: 931-959.

Longley RE, Gunasekera SP, Faherty D and Mclane J, Dumont F (1993) Immunosuppression by discodermolide. *Ann NY Acad Sci* **696**:94-107.

Lovett BD, Strumberg D, Blair IA, Pang S, Burden DA, Megonigal MD, Rappaport EF, Rebbeck TR, Osheroff N, Pommier YG, and Felix CA (2001) Etoposide metabolites enhance DNA topoisomerase II cleavage near leukemia-associated MLL translocation breakpoints. *Biochemistry* **40**:1159-1170.

Ma S, Chowdhury SK, Alton KB (2006) Application of mass spectrometry for metabolite identification. *Curr Drug Metab* **7**:503-523.

Maanen JMS, Lafleur MV, Westmijze EJ, van Maanen JM, van Schaik MA, Lankelma J, and Retel J (1988) Formation of different reaction products with single- and double-stranded DNA by the ortho-quinone and the semi-quinone free radical of etoposide (VP-16-213). *J Natl Cancer Inst* **80**:1526-1533.

Maellaro E, Del Bello B, and Comporti M (1996) Protection by ascorbate against apoptosis of thymocytes: Implications of ascorbate-induced nonlethal oxidative stress and poly(ADP)ribosylation. *Exp Cell Res* **226**:105-113.

Mani S, Macapinlac M, Goel S, Verdier-Pinard D, Fojo T, Rothenberg M and Colevas D (2004) The clinical development of new mitotic inhibitors that stabilize the microtubule. *Anti-Cancer Drugs* **15**:553-558.

Mareel MM, De Mets M (1984) Effect of microtubule inhibitors on invasion and on related activities of tumor cells. *Int Rev Cytol* **90**:125-168.

Mita C, Hammond LA, Lockhart AC, Shah M, Curtright J, Chen T, et al. (2003) A phase I and pharmacokinetic study of XAA296A (discodermolide) administrated once every three weeks in adult patients with advanced solid malignancies. *Proc AACR-NCI-EORTC Int Conf* abstr A252.

Monks TJ, Anders MW, Dekant W, Stevens JL, Lau SS, van Bladeren PJ (1990) Glutathione conjugate mediated toxicities. *Toxicol Appl Pharmacol* **106:**1-19.

Nasr F, Macintyre E, Venuat AM, Bayle C, Carde P, Ribrag V (1997) Translocation t(4;11)(q21;q23) and MLL gene rearrangement in acute lymphoblastic leukemia secondary to anti topoisomerase II anticancer agents. *Leuk Lymphoma* **25**:399-401.

Nguyen L, Chatelut E, Chevreau C, Tranchand B, Lochon I, Bachaud JM, Pujol A, Houin G, Bugat R, and Canal P (1998) Population pharmacokinetics of total and unbound etoposide. *Cancer Chemother Pharmacol* **41**:125-132.

Ng A, Taylor GM, Eden OB (2000) Secondary leukemia in a child with neuroblastoma while on oral etoposide: what is the cause? *Pediatr Hematol Oncol* **17**:273-279.

Nonaka T, Mio M, Doi M, and Tasaka K (1992) Histamine-induced differentiation of HL-60 cells. The role of cAMP and protein kinase A. *Biochem Pharmacol* **44**:1115-1121.

Novartis, A. G. *Annual Report Pursuant to Section 13 or 15(d) of the Securities Exchange Act of 1934 for the fiscal year ended December 31, 2004*, Securities Exchange Commission file number 1-15024, Form 20-F, filed Jan 28, 2005, p 42.

Obach RS (1999) Prediction of human clearance of twenty-nine drugs from hepatic microsomal intrinsic clearance data: An examination of in vitro half-life approach and nonspecific binding to microsomes. *Drug Metab Dispos* **27**:1350-1359.

Obach RS, Baxter JG, Liston TE, Silber BM, Jones BC, Macintyre F, Rance DJ and Wastall P (1997) The prediction of human pharmacokinetic parameters from preclinical and in vitro metabolism data. *J Pharmacol Exp Ther* **283**: 46-58.

O'Brien PJ (2000) Peroxidases. *Chem Biol Interact* **129:**113-139.

O'Neil GW, Phillips AJ (2006) Total synthesis of (–)-dictyostatin. *J. Am. Chem. Soc*.**128**: 5340-5341.

Pang S, Zheng N, Felix CA, Scavuzzo J, Boston R, and Blair IA (2001) Simultaneous determination of etoposide and its catechol metabolite in the plasma of pediatric patients by liquid chromatography/tandem mass spectrometry. *J Mass Spectrom* **36**:771-781.

Paterson I I, Florence GJ, Gerlach K, Scott JP. (2000) Total synthesis of the antimicrotubule agent (+)-discodermolide using boron-mediated aldol reactions of chiral ketones. *Angew Chem Int Ed Engl* **39**:377-380.

Paterson I, Britton R, Delgado O, Meyer A, and Poullennec KG. (2004) Total synthesis and configurational assignment of (–)-dictyostatin, a microtubule-stabilizing macrolide of marine sponge origin. *Angew Chem Int Ed Engl* **43**: 4629-4633.

Paterson I, Britton R, Delgado O, Wright AE (2004) Stereochemical determination of dictyostatin, a novel microtubule-stabilising macrolide from the marine sponge *Corallistidae sp*. *Chem Commun (Camb)* **6**: 632-633.

Pedersen-Bjergaard J, and Rowley JD (1994) The balanced and the unbalanced chromosome aberrations of acute myeloid leukemia may develop in different ways and may contribute differently to malignant transformation. *Blood* **83**: 2780-2786.

Pettit GR, Linchacz ZA, Gao F, Boyd MR, Schmidt JM **(**1994**)** Isolation and structure of the cancer cell growth inhibitor dictyostatin 1. *J Chem Soc Chem Commun* **9**: 1111-2.

Pirmohamed M, Naisbitt DJ, Gordon F and Park BK (2002) The danger hypothesis: potential role in idiosyncratic drug reactions. *Toxicology* **181/182**:55–63.

Pinnix IB, Guzman GS, Bonkovsky HL, Zaki SR, and Kinkade JM Jr (1994) The posttranslational processing of myeloperoxidase is regulated by the availability of heme. *Arch Biochem Biophys* **312**:447-458.

Plant N (2004) Strategies for using in vitro screens in drug metabolism. *Drug Discov Today* **9:**328-336.

Pommier Y, Schwartz RE, Zwelling LA, Kohn KW (1985) Effects of DNA intercalating agents on topoisomerase II induced DNA strand cleavage in isolated mammalian cell nuclei. *Biochemistry* **24**:6406-6410.

Popovic R, Zeleznik-Le NJ (2005) MLL: how complex does it get? *J Cell Biochem* **95**:234-242.

Prakash C, Soliman V (1997) Metabolism and excretion of a novel antianxiety drug candidate, CP-93,393, in Long Evans rats. Differentiation of regioisomeric glucuronides by LC/MS/MS. *Drug Metab Dispos* **25**:1288-1297.

Prentis RA, Lis Y, Walker SR (1988) Pharmaceutical innovation by the seven UK-owned pharmaceutical companies (1964-1985). *Br J Clin Pharmacol* **25**: 387-396.

Pui CH, Behm FG, Raimondi SC, Dodge RK, George SL, Rivera GK, Mirro J, Kalwinsky DK, Dahl GV, and Murphy SB (1989) Secondary acute myeloid leukemia in children treated for acute lymphoid leukemia. *N Engl J Med* **321**:136-142.

Pui CH, Relling MV (2000) Topoisomerase II inhibitor-related acute myeloid leukaemia. *Br J Haematol* **109**:13-23.

Ramachandran PV, Srivastava A, and Hazra D. (2007) Total synthesis of potential antitumor agent, (–)-dictyostatin. *Org Lett* **9**: 157-160.

Relling MV, Nemec J, Schuetz EG, Schuetz JD, Gonzalez FJ, Korzekwa KR (1994) O-demethylation of epipodophyllotoxins is catalyzed by human cytochrome P450 3A4. *Mol Pharmacol* **45**:352-358.

Ritter JK (2000) Roles of glucuronidation and UDP-glucuronosyltransferases in xenobiotic bioactivation reactions. *Chem Biol Interact* **129:**171-193.

Rick O, Beyer J, Kingreen D, Schwella N, Krusch A, Schleicher J, Kirsch A, Huhn D, and Siegert W (1998) High-dose chemotherapy in germ cell tumours: A large single centre experience. *Eur J Cancer* **34**:1883-1888.

Rooney PH, Telfer C, McFadyen MC, Melvin WT, Murray GI (2004) The role of cytochrome P450 in cytotoxic bioactivation: future therapeutic directions. *Curr Cancer Drug Targets* **4:**257-265.

Rowinsky EK (1997) The development and clinical utility of the taxane class of antimicrotubule chemotherapy agents. *Annu Rev Med* **48**:353-374.

Rungger-Brandle E, Gabbiani G (1983) The role of cytoskeletal and cytocontractile elements in pathologic processes. *Am J Pathol* **110**:361-392.

Sabourin M, and Osheroff N (2000) Sensitivity of human type II topoisomerase to DNA damage: Stimulation of enzyme-mediated DNA cleavage by abasic, oxidized and alkylated lesions. *Nucleic Acids Res* **28**:1947-1954.

Sanchez-Pedregal VM, Kubicek K, Meiler J, Lyothier I, Paterson I, and Carlomagno T. (2006) The tubulin-bound conformation of discodermolide derived by NMR studies in solution supports a common pharmacophore model for epothilone and discodermolide. *Angew Chem Int Ed* **45**: 7388-7394.

Sanders M, Shipkova PA, Zhang H, Warrack BM (2006) Utility of the hybrid LTQ-FTMS for drug metabolism applications. *Curr Drug Metab* **7**:547-555.

Schattenberg DG, Stillman WS, Gruntmeir JJ, Helm KM, Irons RD, Ross D (1994) Peroxidase activity in murine and human hematopoietic progenitor cells: potential relevance to benzene-induced toxicity. *Mol Pharmacol* **46:**346-351.

Shearer P, Kapoor G, Beckwith JB, Takashima J, Breslow N, and Green DM (2001) Secondary acute myelogenous leukemia in patients previously treated for childhood renal tumors: A report from the National Wilms Tumor Study Group. *J Pediatr Hematol Oncol* **23**:109-111.

Shin Y, Fournier JH, Fukui Y, Bruckner AM, Curran DP (2004) Total synthesis of (-)-dictyostatin: confirmation of relative and absolute configurations. *Angew Chem Int Ed Engl* **43**: 4634-4637.

Shuker SB, Hajduk PJ, Meadows RP, Fesik SW (1996) Discovering high-affinity ligands for proteins: SAR by NMR. *Science* **274**: 1531-1534.

Silverman L, Campbell R, Broach JR (1998) New assay technologies for high-throughput screening. *Curr Opin Chem Biol* **2**: 397-403.

Sirica AE (1996) Biliary proliferation and adaptation in furan-induced rat liver injury and carcinogenesis. *Toxicol Pathol* **24:**90-99.

Smith AB, Freeze BS, Xian M, Hirose T (2005) Total synthesis of (+)-discodermolide: a highly convergent fourth-generation approach. *Org Lett* **7**:1825-1828.

Smith AB and Xian M (2005) Design, synthsis and biological evaluation of simplified analogues of (+)-discodermolide. Additional insights on the importance of the diene, the C(7)hydroxyl, and the lactone. *Org Lett* **23**:5229-5232.

Soucék P, Anzenbacker P, Skoumalov I, and Dvorak M (2005) Expression of cytochrome P450 genes in CD34+ hematopoietic stem and progenitor cells. *Stem Cells* **23**:1417-1422.

Stewart CF (1994) Use of etoposide in patients with organ dysfunction: Pharmacokinetic and pharmacodynamic considerations. *Cancer Chemother Pharmacol* **34** (Suppl.):S76-S83.

Strobl H, Takimoto M, Majdic O, Fritsch G, Scheinecker C, Hocker P, and Knapp W (1993) Myeloperoxidase expression in CD34+ normal human hematopoietic cells. *Blood* **82**:2069-2078.

Tomer KB (2001) Separations combined with mass spectrometry. *Chem Rev* **101**:297-328.

Tozuka Z, Kaneko H, Shiraga T, Mitani Y, Beppu M, Terashita S, Kawamura A, Kagayama A (2003) Strategy for structural elucidation of drugs and drug metabolites using (MS)n fragmentation in an electrospray ion trap. *J Mass Spectrom* **38**:793-808.

Tyurina YY, Tyurin VA, Yalowich JC, Quinn PJ, Claycamp HG, Schor NF, Pitt BR, and Kagan VE (1995) Phenoxyl radicals of etoposide (VP-16) can directly oxidize intracellular thiols: Protective versus damaging effects of phenolic antioxidants. *Toxicol Appl Pharmacol*1**31**:277-288.

Uetrecht JP (1999) New concepts in immunology relevant to idiosyncratic drug reactions: the "Danger Hypothesis" and innate immune system. *Chem Res Toxicol* **12**:387–395.

Uetrecht JP (2000) Is it possible to more accurately predict which drug candidates will cause idiosyncratic drug reactions? *Curr Drug Metab* **1:**133-141.

van Maanen JM, de Ruiter C, Kootstra PR, Lafleur MV, de Vries J, Retel J, Pinedo HM (1985) Inactivation of phi X174 DNA by the *ortho*-quinone derivative or its reduction product of the antitumor agent VP 16-213. *Eur J Cancer Clin Oncol* **21**:1215-1218.

Van Maanen JM, Verkerk UH, Broersen J, Lafleur MV, De Vries J, Retel J, and Pinedo HM (1988) Semi-quinone formation from the catechol and *ortho*-quinone metabolites of the antitumor agent VP-16-213. *Free Radical Res Commun* **4**:371-384.

Wani MC, Taylor HL, Wall ME, Coggon P, McPhail AT (1971) Plant antitumor agents. VI. The isolation and structure of taxol, a novel antileukemic and antitumor agent from *Taxus brevifolia*. *J Am Chem Soc* **93**:2325-2327.

Watanabe Y, Nakajima M, Ohashi N, Kume T, Yokoi T (2003) Glucuronidation of etoposide in human liver microsomes is specifically catalyzed by UDP-glucuronosyltransferase 1A1. *Drug Metab Dispos* **31**:589-595.

Watkins P (2000) COMT inhibitors and liver toxicity. *Neurology* **55:**S51-52.

Wierecky J, Kollmannsberger C, Boehlke I, Kuczyk M, Schleicher J, Schleucher N, Metzner B, Kanz L, Hartmann JT, and Bokemeyer C (2005) Secondary leukemia after first-line high-dose chemotherapy for patients with advanced germ cell cancer. *J Cancer Res Clin Oncol* **131**:255-260.

Winick NJ, Smith SD, Shuster J, Lauer S, Wharam MD, Land V, Buchanan G, and Rivera G (1993) Treatment of CNS relapse in children with acute lymphoblastic leukemia: A Pediatric Oncology Group study. *J Clin Onco* **11**: 271-278.

Yalowich JC, Kagan VE, Do D, Yang S, Giorgianni A, McDonald P, Fan Y, Day BW, Riviere J, and Wagner JR (2004) Myeloperoxidase-dependent pro-oxidant effects of etoposide: Implications for etoposide-induced leukemogenesis. *Pro Am Asso Cancer Res* **45**:3084.

Yu LJ, Matias J, Scudiero DA, Hite KM, Monks, A, Sausville EA, and Waxman DJ (2001) P450 enzyme expression patterns in the NCI human tumor cell line panel. *Drug Metab Dispos* **29**:304-312.

Zheng N, Felix CA, Pang S, Boston R, Moate P, Scavuzzo J, and Blair IA (2004) Plasma etoposide catechol increases in pediatric patients undergoing multiple-day chemotherapy with etoposide *Clin Cancer Res* **10**:2977-2985.

Zhuo X, Zheng N, Felix CA, and Blair IA (2004) Kinetics and regulation of cytochrome P450-mediated etoposide metabolism. *Drug Metab. Dispos* **32**:993-1000.